**Yousr REKIK**

NANOTECH Master
2018/2019

***The French Alternative Energies and Atomic Energy Commission (CEA)***

17, rue des Martyrs, 38054 Grenoble cedex 9

# Fabrication and characterization of biomimetic hybrid nanoporous membranes

**From 18/02/19 to 14/08/19**

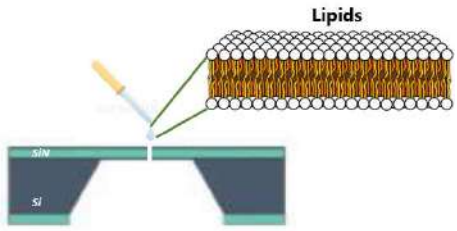


Confidentiality: yes

## Under the supervision of:

- **Company supervisor : Camille RAILLON** Present at defence
  **Camille.RAILLON@cea.fr**

- **Phelma Tutor : Liliana BUDA-PREJBEANU**
  **Liliana.Buda@cea.fr**

**Ecole nationale**
**supérieure de physique,**
**électronique, matériaux**

**Phelma**
Bât. Grenoble INP - Minatec
3 Parvis Louis Néel - CS 50257
F-38016 Grenoble Cedex 01

Tél +33 (0)4 56 52 91 00
Fax +33 (0)4 56 52 91 03

**http://phelma.grenoble-inp.fr**

**Acknowledgements**

I would like to thank Dr. Arnaud BUHOT for having accepted me in his team; CREAB at the SyMMES laboratory at CEA-Grenoble. A special thanks goes to my tutor, Mrs. Camille RAILLON for her valuable advice, guidance and for her precious support. I am also grateful Mrs. Juliette JOUHET for giving me the opportunity to discover the world of plant lipids, for her patience with my silly questions about biology and for her valuable remarks about my report.

My great thanks go to the CREAB team for their great company, to Catherine and Morgane from LPCV/Lipid team for their help and patience.

I would also like to thank M. Pierre-Henri JOUNEAU for his valuable help in transmission electron microscopy experiments and M. Denis MARIOLLE for his priceless advice in AFM experiments and image post processing.

Finally, I would like to thank Mrs. Liliana BUDA-PREJBEANU for her involvement in my internship.

***"Allow yourself to be beginner. No one starts off being excellent", Wendy Flyn***

# Table of contents

# Glossary

**Ligand:** Molecule that specifically bind to ions

**Methyl beta-cyclodextrin (MbCD):** Reagent solution used to increase substance (non-polar) solubility

**Sonication:** Particle and solution agitation process using ultrasonic (>20 kHz) frequencies

**Extrusion:** A process to create objects with a well-defined cross section

**Carboxyl group:** COOH group

**Fatty acid:** Molecule having a long hydrocarbon chain and a carboxyl (-COOH) group. It is the principal component of lipid molecule tail

**Phosphate group:** Contains a phosphorus atom (P) bound to four oxygen residues

**Hydroxyl group:** OH group

**Osmotic pressure:** The pressure needed to be applied to push water across a semipermeable membrane

**Sphingolipids (SLs):** Lipids based on sphingosine in their headgroups (instead of glycerol)

**Steric forces:** Repulsive force between two overlapping electronic clouds

**Buffer solution**: Solution of constant pH

**Oxalic acid ($C_2H_2O_4$)**: Reducing agent

**Vertebrates:** **"**A vertebrate is an animal with a spinal cord surrounded by cartilage or bone" (from Wikipedia)

**HEPES:** (4-(2-hydroxyethyl)-1-piperazineethanesulfonic acid)

# LIST OF ABBREVIATIONS

**RO:** Reverse Osmosis

**TEM:** Transmission Electron Microscopy

**AFM:** Atomic Force Microscopy

**STEM:** Scanning Transmission Electron Microscopy

**Cer:** Ceramide

**Chol:** Cholesterol

**CPEO3:** Cholesterylpolyethylenoxythiol

**DLPC**: 1,2-dilauroyl-sn-glycero-3-phosphocholine
**DPPA**: 1,2-dipalmitoyl-sn-glycero-3-Phosphatidic acid
**DPPC:** 1,2-dipalmitoyl*sn*- glycero-3-phosphocholine
**DPhPC:** 1,2-diphytanoyl-*sn*-glycero-3- phosphocholine
**DOTAP:**1,2-dioleoyl-3-trimethylammonium-propane chloride

**DOPC:** Dioleoylphosphatidylcholine

**DOPS:** Dioleoylphosphatidylserine

**DMPC:** Dimyrisoylphosphatydilcholine

**DPPE:** Dipalmitoylphosphatidyletanolamine

**DSPC:** 1,2-distearoyl-snglycero-3-phosphocholine
**ESM:** Egg Sphingomyelin

**OT:** Octanethiol

**MbCD:** Methyl beta-cyclodextrin

**pSi:** porous Silicon

**PEM:** Polyelectrolyte multilayer
**POPE:** Palmitoyloleoyl-phosphatidylethanolamine
**POPG:** Palmitoyl-oleoyl-phosphatidylglycerol

**POPS:** 1-palmitoyl-2-oleoyl-phospatidylserine
**POPC:** 1-palmitoyl-2-oleoyl-phospatidylcholine

**SiN**: Silicon nitride

**SL:** Sphingolipid

**SM:** Sphingomyelin

**PFQNM:** Peak Force Quantitative Nanomechanical Mapping or Peak Force Quantitative Nano-Mechanics

**$C_2H_2O_4$:** Oxalicacid

**LPCVD:** Low Pressure Chemical Vapor Deposition

# List of figures

# Introduction

## 1. General context

Due to the indiscriminate human activities disrupting the ecological balance, water pollution is becoming a serious threat to both environment and human beings. For instance, about 330 $km^3$of wastewater are reported to be annually generated worldwide (2015). Such avolume is sufficient theoretically to “irrigate millions of hectares of crops”[1].Therefore, dealing with large volumes of produced wastewater to clean and recirculate isone of the difficult challenges we are facing nowadays.

There are different types of **water pollutants** (infectious agents, oxygen demanding wastes, thermal pollution, organic pollutants, inorganic pollutants...). Inorganic water contaminants, mainly heavy metals, are very harmful because of their **high toxicity** and **non-biodegradability**. Furthermore, they are highly water soluble and deposit slowly in soil.

**Heavy metals** are elements whose density exceeds 5g/$cm^3$ such as Arsenic (Ar), Cadmium (Cd) and Mercury (Hg), [2]. Water polluted with heavy metals can be produced from different industrial activities such as cleanroom activities, printed circuit board (PCB) manufacturing, wood processing industries and petroleum refining.

When adsorbed and accumulated in living organisms, these contaminants can cause poisoning, cancer and organ and nervous system damage. That’s why, strict legislation has been set to define limits on the maximum concentration of heavy metals in water discharged in the environment (**Table A.1, Appendix A**).

Conventional methods for heavy metals removal include physical, chemical and biological techniques (Figure A.1, Appendix A). Owing to their ability to remove inorganic compounds that other methods cannot, **chemical methods** have proven to be the most suitable for toxic inorganic compounds removal. In particular, chemical precipitation and membrane filtration techniques are widely used. Whereas chemical precipitation is based on the production of insoluble heavy metals precipitates,a porous membrane is used in membrane-based methods toseparate contaminants from wastewater. In the latter methods, the size of retained pollutants can be controlled by the membrane pore size. **Ultrafiltration (UF)**, **nanofiltration (NF)** and **reverse osmosis (RO)** are examples of membrane filtration methods. In reverse osmosis (RO), polluted water is forced, thanks to mechanical pressure, across a semi permeable polymeric membrane that rejects ions and pollutants while selectively letting water through.

Although membrane-based systems are very efficient for heavy metal removal with values reaching 90% for ultrafiltration[3], their main drawback is their high energy consumption. In order to achieve **zero-energy filtration processes** embedded in **miniaturized water filters**, researchers have been developing alternative approaches and optimizing conventional technologies. Among these alternative approaches, biomimetic membranes; with transport properties mimicking those of **biological nanopores** and **bio-channels;** have been receiving considerable attention in the last years. Biological **nanopores and transmembrane proteins**are nanometric structures spanning the lipid bilayerof cell membranes. They ensure

the communication of the cell with its external environment through the **selective and efficient** transport of molecules and ions from one side of the membrane to the other.

## 2. Motivation of work

Creating robust man-made biomimetic structures is a challenging task requiring both a great understanding of the bewildering complexity of biological processes to be mimicked and a good knowledge of the materials to be used in synthetic systems.

However, researchers succeeded to develop solutions, few of them are already on the market. In this paragraph, two examples of biomimetic membranes are presented.

### 2.1 Aquaporin Inside ® tap water RO membranes

Taking advantage of conventional RO synthetic membranes, the Danish company Aquaporin found in 2007 « took a further step » by introducing the natural water channel protein: Aquaporin in its water filtration products. **Aquaporin** is responsible for the **rapid** and **highly selective** water transport across cell membranes of all organisms from bacteria to humans. It is thanks to the diffusion mechanism of this protein that our kidney cells can filter hundreds of water liters (150-200L)from primary urine each day.

In order to ensure clean water with balanced energy requirements, Aquaporin group developed **tap-water** filtering devices (Aquaporin Inside® tap water RO membranes) for industrial and house use (Figure1) exhibiting 50% higher water permeability compared to conventional RO membranes[4]. They are **wearable** filters with high throughput going up to hundreds of liters per hour (425 L/h) for industrial customers and with low applied pressures (<7 bar).

***Figure 1:*** *Aquaporin Inside® TWRO1812-175 reverse osmosis (RO) membrane element able to produce 28 L/h of permeate water at low applied pressure (4 bar), making it suitable for direct flow water purification. It can fit into house filtration RO systems and it has been reported to be 3 X more efficient than three conventional RO counterparts.Taken from[4].*

Stability over numerous chemical and mechanical stimuli and specific ion selectivity are additional features highlighting biological nanopores as efficient transport structures. Matching ion selectivity at nanoscale in a synthetic platform is very challenging considering the complex surface functionalization to be mastered. In this context, solid state nanopores with chemically modified internal walls are reported in literature as models to mimic biological selectivity of ion channels. A recent example is described in the next paragraph.

### 2.2 Biomimetic potassium-selective nanopores

Few months ago, Acar et al., [5] reported the fabrication of solid-state silicon nitride (SiN) nanopores preferentially conducting potassium ions ($K^+$) over sodium ions ($Na^+$) with a selectivity ratio exceeding 80 for nanopores with effective diameters less than 2nm. Although this value is tens of times less than the real biological potassium channel selectivity, achieving selectivity in solid-state platforms will open new perspectives for the future of biomimetic nanopores.

This ionic (cation/cation) selectivity, surpassing already reported ones by about one order of magnitude[5] [5], originates from nanopore walls coatings with ligands; molecules that specifically bind to ions ($K^+$ in this example). Besides, single-stranded DNA (ssDNA) molecules bound to nanopore entrance enable only cations to enter the biomimetic ion channel playing therefore the role of "cation filters" (Figure 2).

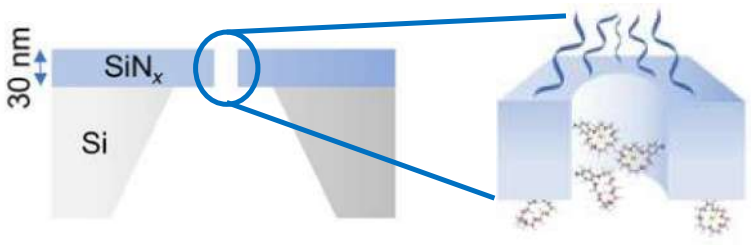


***Figure 2:****Potassium-selective solid state nanopore. (A) Single nanopore with tunable diameter fabricated in a 30-nm thick SiN film. (B) Zoom on the nanopore showing its asymmetric chemical modification; single-stranded DNA molecules located at its entrance and ligand (4'-aminobenzo-18-crown-6 ether) molecules bound to its internal walls. Adapted from Acar et al. [5]*

The latter article emphasizes the current interest of researchers in biomimetic solutions. Moreover, it is added as a solid support for our project since it focuses on ion channels 'transport and selectivity; the two most crucial parameters for a good filtration system whether at macro or at nanoscale.

## I. The project

### 1. Biomimetic hybrid nanopores

As mentioned before, we are inspired by ion channels. These channels facilitate the passage of specific ions across a membrane down their concentration gradient without high energy consumption. This phenomena is called **"facilitated diffusion"**.

In order to be able to build, on the long term, a biomimetic nanoscale filters for heavy metal removal, it is important to mimic the **biological environment** in which channels are integrated. Indeed, the biological cell is surrounded by a 5-nm thick lipid bilayer filled with the different types of nanopores and transporters controlling intracellular/extracellular exchange. These "separation paradigms" (Shen et al., [6]) enable the cell to regulate its volume and its internal osmotic pressure, yet their ex-vitro study is challenging. In fact, biological nanopores have **fixed size and** the cellular lipid bilayer, in which they are

incorporated, has a limited stability; very sensitive to small changes in external parameters such as pH, salt concentration, temperature and mechanical stress.

On the other side, solid-state nanopores based on materials from semiconductor clean room technologies have proven to be a reliable alternative for biosensing applications since the early 90s (Branton et al., [7]). Their originality resides in their tunable diameters and lengths, their support stability, their adjustable surface properties and their potential for integration into fluidic devices and networks. These characteristics allow solid-state nanopores to control single-molecule transport. However, their surface functionalization, through addition of specific molecules is needed to mimic biological selectivity.

In this context, we propose to design hybrid nanoporous membranes combining the robustness of synthetic nanopores with the selectivity of biomolecular interactions (lipids). Our proposed membrane is composed of a silicon nitride (SiN) nanopore acting as a support for a lipid layer deposited on it (Figure 3). The latter layer is intended to mimic the biological lipid layer surrounding our cells. After fabrication, the whole membrane can be used as a model to further incorporate other holey structures to mimic ion channels. It is noteworthy that, for simplicity reason, figure 3 shows a single biomimetic hybrid membrane which is part of a large nanoporenetwork.

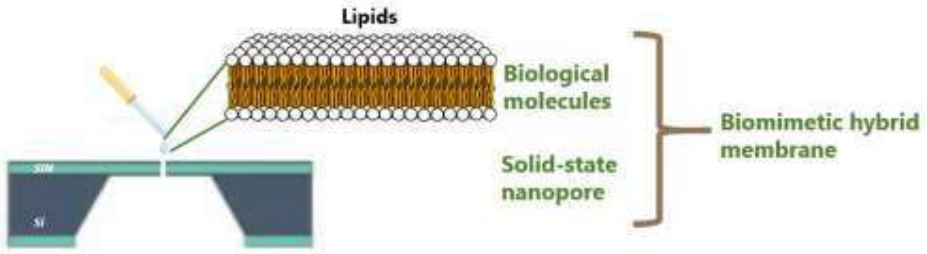


***Figure 3:*** *The structure of the proposed biomimetic hybrid membrane*

## 2. Challenge and objectives

Complexity is the main challenge in biological systems study. To tackle this challenge, we use a **bottom-up** engineering approach. It consists in dividing the system into small systems, studying each sub-system separately and finally linking all the studied processes together and building a whole understanding of the initial system. Projected on our example, this approach is visible in the two-step biomimetic adopted strategy; the first step is mimicking the lipid bilayer (objective of my internship) and the second one is mimicking ion channels (the future of the project).

My internship is the proof of concept step of the project aiming at building a passive biomimetic membrane for water filtration applications. The internship objectives are to:

- Build robust hybrid membranes by suspending lipids on solid-state nanopores using different lipid deposit methods
- Characterize the lipid organization on the surface of and inside nanopores using advanced microscopy techniques

In particular, the question we want to answer concerning the second point is whether lipids form a lipid coating (Figure 4) or a suspended layer inside nanopores. It is worthy to note that both configurations are reported in literature: coating (Yusko et al., [8]) and suspended lipid layer (Han et al., [9])

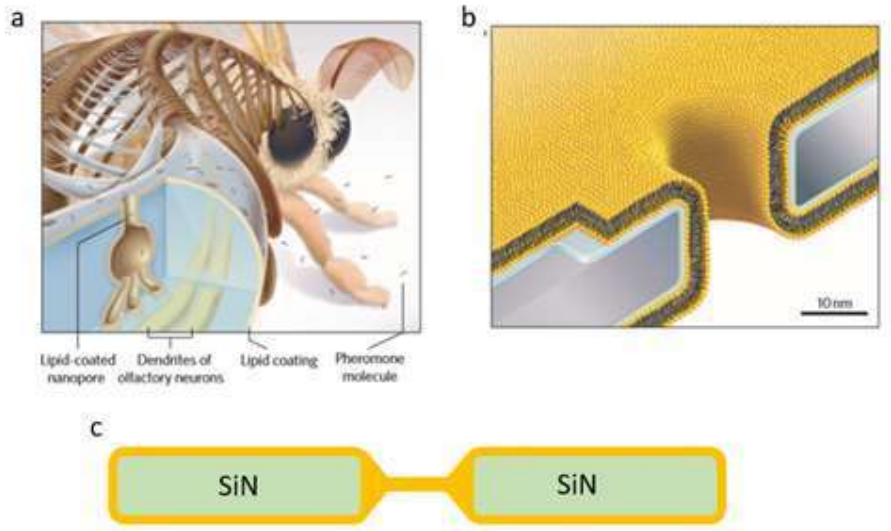


***Figure 4**: Biomimicry and synthetic lipid layers a) Drawing of a cross-section through an olfactory sensillum (sensory organ) in the insect antenna showing lipid-coated nanopore, responsible for the capture of different molecules b) Drawing, to scale, of a lipid-coated (yellow) SiN nanopore (grey) with an intermediate water layer (blue). a) and b) are adapted from Yusko et al.[8] c) Drawing, not to scale, of a suspended layer in a SiN nanopore.*

## 3. Industrial context

This interdisciplinary projectis a collaboration between SyMMES laboratory (Laboratoire de Systèmes Moléculaires et nanoMatériaux pour l'Energie et le Santé) and LPCV (Laboratoire de Physiologie Cellulaire et Végétale), both are parts of CEA-Grenoble. The latter is one of the nine centers of the French Alternative Energies and Atomic Energy Commission (CEA). It was founded in 1995 and counts 115 laboratoires whose activities are distributed between industrial (85%) and fundamental research (15%). The two collaborating laboratories (SyMMES and LPCV) belong to the fundamental research division of CEA-Grenoble.

CREAB (Chimie pour la Reconnaissance et l'Etude d'Assemblages Biologiques) team, where this internship is conducted, is part of SyMMES laboratory. Bringing together the expertise of chemists, engineers and physicts, its research activities are focused on surface chemistry for biosensing applications and analytical applications. Whereas, LPCV is a leader laboratory in the field of plant lipids. Its expertise, in particular that of the lipid team (the project

collaborator) is based on a unique knowledge of lipid metabolism of plant cells and on a mastering of the most efficient methods to produce, quantify and qualify these lipids. PFNC (Technology Platform for Nano Characterization) services were also accessible within this internship.

## II. State of the art : AFM for lipid bilayers

### 1. Lipid description

Cell membrane is composed of a bilayer of lipids with integrated membrane proteins and attached sugars. Lipids are amphipathic molecules with a **hydrophilic (water-loving) head** and a **hydrophobic (water-hating) tail**. The head is stable in an aqueous environment while the tail is stable in a lipid one; which explains the self-assembly of lipids in bilayers. In a bilayer, hydrophilic heads of each monolayer point towards the aqueous medium whereas tails point towards each other (Figure 5).

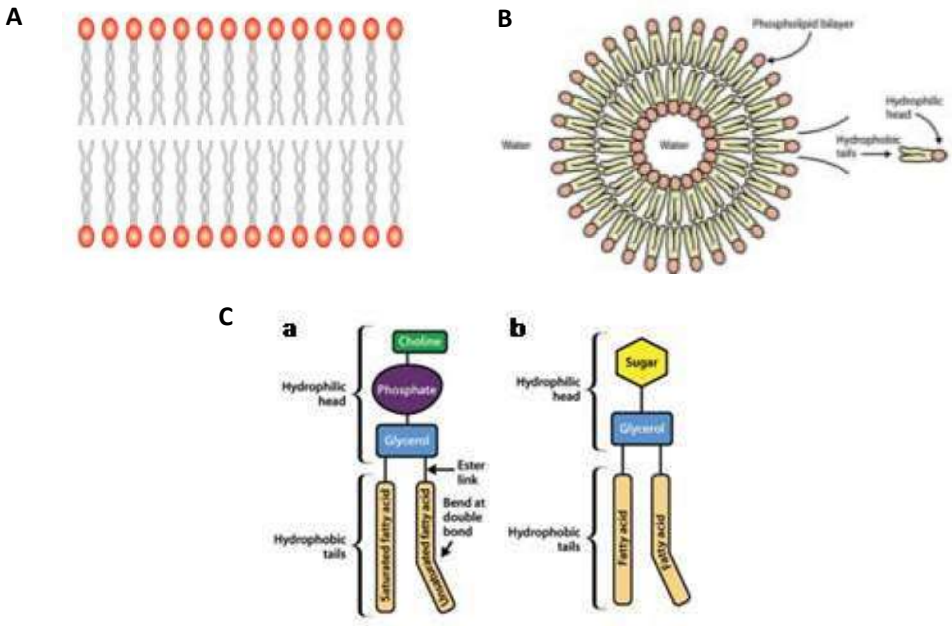


***Figure 5:*** *A and B: Self-assembled lipid bilayers A) Two monolayers or leaflets compose the 5-nm thick lipid bilayer. Hydrophilic heads (red circles) are in contact with aqueous medium and hydrophobic tails face each other, B) Liposome structure with a zoom on one phospholipid. C: Representations of three membrane lipids structure a) Phosphatidylcholine (PC) b) Glycolipid; sugar is a compound having the general formula: $(CH_2O)_n$ with n=3, 4, 5 or 6. Adapted from Watson et al., [10].*

Amphiphilic lipids are the fundamental building blocks of biological membrane bilayers. Regarding the chemical structure of their hydrophilic headgroup, neutral membrane lipids can be divided into two main classes. The first are lipids with a headgroup chemistry dominated by one large electric dipole, such as the most abundant phospholipid species phosphatidylcholine (PC). The second class involves lipids whose headgroups comprise multiple small electric dipoles, typically polar hydroxyl (OH) groups, such as glycolipids. In

nature, membranes in different cell compartments exhibit largely different lipid compositions. Highly dynamic and loosely packed membrane systems, for instance the endoplasmic reticulum or Golgi membranes, which belong to a network of endomembrane compartments all connected via vesicle budding and fusion, are rich in PC lipids. In contrast, structurally more steady and densely packed multilamellar membrane systems, such as myelin sheaths in vertebrates and the photosynthetic membranes (or thylakoids) in plants, exhibit high contents in glycolipids displaying multiple OH groups[11] (Figure 5C).

The main feature of lipids is their insolubility in water and their solubility in organic solvents (type of chemicals vaporizing at room temperature). In water, they form a surface film (monolayer with hydrophilic head in contact with water surface and hydrophobic tails in contact with air) or liposomes. Liposomes, also called micelles, are spheres with lipid bilayers separating two water compartments (Figure 5B).

Commercial lipid nomenclature is usually composed of four or more letters. The two last letters indicate the headgroup e.g. PC phosphatidylcholine, PE phosphatidylethanolamine, PG phosphatidylglycerol and the first ones are related to the nature of fatty acid of the tail e.g. : P : palmitic acid (C16 :0), O : oleic acid (C18 :1), S : stearic acid (C18 :0), M :myristic acid (C14 :0), L : Lauric acid (C12 :0), except for D meaning di- (two fatty acids). For example, DPPC has two palmitic acid in his tail (2x16:0). In general, the ":" symbol indicates the position of the double bond.

Thanks to the crucial role of lipid bilayer in ensuring cell communication with the extracellular environment and its contribution to various cell signaling, its structural and mechanical properties have been widely studied through different characterization techniques.

## 2. Lipid deposition methods

To be able to characterize them, lipids are deposited on a support using different methods. The most used methods: **drop casting, spin coating, Langmuir Blodgett deposition and vesicle fusion** are described in this section.

### 2.1. Drop casting or painting method

Drop casting consists in pipetting small volumes of lipids dissolved in organic solvent (eg. Methanol $CH_3OH$/chloroform $CHCl_3$ mixture) onto the target support. After solvent evaporation, also referred as to thinning process, and thanks to lipid self-assembly, bilayers are formed. When deposited on the support, lipids expand over a defined area (depending on the support total area and the lipid volume) and after solvent drying, the substrate is covered by a thin membrane. This method can be performed in air or in aqueous solution as reported by Lauger et al., [12]. Usually, syringes or pipettes are used to inject lipid solutions. However, other alternatives, like lipid deposition using a paint brush are also reported[13]. Substrates can be chemically functionalized to facilitate lipid adsorption on them. This easy lipid spreading technique has proven to be attractive for lipid structural studies as it allows efficient lipid bilayer packing reaching up 1000 bilayers[14]. Stacking lipid architectures are crucial in some biological membranes such as the thylakoid membrane of plant chloroplast.

A similar deposition technique with well-controlled bilayer number is spin coating

### 2.2. Spin coating

Although spin coating was a well-established technique for inorganic thin film deposition since the eighties, its first use for lipid deposition dates back only to 2002 (Mennicke et al., [14]). Using a spin coater, lipids dissolved in organic solvent are pipetted onto a cleaned rotating substrate (Figure 6c). During the first slower step of this process, lipid solution covers the support surface homogenously. The second step allows solvent drying by quickly rotating the substrate. Further sample exposition to vacuum can be performed to make sure all solvent traces are removed. Furthermore, the dry lipid layer can be hydrated with the appropriate buffer if needed.
Spin coated lipids are characterized by high homogeneity and well-controlled film thickness. Solvent choice is reported to have great influence on the final sample microscale homogeneity. Both lipid and substrate nature should be considered before choosing it. Indeed, the solubility of some lipids is higher in specific solvents compared to others. For example, chloroform ($CHCl_3$) is a suitable solvent for some lipids and propanol ($C_3H_8O$) is preferred for others [14]. For a better surface coverage, solvent and support should also have the same wettability properties; hydrophobic solvent for hydrophobic substrate and hydrophilic solvent for hydrophilic support.
Apart from film thickness, lipid bilayer lateral pressure can be further controlled thanks to Langmuir-Blodgett (LB) method.

### 2.3. Langmuir-Blodgett (LB) transfer

Langmuir-Blodgett (LB) technique is based on the transfer of lipid molecules from a water-air interface to a solid support (Figure 6). First, the substrate is immersed at controlled speed vertically to a lipid monolayer formed at the air-water interface on the Teflon-coated trough of the LB apparatus. A magnetic balance records the surface pressure and allows controlling it during support immersion to monitor lipid packing. Two mobile Teflon barriers (represented by black small rectangles close to lipids on figure 6b) are used to vary the area available for lipid monolayer spreading. Dipping the substrate vertically a second time results in the transfer of a second monolayer and a lipid bilayer is formed on each side of the solid support (Figure 6b). A horizontal immersion of the substrate is also possible and is called Langmuir-Schaefer (LS) transfer. Multiple substrate immersions lead to lipid multilayer formation and therefore, control the film thickness.

The originality of LB deposited lipids resides in their possible asymmetry, i.e., the monolayers can have different lipid compositions. Asymmetric synthetic lipid bilayers better mimic biomembrane leaflets reported to be composed of different lipids. Defect density of the final film is function of surface pressure and substrate lifting speed which should be carefully controlled. Besides, the second monolayer transfer should be quick enough to not alter the diffusion properties of the first monolayer deposited on the solid substrate. High dependency of film features on deposition parameters causes reproducibility problems of LB method decreasing its popularity compared to vesicle fusion deposition technique[15].

### 2.4. Liposome fusion method

Formation of lipid bilayers from liposome (or vesicle) fusion is the most popular lipid deposition method. A suspension of unilamellar vesicles is deposited on a flat substrate (Figure 6a). To prepare lipid vesicles, lipids are first dissolved in an organic solvent. Then, the solvent is totally dried under nitrogen or argon flow. Second, lipids are resuspended in an aqueous solution yielding a suspension of multilamellar vesicles. Sonicating or extruding the obtained vesicles form **unilamellar vesicles**. Sonication is particle agitation using ultrasonic (>20 kHz) frequencies whereas extrusion is a process to create objects with a well-defined cross section (Cf. Appendix D) for more details about liposome extrusion steps). The difference between multilamellar and unilamellar vesicles is the number of bilayers surrounding the liposome. For instance, the liposome of Figure 5B is a unilamellar lipid vesicle.

To distinguish between the two treatment methods, different abbreviations are used: SUVs to refer to small unilamellar vesicles or small sonicated unilamellar vesicles and EUVs for extruded unilamellar vesicles. Large unilamellar vesicles (LUVs) is also used for extruded vesicles to account for the bigger size of the latter vesicles[16], [17]. The vesicle fusion mechanism is not yet fully understood. However, it is known to be a multiple-step process starting with the adsorption of vesicles on the substrate and ending with vesicle rupture and formation of a continuous lipid layer. The adsorption-rupture transition can be direct or triggered by an intermediate step of vesicle fusion (as shown in figure B.1, Appendix B,). Different parameters related to lipid vesicles, physicochemical environment (pH, temperature, osmotic pressure..) and substrate properties influence the final layer structure. While the adsorption step is enhanced by lipids/support electrostatic interactions, vesicle fusion is dependent on vesicle size and rupture step depends on temperature and osmotic pressure[18].

Although vesicle fusion is a very simple deposition technique, reproducing biomembrane asymmetry is a difficult task requiring careful control of the deposition protocol[19].

As mentioned above, LB transfer and vesicle fusion are the two most reported methods for lipid bilayers deposited on solid supports. Their combination was also used[15] in an attempt to overcome each technique drawbacks. The different benefits and drawbacks of the described deposition methods are summarized in Table B.1., Appendix B.

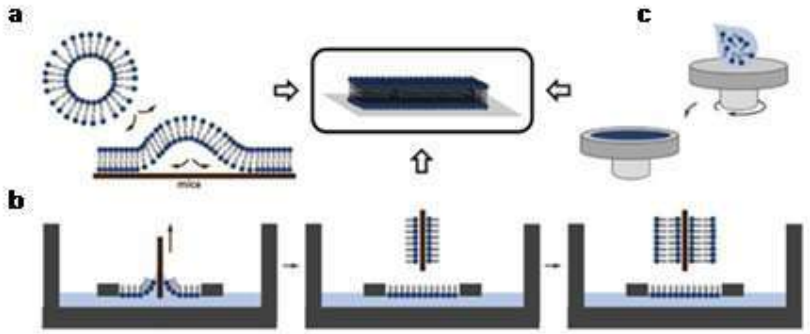

***Figure 6:*** *Different techniques to deposit lipid bilayers on solid substrates a) Liposome fusion method, b) Langmuir-Blodgett (LB) transfer technique c) Spin-coated lipid films. Adapted from Audenis et Giannotti, [20]*

Biomembrane organization study has been attracting researchers' attention for more than a decade now and a wide range of surface characterization techniques have been used for this purpose. Among them, atomic force microscopy (AFM) has been an essential tool to determine lipid bilayer organization at the nanoscale. Additionally, its ability to operate in liquid environment, without any sample fixation, has opened new opportunities to bilayer study under physiological conditions. Besides, it has shed light on membrane lipids' nanomechanical properties by enabling minimal force sensing (piconewton pN to nanonewton nN range). The following section is a summary of lipid structural and nanomechanical properties investigated by means of AFM.

## 3. Structural and mechanical properties characterization of membrane lipids with AFM

### 3.1. AFM imaging modes and AFM force spectroscopy (AFM-FS)

AFM is a scanning probe technique based on a cantilever tip scanning a sample surface while the sample/tip interaction forces are monitored using a feed-back control. Tip deflection is measured by a position-sensitive photo detector. AFM can operate in different modes which can be used for both imaging and force spectroscopy. In **contact mode**, the tip is continuously scanning the sample at a constant deflection (i.e. at constant tip applied force) and the piezo signal generates the scanned surface topography. In **tapping mode**, the cantilever is oscillating close to its resonant frequency and its amplitude and phase are monitored. Contact and tapping modes are usually used for **structural characterization** of lipid bilayers. Determination of mechanical properties is also possible with force spectroscopy experiments.

**AFM-FS and its based imaging modes**

In a standard force spectroscopy experiment, the tip moves downwards and upwards from the sample in cycles and the cantilever applied force, F, is recorded as function of **z-piezo displacement** $\Delta z$ or **tip-sample separation** $\Delta D$. $\Delta D$ is determined from $\Delta z$ using the relationship $\Delta D = \Delta z - \Delta d$ where $\Delta d$ is the cantilever deflection. Figure 7b is a typical force plot on supported lipid bilayer (SLB) with an approach (or approaching) curve (in red) and a retraction (or retracting) curve (in blue). When the cantilever is far from the sample, no interaction exists and no cantilever deflection is measured (Figure 7b. point A). The cantilever is brought closer to the surface and it starts feeling the long-range forces, mainly electrostatic and Van Der Waals forces (Figure 7b. point B). When the gradient of the force overcomes the cantilever spring constant, a jump-to contact is observed (Figure 7b. point C). After this point, increasing the pushing force causes the cantilever to bend upwards while staying in contact with the sample. It is the elastic regime. When the force reaches the critical yield value, the cantilever penetrates through the bilayer and a jump is visible on the approach curve (Figure 7b. point D). The critical yield force or yield threshold force ($F_y$) or

breakthrough force ($F_b$) or punch force is the maximum force the bilayer can withstand before breaking. Breakthrough event is the onset of plastic bilayer deformation. Further increase of the force at point D increases the cantilever deflection (Figure 7b. point E).

In the retraction curve, a hysteresis is observed due to **tip adhesion to the sample**. The tip bends downwards until reaching a critical adhesion force (Figure 7b. point F). After overcoming the adhesion force, the cantilever is completely detached from the sample (Figure 7b. point G).

Before plastic regime, a **variety of forces** contribute to each region of force plot. Figure 7c is a typical force plot on a DOPC lipid bilayer with the corresponding forces taking place in each regime. During approach, the cantilever probes the **long-range electrostatic forces** with lipids, in particular phospholipids as the majority of them are negatively charged. Then, it probes the **short-range hydration and steric forces**, reported to cause a short-range repulsion between two-opposing lipid bilayers[21]. Actually, this repulsion is related to the force required to remove water when both bilayers surfaces come into contact. At higher forces (in the range of nN), the bilayer is elastically deformed before being plastically deformed after its breakthrough.

Approach curve provides information about surface properties (derived from the different interaction forces), sample elasticity (measured from its slope) and sample breakthrough force $F_b$. Retraction curve is used to estimate the adhesion force $F_{adh}$ (or pull-off force) from its minimal value. $F_b$ is the most used FS parameter because it is a fingerprint of the sample translating its mechanical stability. FS quantitative measurements have been reported to complement topographical studies in setting an upper limit to the working set point force applied to the bilayer. In other words, applying a force higher than $F_b$ is highly probable to damage the sample and to decrease therefore image resolution. This complementarity has been enhanced with the use of **FS-based imaging modes** which, simultaneously, scan the sample and record its force distance curves over large areas compared to standard FS conventional measurements. **Force volume mode (FV) (or force mapping mode)**, for instance, saves force curves at each pixel of AFM image. It provides force density maps (e.g. $F_b$ and $F_{adh}$ maps) where topography features are correlated to force measurements. Yet, its slow acquisition time affects the lateral resolution of AFM images. To overcome this disadvantage, **Peak Force Quantitative Nanomechanical Mapping or Peak Force Quantitative Nano-Mechanics (PFQNM)** was developed. In PFQNM, the sample is imaged while its nanomechanical mapping is performed at high resolution. The tip is oscillating at a given frequency and amplitude in z axis and cycles of force curves are recorded. After further curve analysis, mechanical parameters (Young's modulus, deformation, adhesion and dissipation energy) are fitted and matched simultaneously with sample topography. The strength of this mode is the possibility it offers to understand the relationship between the structure and mechanics of scanned samples.

Other FS-based imaging modes were also implemented to deepen into nanomechanical characterization, from which we can cite pulsed force mode (PFM)[22], force modulation to extract viscoelastic properties[15] and force clamp (FC) mode to follow the kinetics of puncture events[20].

Table B.2. in Appendix B summarizes the advantages and disadvantages of **FV, PFM and PFQNM**.

As for biomembrane research, many studies have reported the importance of AFM force spectroscopy (AFM-FS) to understand membrane nanomechanics "within the nanometer realm" (Manyes et al.,[21]) after the publication of the pioneering work of Dufrêneet al.[23] (1999) in this field.

Practically, before performing AFM experiments, lipids are deposited on substrates applying one of the methods detailed in the previous section (cf. **II. Lipid deposition methods**). Depending on the support nature, we distinguish between **supported lipid bilayers (SLBs)** if lipids are deposited on bulk substrates and **pore-spanning bilayers (PSBs)** when lipids are deposited on porous supports. SLB and PSB are two models meant to synthetically model biomembranes.

In the following, **sections 3.2. and 3.3.**deal with **SLBs'** properties while **3.4. and 3.5.**are about **PSBs**. The sixth section explains the effect of different AFM imaging parameters on scan results. It concerns both models.

To avoid repetition, **model 1** and **model 2** can be used to refer to **SLBs** and **PSBs**, respectively. It is worth to note that, in literature, PSBs can refer to polymer supported bilayers (Picas et al.[15], 2012) which are out of the scope of this chapter. Moreover, to avoid making the text more cumbersome, only lipid name abbreviations are used in the reported examples (e.g. PC instead of phosphatidylcholine). Lipid full names are found in list of abbreviations.

**N.B.** In the following text, AFM cantilever and AFM tip /probe refer to the same thing. It is a name "confusion" tolerated in AFM community. But, in reality, the tip is the cantilever part scanning the sample and the cantilever is the substrate to which it is attached.

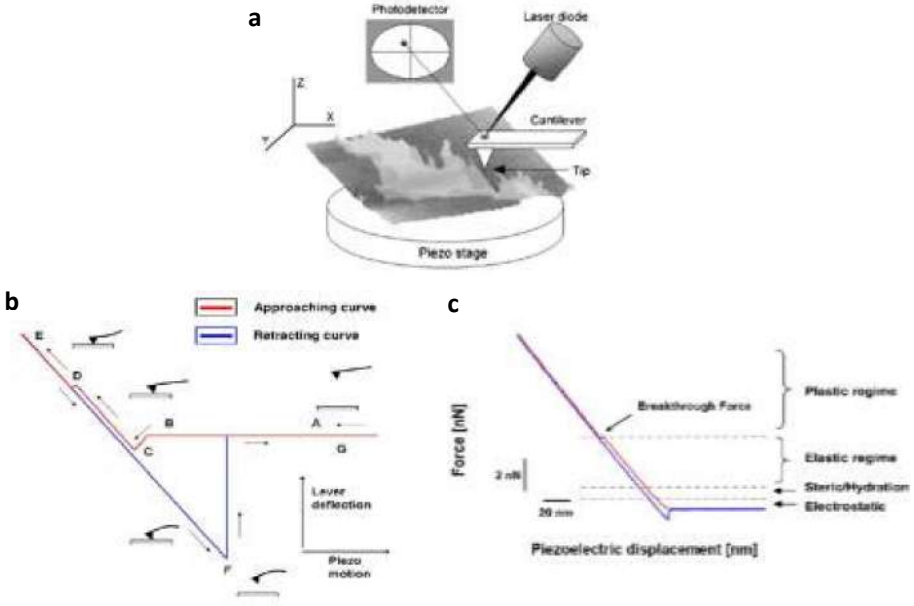

***Figure 7:****a) AFM experimental setup b and c: Force curves on supported lipid bilayers b) Theoretical force plot with the different parts denoted with capital letters (from A to G) and the corresponding cantilever/sample system represented close to each letter. c) Force curves on a DOPC lipid bilayer with the different forces, contributing to each regime, denoted on the right of the scheme. For both plots, cantilever force (lever deflection) is represented as function of the piezo displacement. Adapted from Manyes et al.[21]*

### 3.2. Structural properties of SLBs

AFM has been extensively used for structural characterization of supported lipid bilayers (SLBs). The majority of reported studies used phospholipid bilayers, due to their ability to reproduce biomembrane properties in vivo and their commercial availability.

#### 3.2.1. Study of SLB formation

Stages of SLB formation have been studied as a function of various sample parameters such as lipid concentration[23], and vesicle size and charge for vesicle fusion method[16]. Indeed, electrostatic interaction between the liposomes and the substrate is known to be a key parameter in bilayer formation from the latter method. Besides, SLBs' thicknesses have been estimated using height profiles[23], [24]. For example, Attwood et al.[23] reported a thickness of **5 nm for DOPC bilayer**; which is in agreement with biomembrane thickness.

#### 3.2.2. Study of binary and ternary lipid mixtures

Lateral resolution of AFM has enabled to image and distinguish between different phases (e.g. solid-like gel phase/ fluid phase) coexisting in the same bilayer when several lipids with different fusion temperatures $T_m$ are used and imaged at room temperature[25],[26]. Figure 9 shows the structure of POPE/ POPG mixture.

Imaging binary mixtures containing cholesterol (Chol) has helped researchers to gain insight into the Chol role in SLBs. Cholesterol is a fundamental component of animal eukaryotic cells and is known to form, together with sphingolipids (SLs), nanoscale lateral domains in the cell membrane; called membrane rafts. SLs are lipids based on sphingosine (instead of glycerol). Many articles have highlighted SLB condensing effect of Chol and its enhancing of lipid ordering[22], [27-29]. For example, roughness measurement was recently reported to be decreased by two times after addition of 25 mol % to DPPC/DOPC mixture[29]. Nevertheless, this packing effect depends on SLB chemical composition and on Chol added contents. In fact, Chol dissolves in fluid-like lipids forming an homogenous phase with other lipids, however it can induce a phase heterogeneity when added at specific amounts to gel-phase lipids (e.g. when added at molar fraction below 30 mol % as reported for DPPC[27]).

More complex mixtures containing Chol, phospholipids and SLs, in particular, sphingomyelin (SM) and/or Ceramide (Cer) have been studied[22], [27], [28] and the joint role of Chol and SLs in the organization of phospholipids has been proved.

#### 3.2.3. Influence of substrate roughness on SLB

Although most reported SLB structural characterization were performed on mica substrate, other materials were used as supports to study the substrate effect on lipid bilayers. Increasing support heterogeneity results in loss of bilayer homogeneity. Comparing SLBs

deposited on mica with those deposited on a polymer cushion (polyelectrolyte multilayer, PEM), Dante et al.[30] reported a rather homogenous bilayer on mica (apart from some defects; black regions on figure 8A) and a less-defined SLB topography for PEM (Figure 8B). This was explained by the increased roughness of PEM compared to the atomically flat mica surface. On the other hand, no influence of the substrate on the SLB thickness was reported[24].

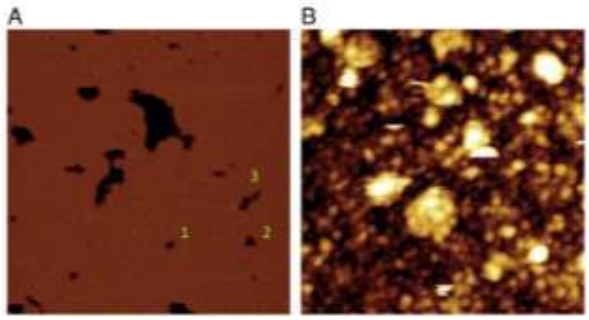


***Figure 8:*** *Substrate effect on supported lipid bilayer topography A) Topographical image of POPC/POPS SLB adsorbed on mica, B) Topographical image of POPC/POPS SLB adsorbed on polymer cushion (PEM). Data scale of A and B: 1µm, z-range = 4.8nm for A and z-range = 14.3nm for B Images were obtained in tapping mode in liquid environment. Adapted from Dante et al. [30]*

### 3.3. Mechanical properties of SLBs

#### 3.3.1. FS as a tool to determine SLB thickness

Breakthrough events on SLB are characterized by a nanometric jump used to measure the bilayer thickness. A thickness ranging between 4 nm and 5 nm was reported in numerous articles, confirming results of AFM topography study and of other analytical surface techniques[21], [23]. When bilayer structure is not well defined (e.g. for rough substrates), it induces uncertainty in height estimation from topographic images. Therefore, AFM-FS measurements can be used as alternatives to overcome this uncertainty[24].

#### 3.3.2. Influence of lipid nature on SLB stability

Lipid nature has a great impact on punch forces[16], [20]. The large range of $F_b$ from several nN (e.g. 3 nN for DPPA[16]) to several tens of nN (e.g. 66nN for DPPC[16]) illustrates the effect of lipid headgroup on the mechanical properties of SLBs. The number of carbon atoms in the lipid tail and the number of unsaturation are also reported to strongly influence the mechanical stability of SLBs [16]. FS has allowed to probe the differences in the mechanical properties between coexisting phases [31].

#### 3.3.3. Influence of cholesterol on lipid stability

AFM-FS has proved the stabilizing effect of cholesterol on lipid bilayers through increase in $F_b$ upon addition of Chol to SLBs[16], [22]. Morandat et al.[16] reported alinear increase of $F_b$with a rate of 0.13 nN and of 0.62 nN per molar percent of Chol (mol %) added to fluid DLPC and gel DPPC, respectively. The increase in mechanical resistance to indentation of Chol/lipid mixtures is, however, dependent on lipid composition and on cholesterol content. In the case of DOPC, $F_b$ is reported to remain approximately constant (in the range of 10 nN – 17 nN) for Chol contents below 50 mol % but increases about 3 times for a Chol amount of

50 mol %, whereas for DLPC SLBs, yield forces linearly increase with progressive addition of Chol (up to 50 mol %)[27].

### 3.3.4. Influence of substrate on $F_b$

The effect of the underlying substrate on SLB structure is accompanied by a variation in the bilayer's mechanical properties, as well. Taking the above mentioned example of POPC (single) and POPC/POPS (binary) SLBs deposited on mica and on polymer cushion (PEM), force mapping reveal a **unimodal distribution** of breakthrough force for both single and binary SLBs deposited on **mica** and a **bimodal distribution** for SLBs on PEM[16],[24]. Quantitatively, the Gaussian fit of the unimodal distribution is centered at 6nN independently from the SLB composition and those of bimodal distributions are centered at 2.3nN and 5.6nN for POPC and 2.2nN and 5.9nN for POPC/POPS[24]. Bilayer heterogeneity explains the two $F_b$ values obtained for SLBs deposited on PEM. This heterogeneity is confirmed by force curves, presenting double breakthrough events for SLB regions on which a double more fluid bilayer is formed on top of the one in contact with the substrate.[24]

### 3.3.5. Adhesion forces

Adhesion force $F_{adh}$, pull-off force or snap-off peak is the minimal value of the retraction force curve. Contrary to breakthrough force $F_{b,}$ which is an intrinsic property of lipid bilayers, adhesion force is highly dependent on tip/sample interaction parameters such as contact area, contact time and tip penetration in the sample and AFM scanning conditions[32].

Owing to the tip/sample interaction nature, $F_{adh,}$ the latter parameter is strongly influenced by local surface properties changes. Therefore, it is necessary to compare adhesion data with topographical images since adhesion contrast differences can be either related to a material change (e.g. a bilayer defect[24], [31]) or to a geometric effect.

Lipid phase is another factor inducing difference in adhesion force values: Gel (i.e. highly packed) phase is characterized by lower adhesion compared to liquid phase[26], [31], [33], [34]. Representative force curves for both fluid and gel phase of POPE: POPG mixture are shown in Figure 9

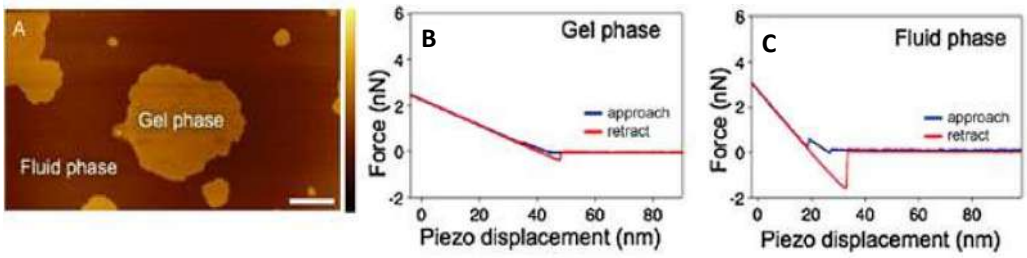


***Figure 9**:Topography and force curves on POPE: POPG (3:1, mol:mol) SLBs A) Topography image showing phase coexistence (fluid/gel) in POPE/ POPG mixture. Color scale is 15nm and bar scale is 5µm. B) andC) Force-piezo displacement plots obtained on gel and fluid phase, respectively. Difference in breakthrough and adhesion forces between both phases is visible. Adapted from Picas et al. (2009) [26].*

Further, tip/sample interaction varies with the scanning medium. Due to the presence of capillary force, adhesion force are higher when scanning in air than when scanning in solution (water or buffer). Indeed, in air, samples are covered with water molecules forming the so-called water meniscus, responsible for the extra force (capillary force) that should be overcome to withdraw tip from the surface. Briefly, adhesion force cannot be understood as an absolute value but rather than the result of interaction of a **specific tip** with a **specific sample** scanned **under specific conditions.**

Despite the fact that SLBs have brought new insights into the study of both structural and mechanical properties of lipid bilayers, they do not perfectly mimic biological membrane. In fact, in biomembranes, lipids can diffuse laterally whereas, in synthetic SLBs, this diffusion is hindered by the presence of the substrate. This is what pushed researchers to build alternative membrane models in the direction of better mimicking biosystems. From these models, we will focus on pore-spanning lipids, subject of the following sections. The examples reported below are extracted from Steltenkamp et al.[35] and Mey et al.[13]

### 3.4. Structural properties of PSBs

Pore-spanning bilayers (PSB), free standing lipid bilayers or lipid membranes denote lipids deposited on porous substrates. PSBs were introduced in 2000[36] as a membrane model to overcome the lack of fluidity of SLBs. In reality, the nanometric water layer reported to be present between lipids and substrate for SLBs[8],[16] was not sufficient to faithfully mimic this fluidity in vitro.
Different parameters have been reported to influence the structure of lipid membranes.

#### 3.4.1. Effect of deposition method and surface functionalization on PSBs

Pore-spanning lipids cover holes or pores introduced in substrates by chemical (reducing agent) treatment or classical cleanroom processes. For example, oxalic acid ($C_2H_2O_4$) was used by Steltenkamp et al.[35] to create pores in alumina ($Al_2O_3$) substrate.

Because of the substrate geometry specificity, compared to bulk supports, the influence of both the deposition method and the substrate surface functionalization and wettability is higher for PSBs than for SLBs.

Mey et al.[13] reported a difference in lipid (DPPC and DPhPC) conformation between solvent-free “supported bilayers” (Figure 10a) and solvent-containing lipid membranes (Figure 10b) deposited on porous silicon. Solvent-free bilayers are prepared by the spreading of giant liposomes on hydrophilic porous silicon and show a **planar structure** with no lipid coating on the nanopore lateral walls, as depicted in the zoomed view of figure 10a. Nevertheless, solvent-containing lipids are deposited via painting method, using a paint brush, on golden-coated substrate functionalized with hydrophobic self-assembled layers of octanethiol (OT) or cholesterylpolyethylenoxythiol (CPEO3). The second type of lipids form a freestanding membrane with nanopore rim coatings. The difference between both conformations is reported to be correlated with each lipid membrane mechanics (Cf. 3.5.Mechanical properties of PSBs)

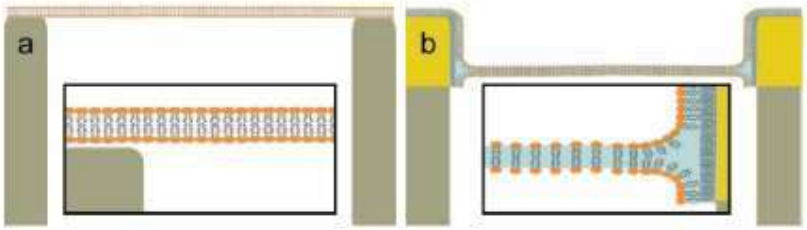


***Figure 10:*** *Schematic representations of different lipid bilayers' conformation inside a pore. a) Solvent-free planar bilayers deposited on hydrophilic porous silicon substrate, b) Solvent-containing pore-spanning bilayer deposited onto functionalized porous silicon (pSi) support. The yellow color on the nanopore rims represents the gold layer deposited on pSi. Before lipid painting, a hydrophobic monolayer of OT or CPEO3 was self-assembled on pSi, as well. Adapted from Mey et al.[13]*

Besides, "nearly planar" pore-spanning bilayers attached to nanopore rims of porous alumina are also reported[35].

### 3.4.2. AFM topography of Covered/uncovered pores

AFM images have allowed to distinguish between **lipid-covered** and **lipid-uncovered** nanopores through topography contrast: darker contrast is observed for uncovered nanopores[35] (Figure 11). Height profiles have also confirmed this nanopore classification as tip penetration in a covered nanopore (70 nm) is reported to be more than 4 times smaller than that in an uncovered pore (300 nm) at a load force of 300 pN. These values are reported for 400-sized nanopores [13]. For pore-spanning lipids, uncovered pores are considered as reference for the covered ones highlighting the importance of relative height or depth in these measurements. In general, tip penetration inside a nanopore is function of the tip geometry and the pore size (i.e. diameter). The first trivial condition is that the tip should have a radius smaller than the nanopore diameter to be able to enter it. This parameter dependence highlights the importance of a complete reporting of all AFM imaging parameters to be able to extract significant conclusions especially when scanning non-planar geometries like nanopores. With a 15-25 tip size, the tip indentation depth is 400 nm for pores with a diameter of 225 nm a 550 nm for pores with a diameter of 400 nm[13].

Moreover, different tip penetration depths are reported with **two different cantilevers** used to scan 90 nm-sized alumina nanopores[35]. **Scan direction** has also an effect on the shape of nanopore symmetry displayed on AFM images or determined from height profiles. Otherwise stated, two types of interactions should be considered for nanopores when they are scanned: tip/nanopore center interaction and tip side/nanopore wall interaction (lateral interaction). The lateral interaction of an AFM tip with bilayers coating the rim of a 90-nm sized nanopore results in an asymmetry in the nanopore shape[35] as shown in figure 11C (second nanopore of the dashed line profile).

### 3.4.3. Influence of force set point on suspended lipid bilayers

Scanning force set point or the force applied during sample scanning is another parameter affecting the nanopore topography, particularly when imaging in contact mode. Thus, a first scan at low force (hundreds of piconewtons) is preferred to assess the capacity of lipid membranes to withstand tip contact. Increasing the force set point may break freestanding

lipid bilayers increasing, therefore, the number of uncovered nanopores. For example, imaging alumina 33 nm-sized nanopores at higher set point (2.7nN) breaks the bilayer inside them (Figure11B), which is not observed for imaging at 0.9 nN (Figure 11A) [36].

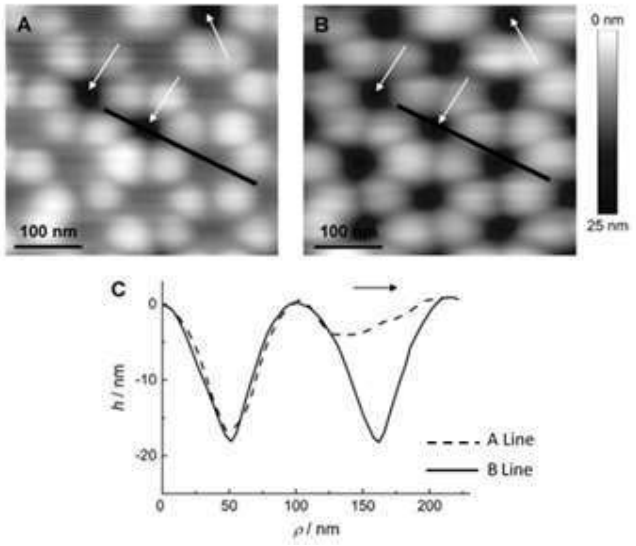


***Figure 11:*** *Effect of load force increase on pore-spanning bilayersA) Topographic images of alumina nanopores covered with positively charged lipid bilayer imaged at low force set point (0.9 nN). Nanopores with darker contrast indicated by white arrows are uncovered with lipids, B) AFM topography of the same region imaged at higher force (2.7 nN)C)Height profiles along A) nanopores in dashed line and along B) nanopores in solid line. The legend on the bottom right is added to the original image. The scan direction is from left to right as indicated by the black arrow. Nanopores have a 33-nm diameter. AFM contact mode in aqueous solution was used. Adapted from Steltenkamp et al.[36]*

Not only the structure of lipid membrane is different from that of SLB but also their nanomechanical features.

### 3.5. Mechanical properties of PSBs

It is worth mentioning that the originality of model 2 resides in the opportunity it offers to study lipid bilayer **bending and stretching**, not possible with model 1. With SLB, only compression can be studied and the elastic response of the bilayer is usually linked to the substrate properties. Table III in Appendix B summarizes the differences between both models. The substrate effect between the two models was quantified by Nussio et al.[37] through variation in breakthrough forces of DMPC and DPPC bilayers from porous silicon to bulk silicon: a 2.5-fold increase in $F_b$ was reported when lipids were deposited on Si compared to pSi case.

#### 3.5.1. Influence of the point in which the force spectroscopy experiments are performed

Contrary to model 1, for which force spectroscopy measurements are independent on the scanned lipid region, FS for model 2 are highly dependent on the nanopore part where indentation experiments are performed. When the tip force is applied on the nanopore center, a fully elastic response represented by a continuous diagonal line in force curves is

reported [13], [36]. However, an infinite repulsion at maximum tip penetration, shown through a vertical line in the force curve (red line in figure 12b), is observed for tip indentation on nanopore rim. Practically, force measurements are conducted for both nanopore rim and center and the depth of jump-to contact point in the nanopore rim's force plot is extracted. It is the relative zero used to measure lipid bilayer thickness as the bilayer extension starts from this point.

Additionally, the bilayer rigidity is reported to be higher when the tip indents it near the nanopore rim [34]. In this example, bilayer rigidity is assessed from its apparent spring constant i.e. from the linear part slope of its force curve.

### 3.5.2. Complexity of force curves interpretation

Taking into account lipid conformations inside nanopores, explanation of FS force curves is not straightforward.

**Different scenarios of membrane rupture [13]**

As for model 1, when the force applied to the lipid bilayer is higher than its $F_b$, a rupture is observed via the sudden jump in force approach curve. Figure 12a is an example of force curve, recorded at a nanopore center, showing a single bilayer breakthrough event. Multiple ruptures are also reported for PSBs (Figure 12b). This unusual aspect is attributed to incomplete breakthrough events or partial breakthrough for which just a bilayer part is broken.

Different scenarios (Figure 13) can be envisioned to explain lipid membrane rupture. A first scenario (Figure 13c and 13d) is **local bilayer break**. The tip can exercise a local force on lipids resulting in a pore formation in the tip/sample contact area. Growing progressively with the force application, the pore can reach a critical radius at which the bilayer destructs locally. If the rupture is expected to be close to tip/bilayer contact region in the first scenario, the second one hypothesizes a rupture away from it (Figure 13e). This highlights the stochastic nature of this event. A third scenario (Figure 13f) focuses on the tip effect; if an imperfect tip indents the bilayer forming a small membrane hole. The fourth scenario is the simplest one with a total rupture of the lipid membrane. As a result, the cantilever relaxes and hits the nanopore wall below the surface (the end of the porous part).

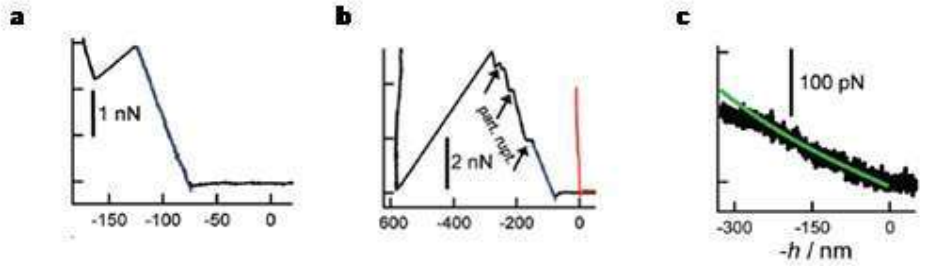


*Figure 12: Force indentation curves of various pore-spanning lipid bilayers on porous silicona) Force curve obtained at a nanopore center of a DPhPC bilayer deposited on a self-assembled OT monolayer on a 225nm-sized nanopore. A single rupture event is recognized, b) Force curves of the same lipid bilayer deposited on a larger nanopore (600-nm sized). Partial rupture events are indicated by the arrows. The black curve is the one obtained at the nanopore center and the red one at the nanopore rim, c) Black curve:*

*force curve of a solvent-free lipid bilayer (prepared from GUVs) deposited on a 250-nm sized nanopore of a hydrophilic pSi. The green curve is a theoretical curve fit. Adapted from Mey et al.[13]*

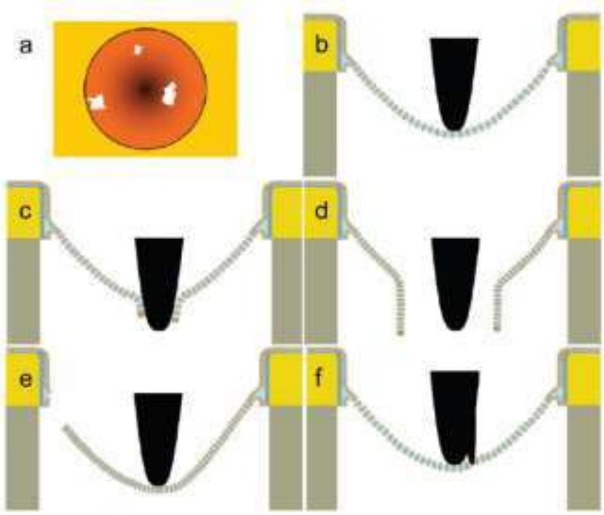


***Figure 13:*** *Illustration of possible scenarios conceivable for lipid membrane rupture inside a nanopore.a) Top view of a pore-spanning bilayer with a local rupture. b) Lateral view of the tip indenting the freestanding lipid bilayer c) and d) First scenario ; local bilayer rupture after a pore is formed in its center e) Second scenario ; stochastic rupture event; away from tip/bilayer contact f) Third scenario ; partial breakthrough caused by a tip inhomogeneity (Double tip example is depicted here). Adapted from Mey et al. [13]*

### 3.5.3. Influence of the tip size

Larger forces need to be applied to larger tips to achieve the same penetration in the same nanopore. This is reported by Steltenkamp et al [36]. As a consequence, higher rupture forces are recorded with larger tips.

### 3.5.4. Lipid membrane rigidity

Lipid rigidity can be either evaluated either from the max force the lipid can withstand or from the apparent spring constant (as explained above). It is influenced by lipid conformation inside nanopores and by nanopore size.

#### 3.5.4.1. Influence of lipid conformation inside nanopores

Planar lipid conformation inside nanopores (Figure 10a) is reported to be more stable than freestanding bilayers (Figure 10b). This comparison is similar to the one between SLBs and PSBs; SLBs are known to be more stable than PSBs. Stability difference is assessed from force curves; a rupture event is observed for solvent-containing freestanding lipid bilayers (Figure 15a) and not for solvent-free planar bilayers of DPhPC and DPPC (Figure 12c) [13].

#### 3.5.4.2. Influence of nanopore size on PSB rigidity

Lipid bilayer rigidity is reported to be inversely proportional to nanopore diameter. Quantitatively, a 1.4-fold increase in the bilayer apparent spring constant is observed when comparing lipids deposited in a 33-nm sized nanopore to PSBs inside a 90-nm sized one (Steltenkamp et al.) [36].

#### 3.5.4.3. Influence of the surface functionalization on the mechanical parameters

Different behaviors dominate the mechanical response of PSBs as function of the surface functionalization of the substrate they rest on. Prestress dominates the response of hybrid bilayers deposited on a functionalized substrate. Prestress is a homogenous tension applied laterally on PSB by a self-assembled OT layer, for instance[13]. This lateral tension results in a freestanding membrane with lateral coatings. On the other hand, lateral tension and bending govern the mechanics of bilayers deposited on a non-functionalized surface.[13]

### 3.5.5. Adhesion forces

Adhesion force between tip and PSBs is reported to be of electrostatic nature. This is the case of(positively charged lipids) for which an electrostatic attraction with the negatively-charged SiN tip is observed[36].Furthermore, lateral interaction of the tip with the inner nanopore wall is also reported to be at the origin of a second snap-off peak[36].

## 3.6. Influence of AFM scanning parameters and conditions on lipid scanning

Both structural and mechanical data of scanned lipids can be affected by various scanning conditions.

### 3.6.1. Tip influence

#### 3.6.1.1. Tip choice

Since the tip is the AFM part in contact with the sample, any change in its surface properties or shape highly affects the quality of the scan. First, depending on the purpose of the AFM experiment (imaging or indentation) and on the nature of the sample to scan, the tip should be carefully chosen. For example, stiffer tips are required to indent stiffer lipid phases. In this context, Steltenkamp et al.[36] reported the use of two different cantilevers with different spring constants to indent gel-phase and fluid-phase lipids.

#### 3.6.1.2. Tip contamination

Owing to the fluid nature of lipids, these molecules can be adsorbed on the tip apex causing “tip contamination”. As a result, a loss of contrast on topography images is observed, leading to inconsistent interpretations. As for AFM-FS, force curves recorded with a contaminated tip reveal two breakthrough events; one of the tip bilayer and one of the support bilayer[21],[25]. Due to “sticky tip”, FS experiments are reported impossible to conduct in some cases (which is not the case for imaging) [22].

### 3.6.2. Scan duration and multiple scan effects

During a long continuous scan, lipids can be removed by the tip[32], [38]. Recently, Jiang et al.[38] reported the removal of DLPC/DSPC SLB domains (Figure14).Scanning a fluid phase bilayer more than one time enhances its adhesion to the tip and favors tip gathering effects. That is to say, the tip can contribute to lipid spreading through enlarging lipid patches[23].

Lipid rupture of pore-spanning bilayers can be another effect of multiple scan even at low load force (Figure 14), as reported by Mey et al.[13]

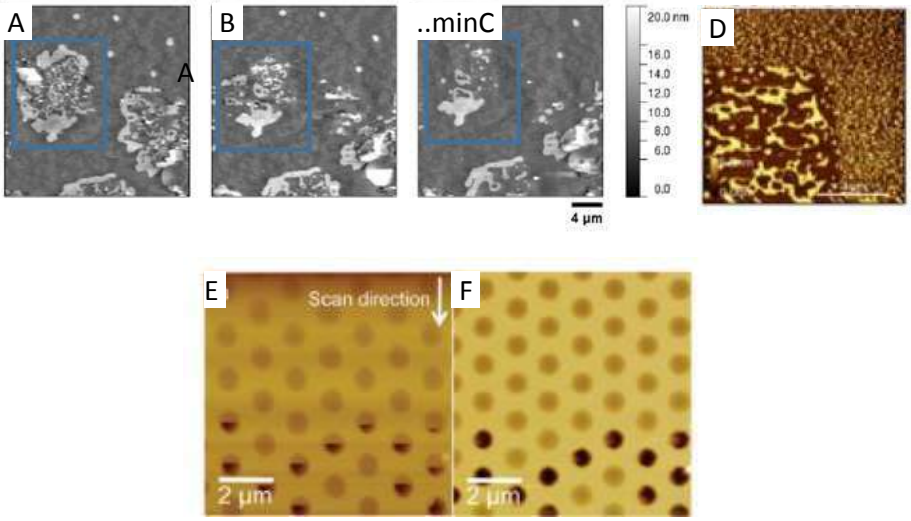


***Figure 14:*** *Multiple scan effects on SLBs and PSBsA, B and C: Successive topographic images of continuous scan of DLPC/DSPC supported lipid bilayers deposited on glass. Bright domains are progressively removed from A to C. Images were obtained in light tapping mode under aqueous immersion conditions. Adapted from Jiang et al [39] D)Topographical image of DOPC bilayers on mica. The image shows a corner at the boundary between a previously scanned region (big lipid patches, bottom left) and region scanned once (small patches). Lipids were imaged in pure water. Z-range: 5 nm and scale bar = 4 µm. Adapted from Attwood et al.[23]E and F: are topography images of DPhPC/DPPC pore-spanning bilayers deposited on 400-nm sized nanopores of silicon. A first scan of the region (E) shows rupture of PSB (dark aspect) in some nanopores whereas second scan (F) displays "open pores pattern" of the same nanopores (total rupture of PSB inside them). E and F were obtained in contact mode at a load force of 300 pN. Adapted from Mey et al.[13]*

### 3.6.3. Effect of applied force

During AFM scanning, the load force, F should not be too low so as to enhance tip tracking across the sample, especially for vesicle fusion bilayers. In fact, partially fused vesicles or vesicles trapped between two planar ruptured domains maintain partially their round shape rendering the bilayer surface not easy to scan. Hence, the need for a good tip tracking. This force should not be too high, neither to avoid sample damage [23].F value should also be considered when measuring bilayer thickness [23], [24]: a high value induces sample compression and as a consequence, the height is underestimated and for a low value, the contribution of long-range repulsion forces results in an overestimation of the measurement.

Therefore, for a good scan quality, AFM experiments should be well designed.

In a nutshell, AFM has proven to be a powerful tool well-suited to characterize structure and nanomechanics of lipids deposited on different types of supports (bulk and porous substrates)

## III. Characterization of lipids deposited on SiNnanoporous membranes

In order to characterize lipid deposited on SiN nanoporous membranes, first, two plant lipids were extracted from Arabidopsis thaliana leaves. Arabidopsis is a plant model commonly used in plant biology studies. Second, lipids were prepared and deposited on SiN membranes using different methods and then, the pore-spanning lipid bilayers were characterized by different microscopy techniques: fluorescence microscopy, transmission electron microscopy (TEM) and atomic force microscopy (AFM).

### 1. The used lipids

Two glycerol lipids were tested: PC and DGDG. Figure 15 is sketch of these two lipids highlighting their main difference: head polarity. In fact, phosphatidylcholine (PC) has a polar head whereas digalactosyldiacylglycerol (DGDG) is a neutral lipid specific of plant membrane. The lipid extraction protocol is found in Appendix C

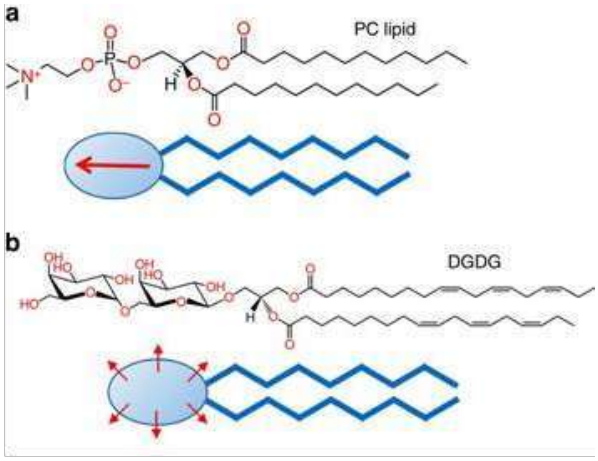


***Figure 15:*** *Structure of plant used lipids showing their head polarity a) PC structure b) DGDG structure*

DGDG neutrality makes it well-suited for future incorporation of charged molecules, like DNA, in hybrid biomimetic membranes. In fact, for example, in the case of DNA, repulsion between DGDG and DNA is reduced and DNA can be better incorporated in the membrane for the long termobjective of the project (water filter fabrication).However, the majority of experiments used PC lipids.

### 2. SiN membranes

The used nanoporous membranes were bought from an electron microscopy grid supplier.

They are 3-mm TEM grids with a 200-nm thick nanoporousSiN membrane deposited by low pressure chemical vapor deposition(LPCVD) on a 200-µm thick bulk Si. On the SiN membrane, an array of more than $10^5$nanopores with a diameter of 100 nm is fabricated (Figure 16). SiN was chosen to be used as lipid support thanks to its mechanical robustness, insulating properties, chemical stability and its easy surface functionalization. It is widely used in nanopore sensing community.

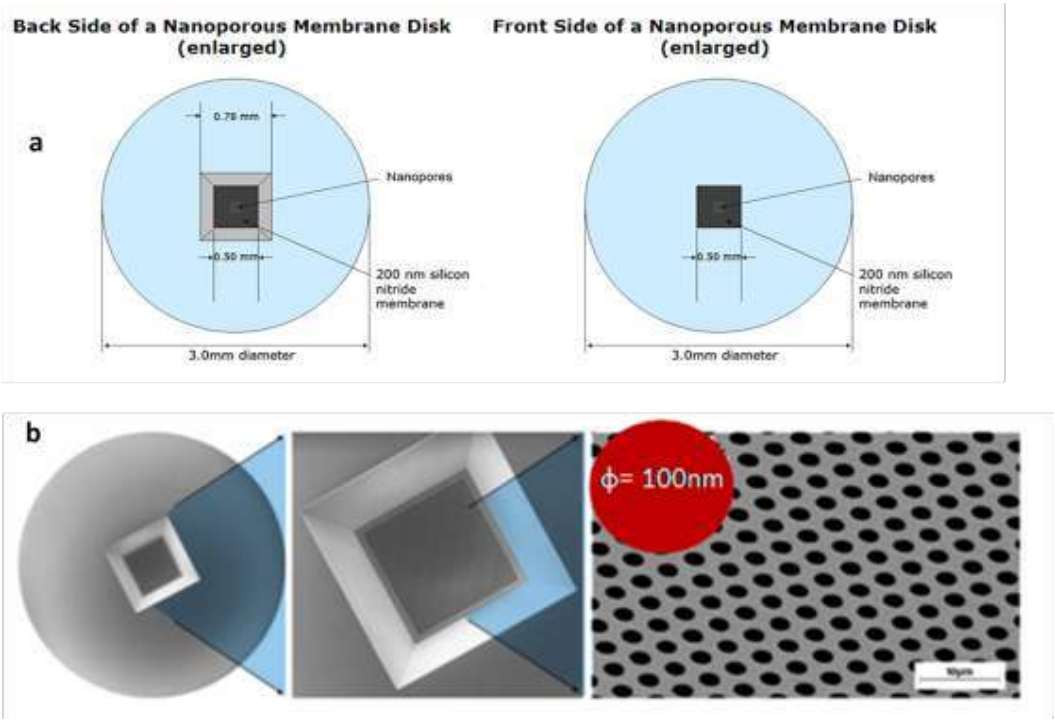


***Figure 16:*** *TEDPELLA TEM grids a) Sketch of back side and front side of a SiN nanoporous membrane b) SEM images of SiN membrane back side with a zoom on nanopore network. Adapted from TEDPELLA website*

## 3. SiN nanoporous membranes characterization

In this section, results of different characterization techniques performed on SiN nanoporous membranes are reported.

After their extraction, lipids were drop-casted on SiN membranes (simplest method) and imaged by fluorescence microscopy.

### 3.1. Fluorescence imaging of SiN membranes

In order to verify adhesion of drop-casted lipids to solid membranes, two TEM grids: a control grid and a second one with DGDG, labeled with a fluorescent lipid (NBD-PC), deposited on it were imaged with an upright optical microscope in fluorescence mode using different magnifications. Figure 17 shows fluorescence images of both membranes. Fluorescence signal of control grid is the optical contribution of all nanopores. On the latter grid, SiN membrane and its nanopore network are well distinguishable; which is not the case for the grid with lipids. The blurry corners of the second grid (Figure 17) led us to conclude that after solvent evaporation, lipids tend to stay on SiN membrane confirming their deposition on it. As nanopore size is below optical microscopy resolution (about 200 nm), higher resolution microscopy was needed to further characterize conformation of lipids inside nanopores.

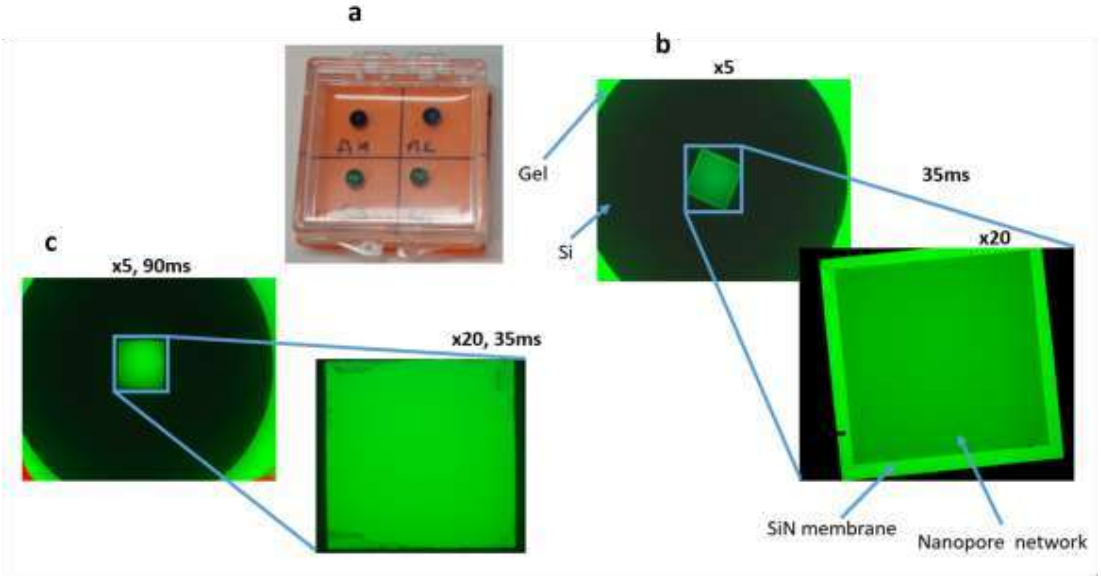


***Figure 17:*** *TEM grids and their fluorescence images.a) TEDPELLA TEM grids deposited on a gel pack. Fluorescence images of A1 and A2 (control and sample grids, respectively) are shown in b and c. b) Fluorescence images of control grid with a zoom on SiN membrane and its nanopore network. The gel (gel pack) is fluorescent. c) Fluorescence images of sample grid covered with fluorescent DGDG (an amount of quantity n=3.10$^{-13}$mol was deposited). Exposure time were 35ms and 90ms and magnifications were x5 and x20 for both grids.*

### 3.2. Transmission microscopy characterization of SiN membranes

The same grids imaged in optical microscopy were then observed in transmission microscopy using conventional transmission microscopy mode (CTEM) and scanning transmission microscopy (STEM) modes. For both modes, images are formed by transmitted electrons through a sample but in STEM, the electron beam is a fine spot and is raster- scanned over the sample (cf appendix for image…). Besides, it enables the use of more transmitted signals than in CTEM, such as the signal of electrons scattered at large angles (detected using a high angle annular dark field (HAADF) detector).

The TEM/STEM images are reported in figure18. The halo observed around nanopores in control membrane is microfabrication process-related. Unlike control membrane, the lipid-covered membrane shows a **blurry aspect** on nanopores; it is the **fingerprint** of lipid presence. For unknown reason, this grid was broken during imaging and a zoom on its edges (Figure18c) shows a superposition of lipid bilayers with a “hair-like” aspect. Although, TEM experiment proved successful deposition of lipids on the nanoporous membrane, no conclusion could be derived about nanopore covering with lipids as the latter fluidity prevented focus adjustment on the former.

For pore-spanning lipid characterization, another nanometric resolution microscopy ought to be used.

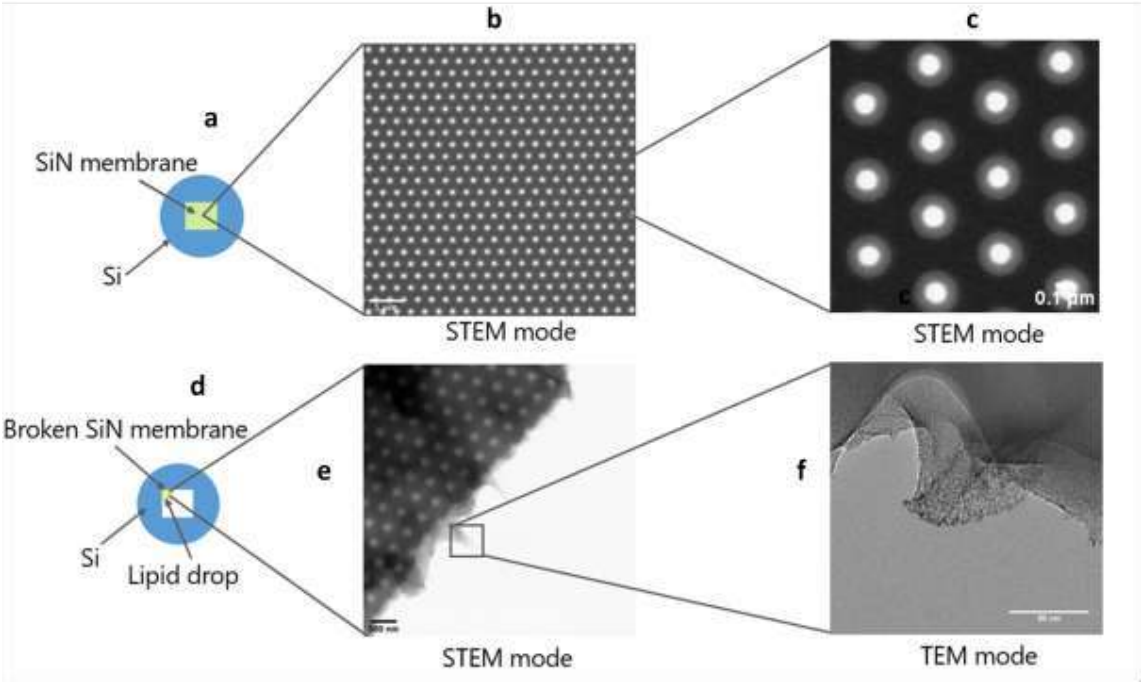


***Figure 18:*** *TEM/STEM images of SiN nanoporous membranes with and without lipids.a and d: Schematic illustration of membranes without (a) and with lipids (d) (broken). b and c: Bright field STEM images of control membrane at magnifications of x288 and x2177, respectively. e and f: STEM and TEM (bright field) images of lipid-covered (DGDG, n=3.10$^{-13}$mol) membrane at magnifications of x1021 and x10796, respectively.*

### 3.3. AFM imaging of lipids on SiN nanoporous membranes

Motivated by the large literature body on lipid bilayer characterization with AFM (Cf. III. State of the art: AFM for lipid bilayers) and by the versatility of this microscopy, AFM was the next imaging tool of lipids deposited on SiNnanopores. AFM Peak Force Tapping™ mode (PFT), developed by Bruker (microscopy supplier), was used. It is a mode where the cantilever is oscillating at a frequency well below its resonance frequency. By keeping a constant normal force between the tip and the sample, PFT overcomes the drawback of tapping mode consisting in tip and sample damage of tip and sample caused by high non-controlled forces.

There are two imaging possibilities with PFT mode: Scan Asyst and PFQNM. In Scan Asyst, automatic optimization of all imaging parameters including peak force is performed. In PFQNM, spectroscopic information from each image pixel is analyzed in real time and different nanomechanical properties (modulus, adhesion force, and deformation depth and dissipation energy) are extracted (Figure 19) and quantified. Moreover, peak force set point i.e. the force applied by the tip on the sample can be controlled.

To differentiate between Scan Asyst and PFQNM, they are referred to as AFM modes in the following parts.

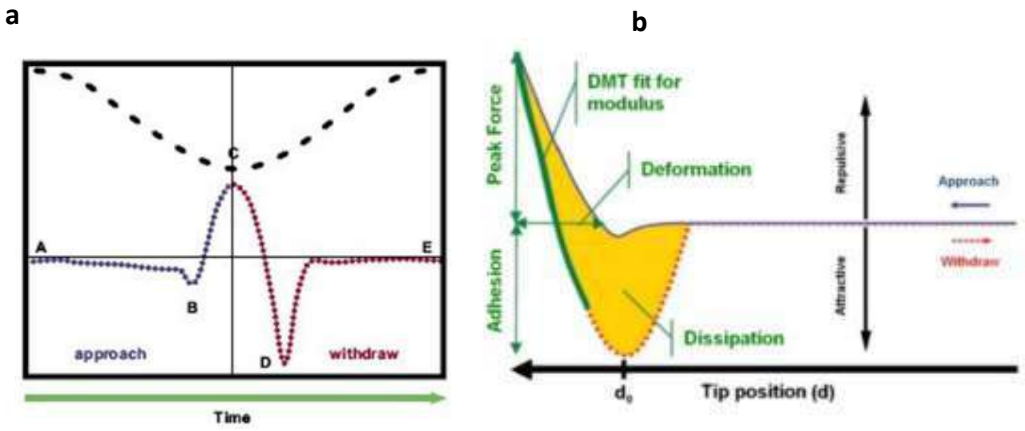


***Figure 19:*** Force curves and information extracted from them. a) Force (solid line) and Z position (dashed line) plots as function of time. B is the jump-to-contact point, C is the point corresponding to peak force and adhesion is determined from point D. b) Force plot as function of the separation (tip position) with the different information extracted from each plot portion. Adapted fromhttps://www.bruker.com/fileadmin/user_upload/8-PDF-Docs/SurfaceAnalysis/AFM/ApplicationNotes/AN128-RevB0-Quantitative_Mechanical_Property_Mapping_at_the_Nanoscale_with_PeakForceQNM-AppNote.pdf

All scans reported in 3.3.1 and 3.3.2. are conducted in air with a SCAN-ASYST-AIR probe (figure 31)

### 3.3.1. Scan Asyst imaging of SiN nanoporous membranes with and without lipids

AFM imaging was first performed on control membranes. Topographic image of a control membrane with four nanopore height profiles are shown in figure 20. A halo is observed around nanopores; which could be explained by a curved section of the SiN membrane at nanopore rims. A loss of nanopore asymmetry is also observed in height profiles through the second valley appearing during tip retraction from the nanopore (scan direction is from left to right). Real nanopore asymmetry hypothesis is rejected since not observed neither on TEM images nor on SEM ones (according to supplier images). Therefore, an AFM-specific feature is behind this observation. It results from the different tip/surface interactions arising during nanopore scanning. In fact, while entering (left) the nanopore, the tip apex is contacting the surface whereas the tip side is contacting the nanopore rim when going out (right). Nanopore asymmetry loss highlights the importance of **scan direction** in constructing the structure topography.

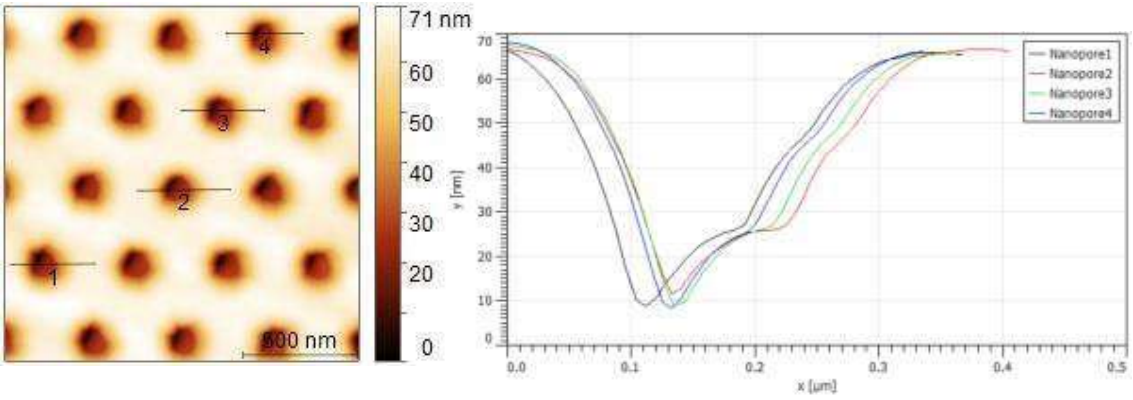


***Figure20:*** *Topographic image (left) of control membrane scanned in Scan Asyst mode and height profiles (right) of 4 of its nanopores. Image was flattened and rotated with Gwyddion. Height profiles along black horizontal lines were also plotted with Gwyddion.Zero height relative to minimum tip penetration. Scan direction: from left to right.*

Drop casting lipids on a control membrane and imaging it yielded topographic images shown in figure 21.

Lipid small islets (bright spots) are formed on the membrane and as for TEM images, a blurry aspect is visible around nanopores.

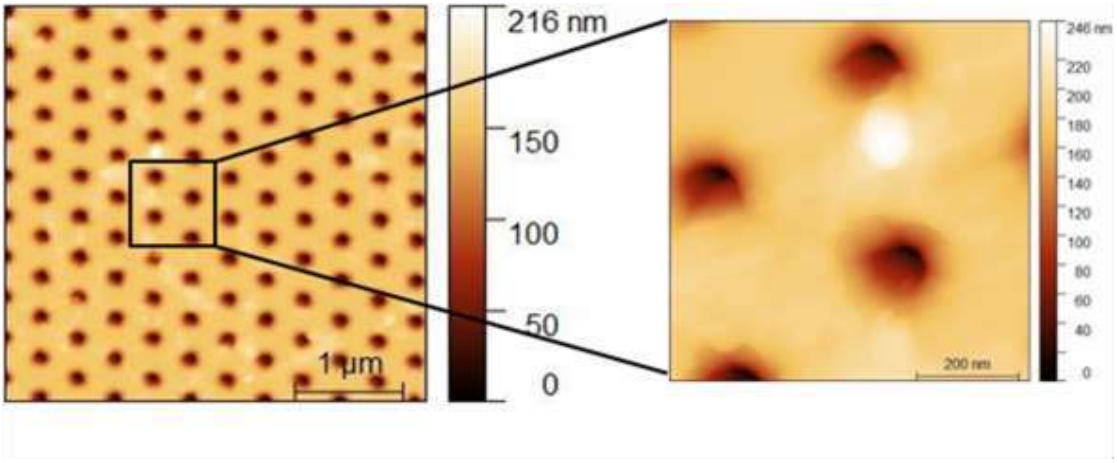


***Figure 21:*** *Topographic images of lipid-covered membrane scanned in Scan Asyst (left) and a zoom on it (right). Membrane was covered with $n_{min}$ of PC (equivalent to a single bilayer on the whole grid). Image was flattened and rotated with Gwyddion. Relative height zero. Scan direction: down.*

In order to characterize homogeneity of lipid spreading on nanoporous membrane, different regions were scanned. Figure 22is the result of two local scans with the corresponding 3D height profiles reported for each scan. Almost no lateral lipid aggregates are observed in the second scan compared to the first one, emphasizing the non-uniformity of **lateral lipid spreading**. This uniformity can also be seen for higher deposited lipid amount (100 times

higher) when very thick (70-nm thick) lipid islet can cover the whole surface of a single nanopore (Figure23).

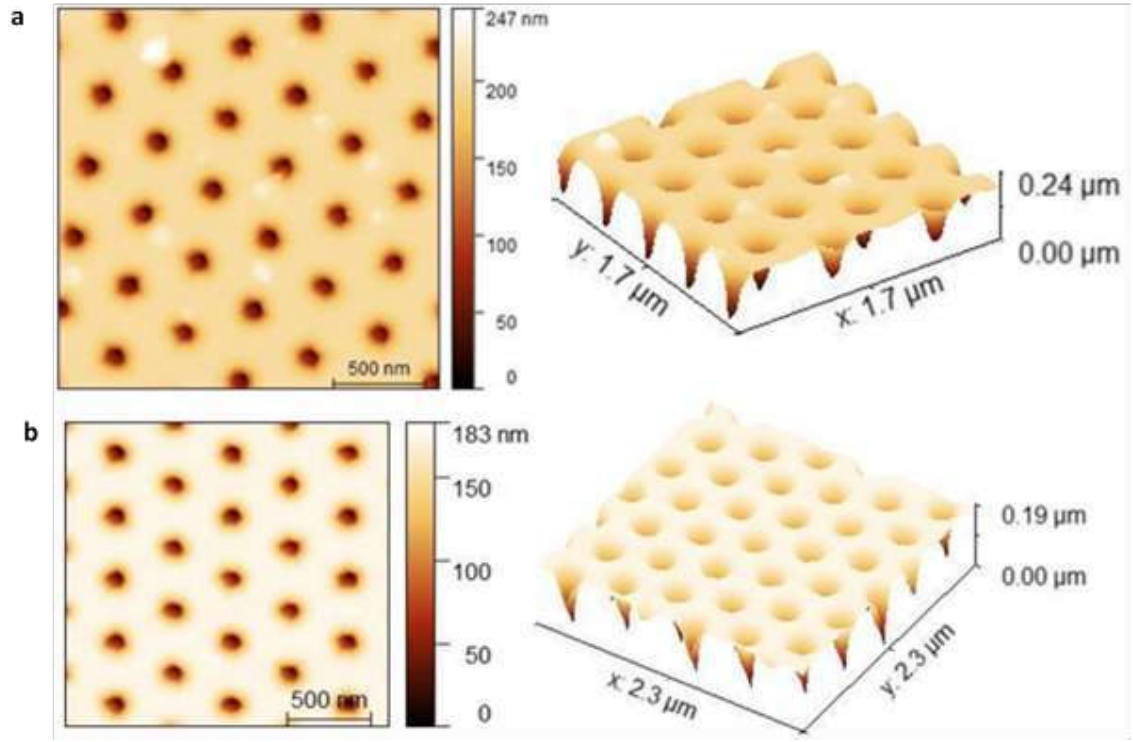


***Figure 22:*** *Non-uniform lateral lipid spreading: topographic images and 3D height profiles of two local scans of a PC-covered membrane (with $n_{min}$). a) 2D and 3D topography of a region showing lipid islets on membrane surface (brighter part on 2D and 3D topography) b) 2D and 3D topography of a region with almost no lipid islet on membrane surface. Images were flattened (second image rotated) with Gwyddion. Relative height zero. Scan direction: down*

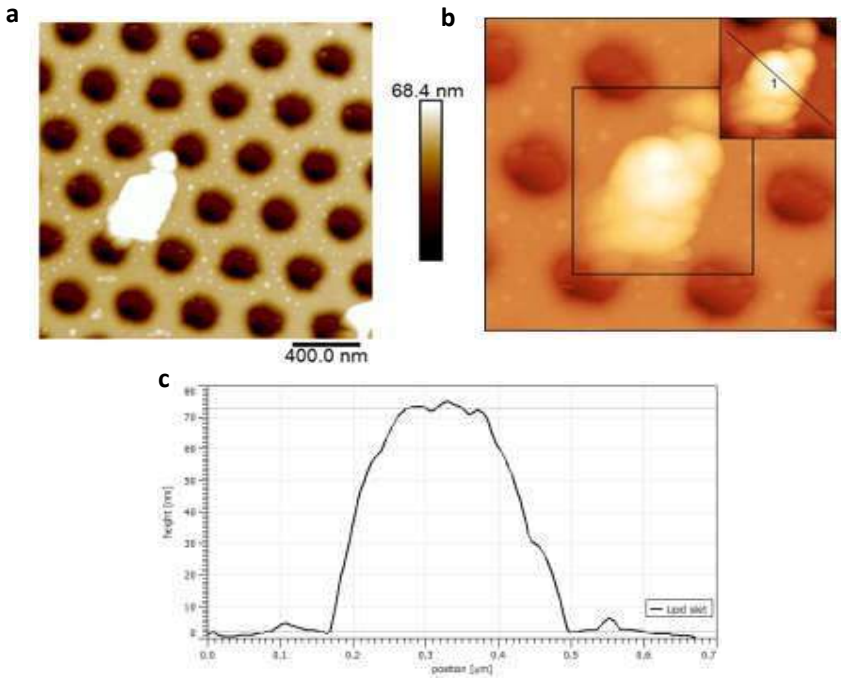


**Figure *23:*** Lipid packing a) Topographic image of PC-covered membrane (n=100* $n_{min}$) showing a thick lipid patch covering one nanopore and small islets spread on the membrane surface highlighting lipid spreading non-uniformity. Image flattened with Nanoscope Analysis. Relative height zero. Scan direction: down b) Zoom on the thick lipid patch and a crop to it with the performed height line on the top right. c) Height profile of lipid patch showing a thickness of 70 nm. b) and c) were obtained with Gwyddion

Although a focus adjustment on lipid islets inside nanopores gave a qualitative idea about nanopore covering, we could not quantitatively characterize this aspect with Scan Asyst. As lipids are softer than SiN, we expected an adhesion difference between SiN scanning and lipid scanning. That's why, samples were imaged in PFQNM mode.

### 3.3.2. PFQNM imaging of SiN nanoporous membranes with and without lipids

Height and adhesion signals were recorded for membranes with and without lipids in PFQNM mode. Figure 24 summarizes the topography and adhesion images of both membranes where lipid-functionalized membrane was covered with a lipid number of moles equivalent to a spreading of a single bilayer on the whole grid surface ($n_{min}$, theoretically estimated). No difference between nanopores is observed for control membrane while some nanopores show higher adhesion than others for lipid-covered one. The encircled nanopore on the bottom images has a higher height and a lower adhesion compared to other nanopores. This predicts the presence of lipids inside it but do not give more information about the other nanopores especially that they have similar topography but different adhesion values(Figure 25b). Height profiles on this nanopore (nanopore1) neighborhood ~~zoom~~ are displayed in figure **25a**. A tip penetration ratio of about 1/3 is measured between nanopore 1 and its neighbors, confirming its full covering with lipids. Correlating adhesion and topography data in a 3D mixed profile (figure 25d), in which the false color represents

adhesion values, further provides additional information to distinguish between different nanopores: the almost fully-covered one, “open” nanopores (non-covered nanopores) and partially-covered nanopores (nanopores with intermediate features).

Superposition of adhesion and topography profiles (Figure 26) further highlights the correlation between these two signals; topography valleys superpose with adhesion peaks inside nanopores and the three types of nanopores (covered, non-covered and partially-covered) have different adhesion profiles; covered nanopore does not present a peak, partially covered nanopores present two peaks and “open” nanopores present a single peak.

As a consequence, PFQNM mode proved its originality to provide further insight into pore-spanning lipids structure through correlation between topography and adhesion images. Through analysis of these images, we concluded a lateral (on the membrane) and vertical (in nanopores) non-uniformity of lipid spreading. Hence, the need for an optimization of the deposition protocol.

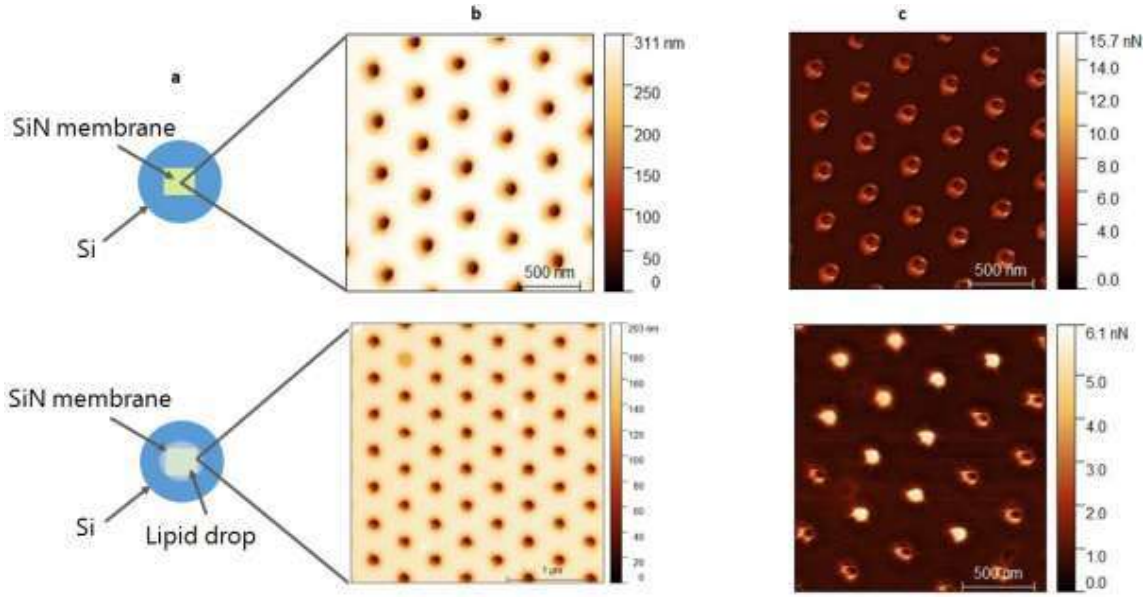


***Figure 24:*** *PFQNM images of SiN nanoporous membranes with and without lipids.a) Schematic illustration of membranes withoutand with lipids. b) Topographic images of control and sample membranes. Images of sample membrane was rotated c) Adhesion images of both membranes. Relative zero adhesion. Auto Control (of scan parameters) was chosen for both scans. Images were flattened with Gwyddion. Relative height zero. Scan direction: down*

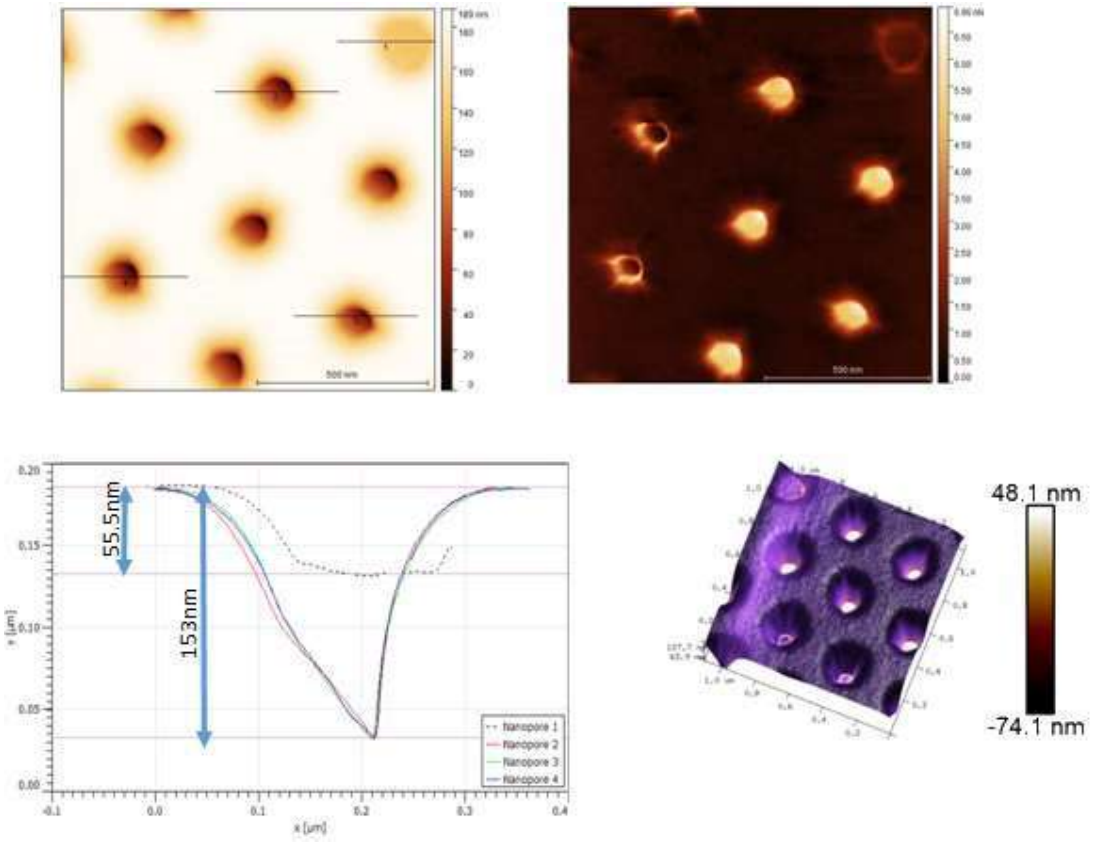


**Figure 25:** Nanopore covering with lipids a) and b) Topographic and adhesion images of PC-covered membrane (n=$n_{min}$) and its corresponding height profilesc) along black height lines d) False color mixed profileof height and adhesion. Height profiles were obtained with Gwyddion and images were flattened with Gwyddion. Mixed profile was obtained with Nanoscope Analysis.

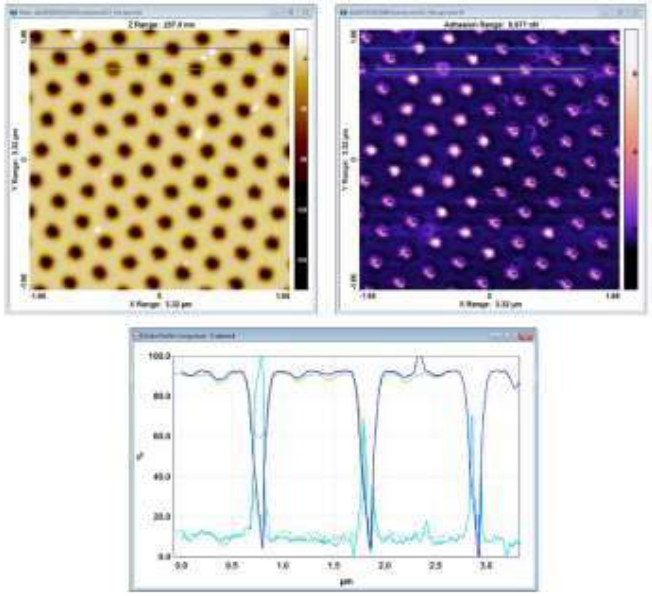

***Figure26:*** *Topographic, adhesion images and their corresponding superposed profiles of the same membrane as for figure 25 where a large region is scanned. Images wereflattedned with Nanoscope Analysis and profiles were obtained in SPIP*

**AFM imaging of sonicated and non-sonicated lipids**

Practically, two parameters can influence lipid spreading on a solid support: lipid solution homogeneity and the deposited amount of quantity (nmol). The second parameter was expected to increase the percent of lipid-covered nanopores on nanoporous membranes.

To ensure a better homogeneity of lipid solution, the effect of sonication on lipids was tested. Sonicated*($n=2000*n_{min}$)* and non-sonicated DGDG*($n=n_{min}$)* were pipetted on 100-nm thick bulk SiN and imaged in PFQNM. Bulk SiN (planar surface) and not nanoporous membrane was used in this experiment in order to reduce the geometrical effect induced by nanopore presence on AFM scanning. The obtained images are displayed in figure27.Sonicated lipids present a better surface coverage compared to non-sonicated ones showing smaller lipid domains. Thanks to this observation, sonication was used in the following characterization experiments. The thickness of sonicated lipids is higher, which is related to its high deposited amount of quantity and not to a sonication effect.

A study of the effect of deposited lipid amount of quantity was also conducted by varying nmol in the range of $10*n_{min}$ to $10^5*n_{min}$. A nonlinear variation of lipid bilayer thickness as a function of nmol was observed and no quantitative conclusion could be derived. However, in order to avoid both a small surface coverage with a small nmol and multiple bilayer stacking preventing nanopore interior imaging with a high nmol, an intermediate number of moles (100 $n_{min}$) was chosen to be used in almost all experiments.

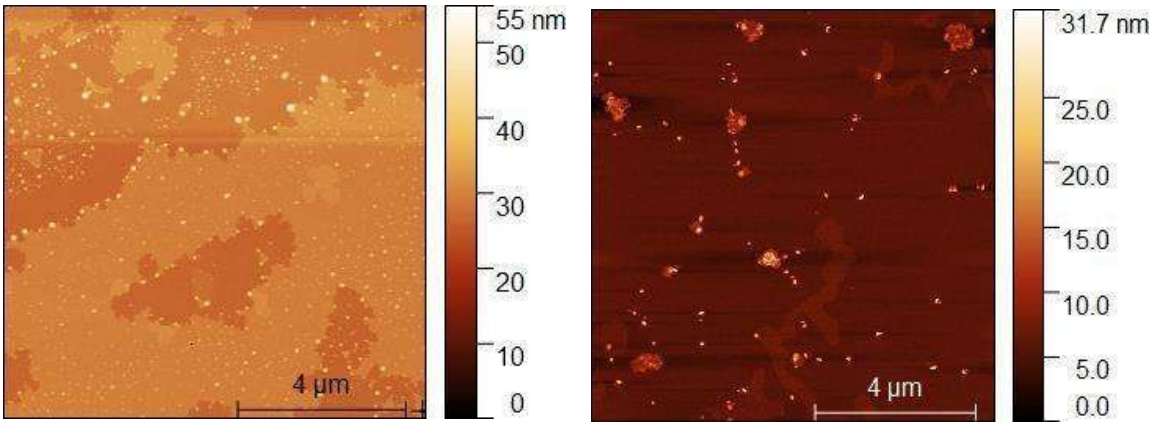


***Figure27:*** *Effect of sonication on lipid bilayer homogeneity. a) Topographic image of sonicated DGDG b) Topographic image of non-sonicated DGDG ($n=n_{min}$). Here, $n_{min}$ refers to DGDG. Images were flattened with Gwyddion. Relative height zero. Scan direction: down*

Since drop casting method is a "random" deposition method in which spatial spreading of lipid solution on nanoporous membrane cannot be controlled, lipid thickness deposited in nanopores was evaluated with respect to control membranes.

**Lipid thickness assessment**

ABA scanning configuration, was used in lipid thickness evaluation experiments. In this configuration, control membrane (A) was first scanned then, the sample membrane with deposited lipids (B) was scanned and finally A was rescanned. The three scans were

performed successively in the same experiment with the same tip. In general, ABA configuration is used to verify soft material deposition on a support via simultaneous analysis of structure and nanomechanical parameters variation and to assess tip/material interaction effect on scan quality.

PC layer thickness was measured using height profiles of randomly chosen nanopores on micrometric scanned regions of control and sample membranes. To account for different errors related especially to imprecision in nanopore center determination, all extracted values were averaged over each scan nanopores. Figure 28 represents the different height profiles of control nanopores and of nanopores covered with PC liposomes $n_{PC}=100*n_{min}$. An average lipid thickness of about **30 nm** was measured inside nanopores: average tip penetration in control nanopores was estimated to 65 nm (Figure 28A), average tip penetration in sample membrane nanopores was estimated to 35nm (Figure 28 B). Lipid layer thickness was calculated by subtracting the second value from the first one. Values around 40 nm were found for drop casted lipids scanned in an ABA configuration. We recognize lateral tip interaction with the nanopore wall in height profiles of control membrane. Besides, these profiles are not superposed (Figure 28 A), this could be explained by the angle between the tip and the membrane, i.e., when the membrane is not vertical, the angle at which the tip enters nanopores varies from a nanopore to another. During the second scan of control membrane (second A), a tip penetration smaller than the one of the first scan was found. This could be explained by the increase of tip radius by lipids adsorbed to it**.**

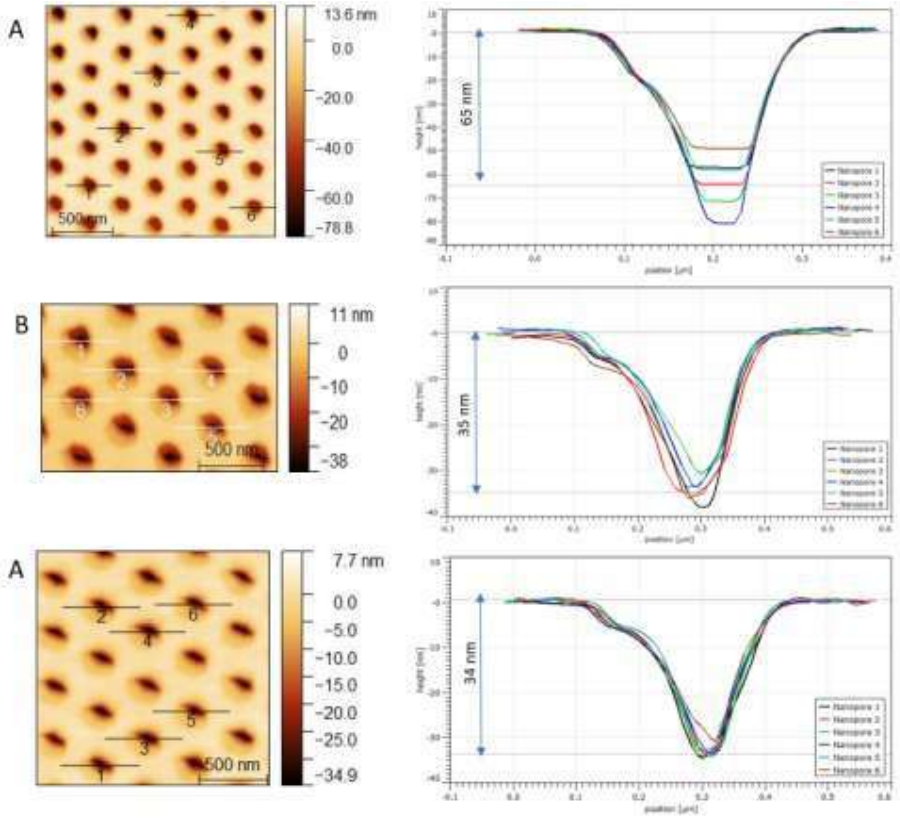


***Figure 28:*** *Lipid thickness assessment. Topographic images and height profiles of randomly chosen nanopores on control and sample membrane (with* $n_{PC}=100n_{min}$) scanned in two different regions.

Average tip penetrations are reported for each scan. Image flattening and height profiles were performed with Gwyddion.

### 3.3.3. AFM characterization of different lipid deposition methods

In order to compare the effect of lipid deposition method on bilayer spreading on SiN, the three four deposition methods, described in lipid deposition methods (cf III. State of the art: AFM for lipid bilayers)**drop casting, spin coating, Langmuir Blodgett method and liposome method** were tested.

To characterize their structure, PC solutions prepared with these four methods were deposited on bulk SiN and imaged with AFM. A large scan of 10 µm was recorded for each method and average peak-to-valley roughness (Cf. VI. Materials and Methods) wasextracted. Figure 29 depicts the scans of drop-casted lipids, spin coated lipids, deposited liposomes and LB deposited lipid film. Small lipid domains shown on scans of lipids deposited by four methods emphasize the non-homogeneity of the formed bilayers. Although, wider lipid domains characterize liposome sample, the surface is not fully covered and the signal saturation proves a rather vertical packing of liposomes. An average (over three lines) roughness of about 24 nm +/- 1 nm was found for these three scans.

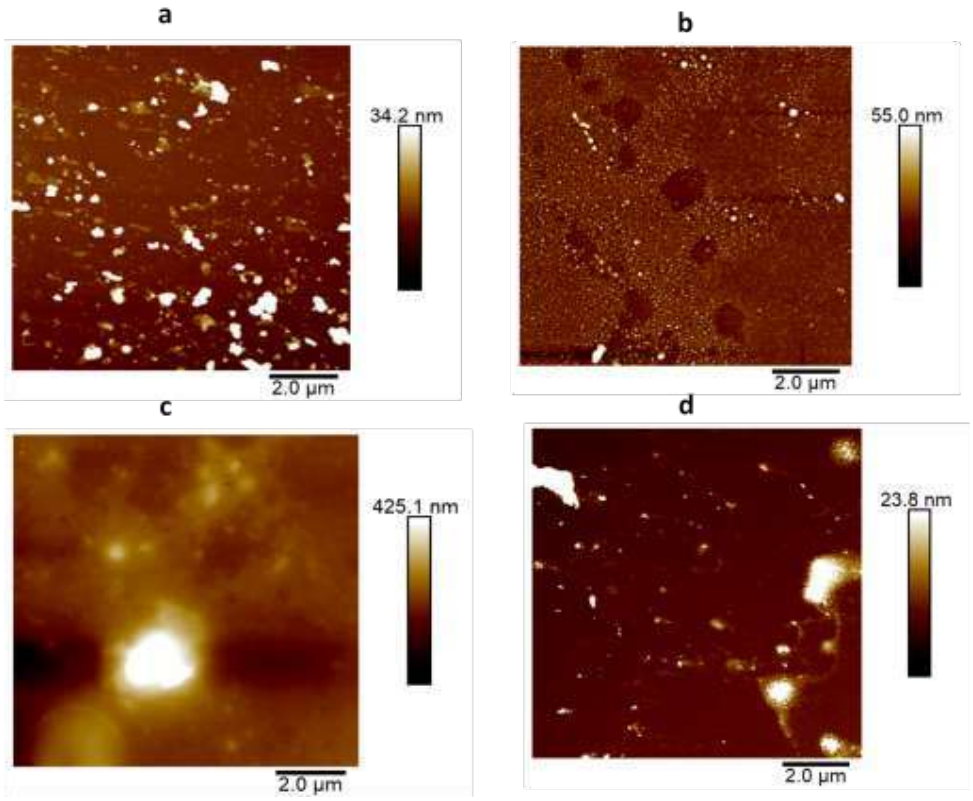


**Figure 29:** Surface coverage of three lipid deposition methodsa) Topographic image of drop-casted lipids prepared b) Topographic image of spin-coated lipids c) Topographic image of deposited liposomes d) Topographic image of LB Lipid film. The three samples were deposited on bulk SiN. Images were flattened with Nanoscope analysis

Getting advantage of the possibility to vertically control the surface coated with lipids, bulk SiN was partially covered with LB deposited lipids and successively scanned over a vertical range of 54 µm, from the top to the bottom, in order to characterize SiN/SiN with lipids interface. Figure 30 is the result of the assembled successive scans. Although the interface was distinguishable in optical imaging (in AFM), a clear straight interface between both sample parts (SiN on the top and SiN with lipids on the bottom) is not visible on recorded scans. Like other deposition methods, lipid small domains are observed for LB lipid films. The average thickness of these scans was about 5nm. No conclusion could be derived from this experiment since this thickness is within the roughness tolerance of bulkSiN.

**Figure 30:** Successive scans (7scans) of LB lipid film. The SiN part is represented to the left and SiN/lipids part is to the right. All scans had a size of 10µm and a Zrange of 10nm. Images were flattened with Nanoscope Analysis

As reported above, the different deposition methods did not result in homogenous lipid bilayers on bulk SiN and further optimization deposition protocols should be carried on.

### 3.3.4. Influence of different AFM scan conditions on lipid bilayer characterization

Varying AFM scan conditions, influence of tip, of scanning medium and of multiple scan were studied on lipids, prepared with different methods and deposited on SiN membranes. The effect of lipid scanning(in other words, tip/lipid interaction) on membrane characterization was also evaluated

**Tip influence on nanopore characterization**

To assess the effect of scanning tip on the nanopore constructed topography, two cantilevers with different sections were used to scan lipid-covered nanopores: SCAN ASYST-AIR with a triangular section and SAA-HPI-SS with a rectangular one. The first probe has a double nominal radius (2nm) to the second (1nm). In addition, SAA-HPI-SS (Figure 31) is tilt-compensated and is more resistant to laser fluctuation. Tip penetration statistics over tens of nanopores covered with drop casted lipids and liposomes, scanned in air respectively with SCAN ASYST-AIR and SAA-HPI-SSwere performed. Figure32 illustrates a part of the analyzed height profiles. For SCAN ASYST-AIR, an average tip penetration of 150 nm was measured whereas, for SAA-HPI-SS, a value of 200 nm was measured. This is related to the small radius of SAA-HPI-SSand therefore its ability to penetrate deeper in the nanopore.

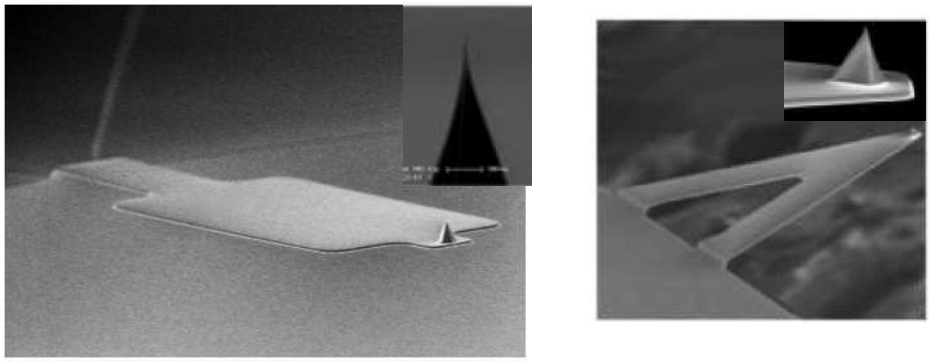

a b

***Figure 31:*** *SEM images of AFM tested probes. a)* SAA-HPI-SS*, b) SCAN ASYST-AIR. On each image, there is a zoom on the tip apex on the top right. Taken from Bruker probes website*https://www.brukerafmprobes.com/

However, as 200 nm is the thickness of the whole SiN membrane and as we expect the tip to penetrate less when lipids are deposited in nanopores, this value can be considered as the maximum local penetration depth found for nanopores not covered with lipids or covered with a very thin bilayer, as a result of a non-uniform lipid spreading.

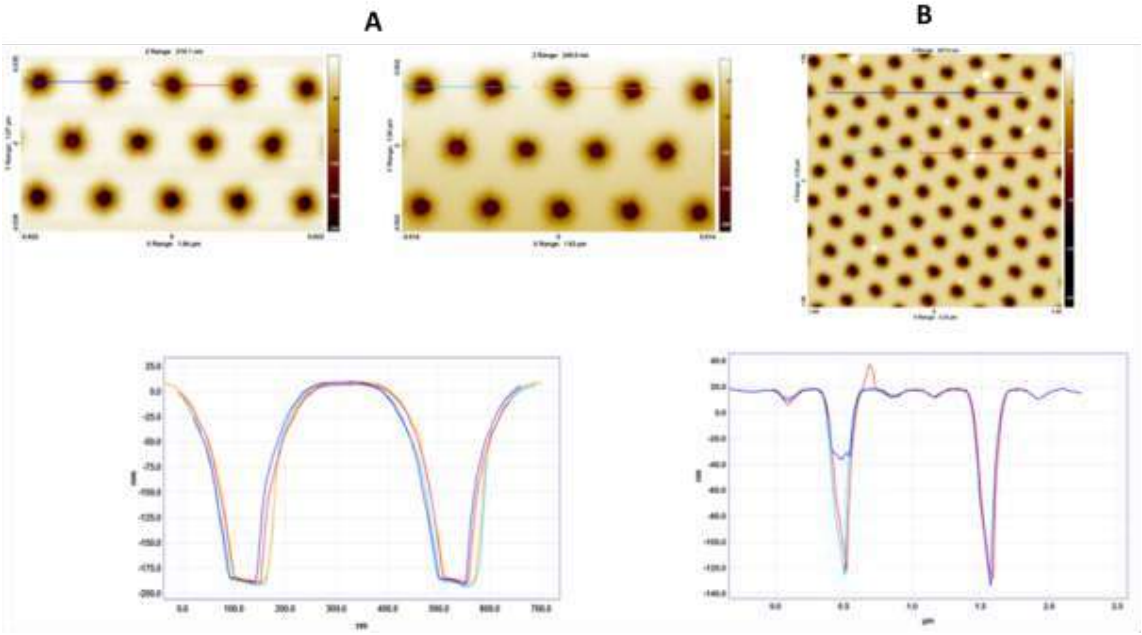


***Figure 32:*** *Part of the height profiles of liposomes and drop casted lipids used in tip penetration estimation of both used tips. A) Topographic images and height profiles of liposomes imaged at 1nN (left) and 2nN (right) load force in air with* SAA-HPI-SS. B) *Topographic image and height profiles of drop casted lipids imaged in air with SCAN ASYST-AIR. The other analyzed profiles are for nanopores on the other lines for liposome sample and are distributed along the scan for drop casted lipids. Images were flattened in Nanoscope Analysis and height profiles were obtained in SPIP.*

**Influence of the applied force on tip penetration**

Two set point forces (1nN and 2nN) were applied during scan, in air, of spin coated and liposomes deposited on SiN membranes with SAA-HPI-SSso as to determine effect of applied force on nanopore constructed topography. Figure 33shows the height profiles of the analyzed nanopores. For both lipid types, an average tip penetration of 200 nm was found for the two load forces. As a result, nanopore structure is independent on the tip applied force and therefore, quantitatively extracted parameters are not neither overestimated nor underestimated (cf. III. State of the art: AFM for lipid bilayers). The double valleys observed on one of the analyzed nanopore (in blue)of the liposome sample can be explained by the presence of a thicker lipid bilayer inside it compared to its neighbors.

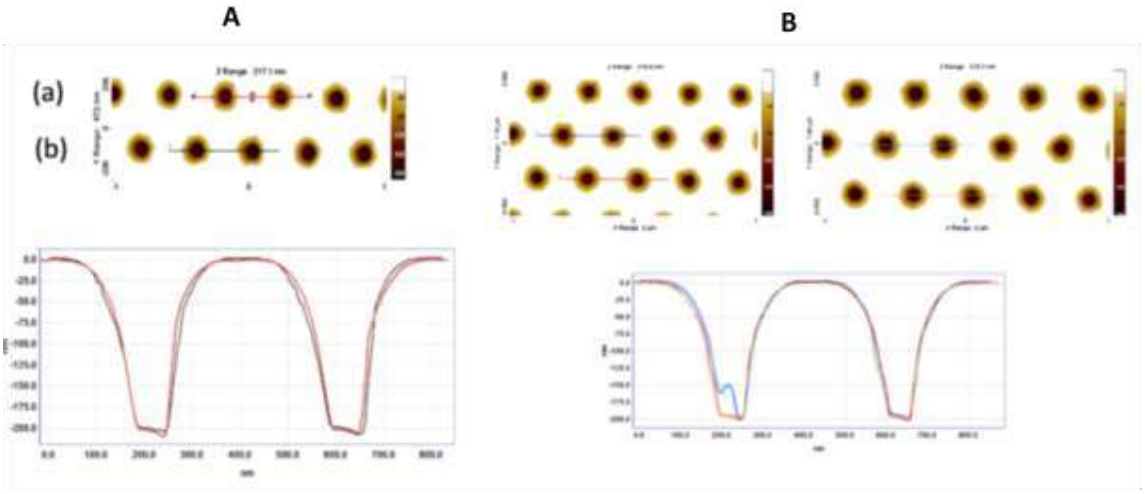


***Figure 33:*** *Influence of peak force on tip penetration A) Topographic image and height profiles of spin coated lipids imaged in air at 1nN (a) and 2nN (b) (on the same scan region) B) Topographic image and height profiles of liposomes imaged in air at 1nN (left) and 2nN (right). Images were flattened in Nanoscope Analysis and height profiles were obtained in SPIP.*

**Influence of PF set point on SiN adhesion**

Effect of applied force on SiN adhesion was also studied on liposome-covered membrane scanned in immersion condition with PEAKFORCE-HIRS-SSB tip. In the latter scan conditions, the sample is scanned when it is immersed in a buffer (HEPES solutionin this case) drop.

A force ABA configuration was used: first,a PF= 5nN was applied to the sample, second, a 10 nN was applied and finally, a second scan with 5nN was performed. Adhesion images of these scans with their SiN corresponding sections and adhesion histograms are represented in table 1.The adhesion images display values in the range from 1nN to 10nN. The x deviation between three scans originate from thermal drift. Besides, a loss of adhesion contrast is visible from the first to the third scan. Adhesion section depicts the local variation of adhesion and histogram representation shows a global distribution over the scanned region. Histogram central values are extracted and plotted as a function of scan number (Figure 34). A nonlinear adhesion variation is observed and SiN adhesion of the first 5 nN

scan (adh1) is not recovered in the second 5nN scan. Two possible scenarios can cause this adhesion variation

- A material change i.e. a lipid bilayer could be broken upon application of relatively high forces (10 nN) changing therefore adhesion value.
- A tip/lipid interaction effect i.e. lipids could be adsorbed on the tip and their interaction with those deposited on the support would be measured instead of tip/lipid interaction forces.

To verify which scenario occurred, SiN adhesion of a freshly scanned region in the neighborhood of the already scanned one should be quantified and if adh1 value will be recovered, the first scenario is most probable to have occurred. Otherwise, lipid adsorption to the tip is more probable.

| Force | 5nN | 10nN | 5nN( second scan) |
|---|---|---|---|
| Adhesion image | 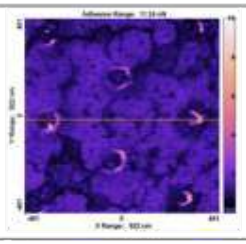 | 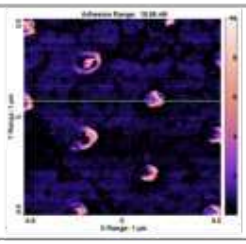 | 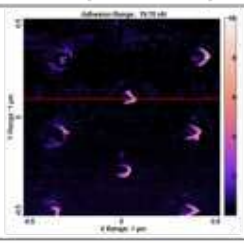 |
| Section | 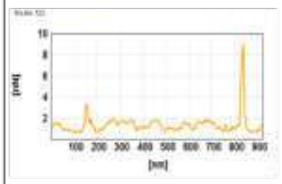 |  | 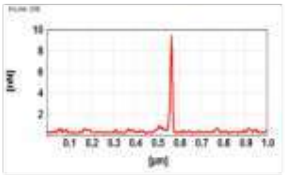 |
| Histogram | 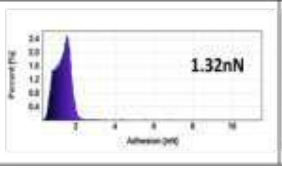  | 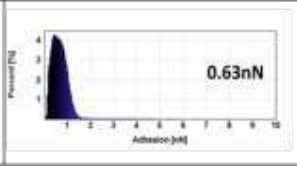  | 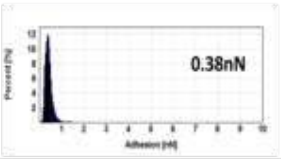  |

***Table 1:*** *Effect of Peak force set point on SiN adhesion (imaging in fluid)*

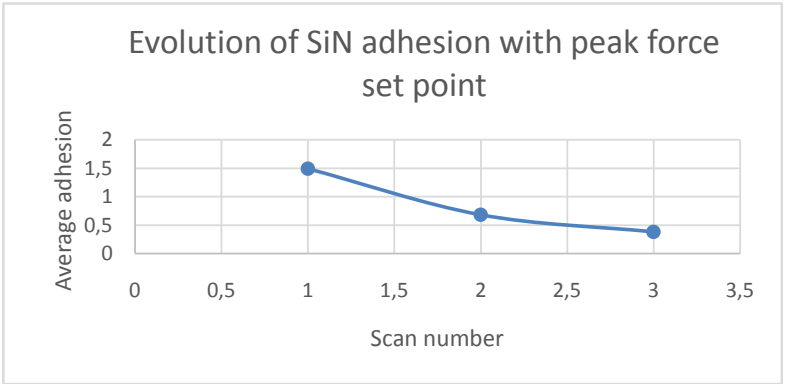

***Figure 34:*** *Average adhesion (around nanopores) as a function of scan number for a liposome sample imaged in immersion conditions scanned in an ABA force configuration. Data was extracted from SPIP analysis (see Table 1).*

**Influence of the scanning medium on lipid deposition inside nanopores**

Scan medium effect on lipid-covered membrane structure was also studied by comparing the height distribution of two samples covered with liposomes and scanned in air and in immersion conditions. Topographic images and height histograms of the two samples are reported in figure 35. Height histograms correspond to a 300 nm z range and the background of topographic image is set to zero. The decrease in percent of points having a depth of 200 nm (with respect to the relative zero) in the liquid-scanned sample, corresponding to "open nanopores", suggest a better lipid covering of nanopores in liquid. Although this air/liquid comparison was rather promising, no quantitative conclusion could be derived since it is not the same sample that is scanned in both media.

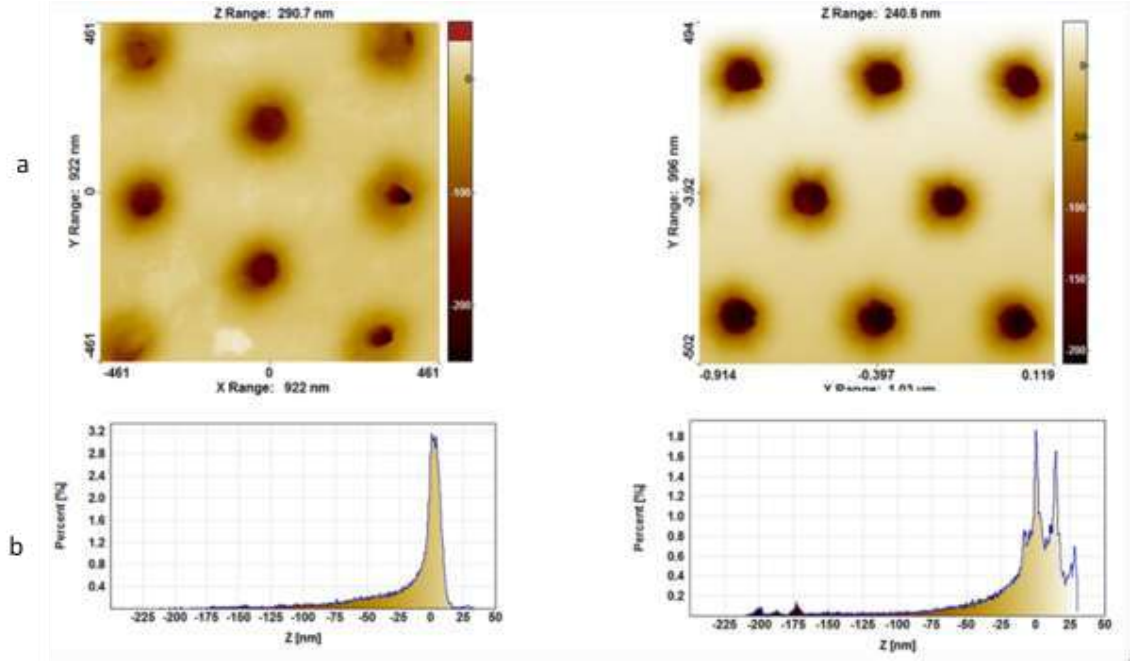


***Figure 35:*** Influence of the scanning medium on lipids inside nanopores*. a) Topographic image (cropped from a larger scan) and the corresponding height histogram of liposomes imaged in air at 2nN. b) Topographic image and the corresponding height histogram of liposomes imaged in immersion conditions at 5nN*

**Assessment of tip/lipid interaction**

Tip scanning effects were also evaluated in ABA sample configuration. Figure36 shows force curves (force spatial and temporal evolution) of ABA successive scans (with SCANASYST-AIR probe) of control membrane (first scan), membrane with drop-casted lipids ($100n_{min}$) and control membrane (second scan).Curve oscillations observed on retract curves of the second control membrane scan and not on the first one could be explained by the progressive removal of lipids from the tip when the latter goes away from the surface. Diameter enlargement (by 10% and by 40%) of control membrane nanopores after lipid scan was also observed. This is in agreement with the hypothesis of lipid adsorption on AFM tip. Because of the wide variability range of diameter increase, the effect of lipid scan on nanopore diameter is reported as a qualitative observation.

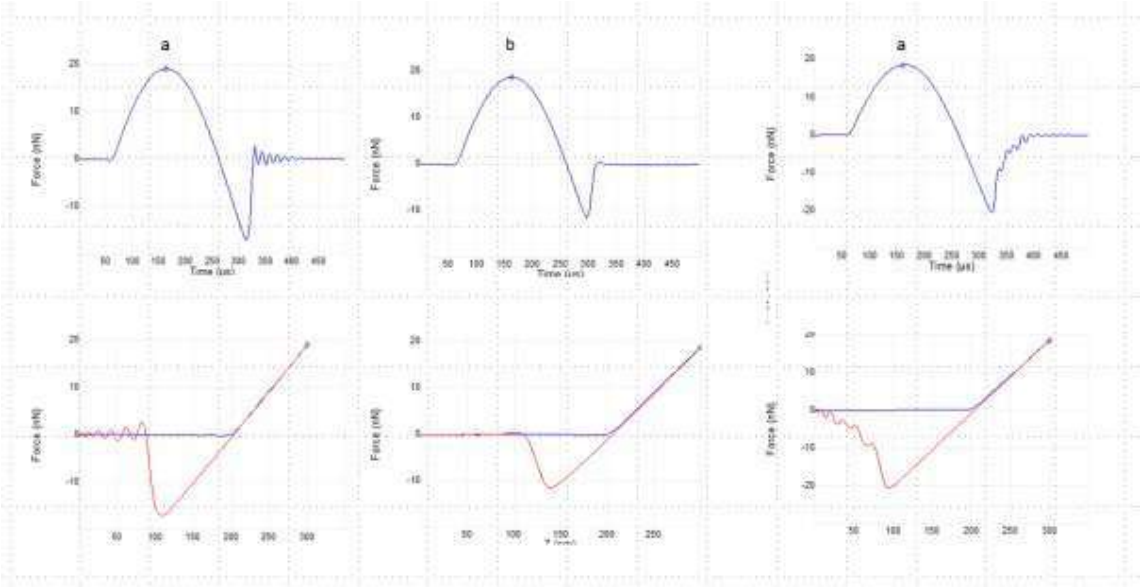


***Figure 36:*** *Force plots of ABA scans with a PC-covered($n=100*n_{min}$) membrane. The top curves show the temporal evolution of force and the bottom ones show its spatial evolution. On the latter forces, blue curves are approach curves and red curves are retract ones.*

To crown all, AFM images of nanoporous membranes should be interpreted with high caution since they are the result of correlation between both tip and sample geometries.

## Conclusions and perspectives

Different microscopy techniques (fluorescence, transmission microscopy and AFM) were used to characterize structure of lipid bilayers inside SiN nanopores. While fluorescence and transmission microscopy served as a positive control to verify successful lipid deposition on SiN membrane surface, AFM was used to deepen into structure of pore-spanning nanopores. Lipids prepared with four different methods were scanned in Peak Force Tapping (PFT)mode with its two variants (Scan Asyst and PFQNM), in air and in water media, with different tips and under different applied forces. Non uniformity of lipid spreading was reported and was the main challenge of the internship.

Scanning lipids with PFQNM highlighted the correlation between topography and adhesion signals in evaluating the surface coverage of lipid bilayer. Additionally, lipid bilayer thickness through comparison of control membranes and lipid-covered membranes was estimated.

Comparing structure of drop casted, spin coated, LB film lipids and liposomes on bulk SiN revealed a non-full surface coverage by lipids but liposome showed a better lateral spreading over the scanned region.

Finally, scanning under different conditions emphasized on the tip/sample interaction nature of AFM principle and on the scan medium effect. Scanning in immersion conditions could bring better nanopore covering with lipids.

As a proof of concept work, this internship was a good starting point for the long-term project since it explored different characterization issues of the biomimetic system and highlighted the originality of AFM to tackle some of these issues.

However, further optimization of the characterization protocol is needed. Experiments should be carried on to improve lipid spreading uniformity inside nanopores. Nanopore diameter effect on lipid uniformity can be studied by spreading lipids on nanopores with different diameters. Besides, lipid deposition protocols should be further optimized by addition of cholesterol, for example, as it is reported in literature to stabilize lipid bilayers (Cf. III. State of the art: AFM for lipid bilayers). Surface functionalization prior to lipid deposition on nanoporous membranes can also be tested.

Finally, this internship has been a great research experience for me. It gave me insight into fundamental research, offered me an opportunity to discover interdisciplinary projects and to gain valuable experience in advanced microscopy and in particular in AFM.

# IV. On the internship

## I. Internship Gantt diagram

During the internship, we addressed the key challenges by dividing the project into tasks detailed in table 2

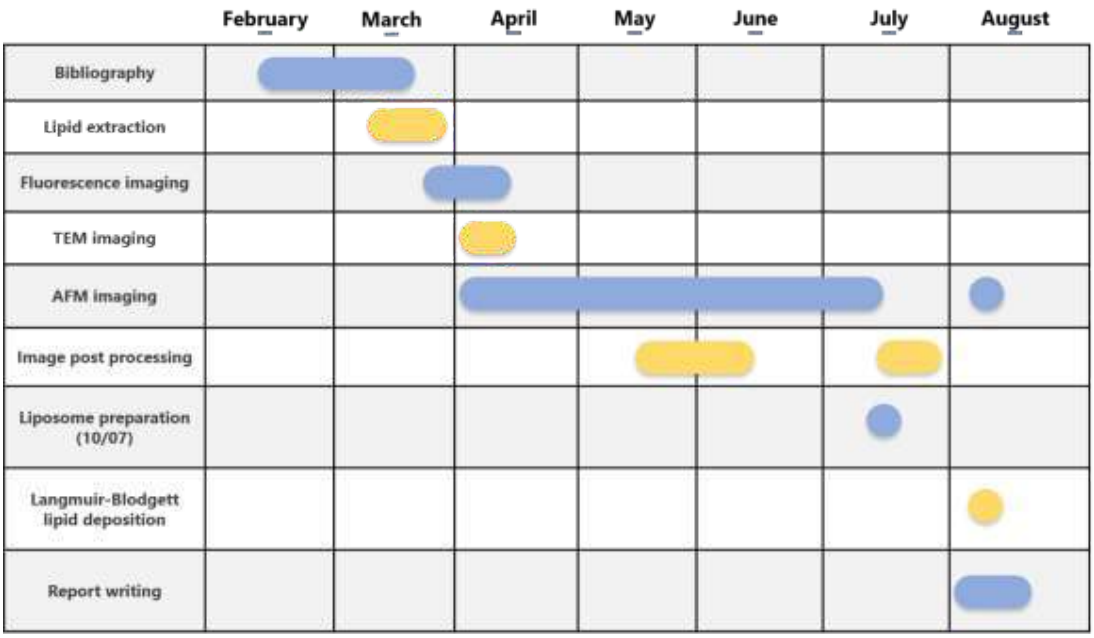


**Table 2: The internship Gantt diagram**

## II. Cost analysis

The total internship cost was estimated to 16 575 €. The detailed monthly costs are detailed in table 3

| | | February | March | | April | | May | June | July | | | August | | |
|---|---|---|---|---|---|---|---|---|---|---|---|---|---|---|
| Yousr (Intern) | Time | 100% (half of the month) | 100% | | 100% | | 100% | 100% | 100% | | | 100% | | |
| | Cost | 650 | 1300 | | 1300 | | 1300 | 1300 | 1300 | | | 1300 | | |
| | Resources | | Lipid extraction equipment | Fluorescence microscope | TEM | AFM* | AFM* | AFM* | AFM** | Software | Liposome preparation | AFM Microscope | SiN membrane | Cantilever |
| | Cost | | 150 | 300 | 300 | 708,5 | 708,5 | 708,5 | 1508,5 | 500 | 100 | 300 | 50 | 26 |
| Camille (Tutor) | Time | 5% | 10% | | 10% | | 10% | 10% | 10% | | | 10% | | |
| | Cost | 200 | 400 | | 400 | | 400 | 400 | 400 | | | 400 | | |
| Juliette (Collaborator) | Time | | 5% | | | | | | | | | | | |
| | Cost | | 165 | | | | | | | | | | | |
| Monthly cost | | 850 | 2315 | | 2708,5 | | 2408,5 | 2408,5 | 3808,5 | | | 2076 | | |
| | | | | | | | | | | | | Total cost | | 16575 |

**Table 3: Cost analysis**

*AFM costs were calculated considering a weekly average of 5 hours and 15 min

** Apart from the “standard” AFM cost in the laboratory, an AFM experiment in PFNC Minatec was conducted in July

# V. Materials and methods

## Materials and instrumentations

Lipids were extracted in the LPCV (CEA Grenoble) laboratory
Fluorophore (NBD-PC) was purchased from Avanti Lipids and stored at -20°C
Methanol was purchased from Sigma Aldrich and chloroform was purchased from Honey Well (Ruedel-De-haen). HEPES powder was purchased from Euromedex Manpack
SPS WAFER SPINNER Spin 150 was used for lipid spin coating
A TRANSONIC 175 (Prolabo) bath sonicator was used for lipid sonication
Silicon Nitride cantilevers: SCANASYST-AIR (nominal spring constant k=0.4 N/m), SAA-HPI-SS (nominal spring constant k=0.25 N/m) and or SAA-HPI-SS (nominal spring constant k=0.12 N/m) were purchased from Bruker
A Langmuir-Blodgett trough from KSV INSTRUMENTS LTD was used for LB lipid film deposition
PELCO Holey Silicon Nitride Support film (100nm pores) TEM grids were purchased from TEDPELLA

## Lipid handling and solution preparation

**Phosphatidylcholine (PC) and digalactosyldiacylglycerol (DGDG)**plant lipids were extracted from Arabidopsis thaliana's leaves, as detailed in Appendix D. To avoid their oxidation, lipids are stored dried (with a nitrogen or argon) at -20°C. To prepare lipid solutions, lipids were dissolved in chloroform/methanol $CHCl_3$/MeOH (1:2, volume:volume), aliquots were prepared and stored dried at -20°C in glass vials. To prepare lipid solutions, glass syringes were used.
1 ampoule (1mg) **of fluorophore** (NBD-PC, emission wavelength **λ= 533nm** and absorbance wavelength **λ= 474nm**) was dissolved in 1ml of $CHCl_3$/MeOH (1:2, volume:volume).

## Theoretical calculation of $n_{min}$ (lipid quantity of matter equivalent to cover the whole TEM grid with a single lipid bilayer)

Only lipid headgroups areas were considered: DGDG (headgroup area: 0.78$nm^2$) and PC (headgroup area: 0.67$nm^2$). Under these considerations, 3.5 $.10^{-11}$mol was found for a PC single bilayer and 3.$10^{-11}$mol for a DGDG single bilayer.

## Lipid solution drop casting

5µl was pipetted on the SiN membrane with a pipette and a plastic tip. Lipids were sonicated in the bath sonicator during about 5 minutes

## Liposome solution preparation

Liposome solutions were prepared as detailed in Appendix[23] E or as reported in Attwood et al.[23][23] for POPC and stored at -4°C. A volume of 5µl or 10µl was pipetted on SiN membranes

## Lipid Spin coating

5µl or 10µl of lipid solution was pipetted on SiN membranes. The membranes were rotated at 500 rpm (rotations per minute) during 10 seconds for the first step and at 1000 rpm during 20 seconds for the second step.

## LB lipid film preparation

A bulk sample was partially dipped at a surface tension of 24mN/n and at a rate of 4mm/min.

After covering with lipids, TED PELLA TEM grids were rinsed with chloroform ($CHCl_3$), ethanol (EtOH) and deionized waterto be reused in other experiments.

### Fluorescence microscopy

Fluorescence imaging was performed with an upright fluorescence microscope ZEISS AxioScope using the GFP filter and a x0.63 camera adapter. 35ms and 90ms exposure times were used.

### Transmission electron microscopy

Transmission electron microscopy experiments were performed with FEI Tecnai Osiris TEM in Conventional Transmission electron microscopy (CTEM) and STEM (Scanning Transmission electron microscopy) modes using a voltage of 200 kV. Images in bright field (BF) and in High-Angle Annular Dark Field (**HAADF**) were saved.

### Atomic force microscopy (AFM)

All AFM imaging was performed using a Bruker Dimension ICON AFM in Peak Force Tapping (PFT) mode with its two variants Scan Asyst and Peak Force Quantitative Nanomechanical Mapping (PFQNM). Scan Asyst imaging was conducted in air with SCANASYST-AIR cantilevers. PFQNM imaging was conducted either in air (using SCANASYTST-AIR or SAA-HPI-SS SiN cantilevers) or in buffer (HEPES) solution (using PEAKFORCE-HIRS-SSB SiN cantilever).

For Scan Asyst imaging, Auto control was used to reduce tip damage and scanner drift

For imaging in PFQNM with SAA-HPI-SS cantilever, calibration of nanomechanical mapping parameters was performed:

- Deflection cantilever sensitivity calibration by scanning a sapphire (stiff material) sample

A static calibration was first performed to verify the tip status applying a Z ramp of 300nm (ramp size). The trigger threshold was 0.15 V. 5 force curves were saved, corrected with baseline correction and the average sensitivity was extracted and saved. Second, a dynamic calibration using a frequency of 2 kHz and an amplitude of 37.5 nm was performed to calibrate the sensor signal with the position of the piezo scanner. QNM synchronization distance (translating the percent of tip indentation in the sample) was saved to be used in the further mechanical characterization of other samples.

- Cantilever spring constant calibration (using the value of sensitivity determined in

sensitivity calibration) by thermal tune (link of the cantilever spring constant to its Brownian motion. A thermal tune range of 1 to 100 kHz was chosen and data was fitted to a Lorentzian function.

Details of the calibration steps are found in Bruker user guides.

### Sample preparation for fluid imaging

Sample: Liposome -covered membrane (liposome suspension prepared in LPCV, cf. Appendix E)

The cantilever (PEAKFORCE-HIRS-SSB) was fixed on Bruker fluid holder. A PDMS adhesive frame was glued onto a bulk Si sample. Then, SiN membrane was glued on bulk Si with a double-sided adhesive. A 10-µl drop of 1mM liposomes suspension in 20mM HEPES pH7.3, 100mM NaCl (buffer) was pipetted on the membrane and the sample was immersed with vesicle buffer.

### Image post processing

TEM and fluorescence images were post processed using FIJI software.

AFM images were flattened with Gwyddion (2.53) and Nanoscope Analysis (1.9). Height profiles were extracted and analyzed with Gwyddion and SPIP (6.7.2). Adhesion sections, adhesion histograms and height histograms were extracted and analyzed with SPIP.

Roughness measurements for lipids deposited on bulk SiN were conducted by extraction average roughness (the difference between the highest peak and the lowest valley within a scan line). For each sample, roughness was averaged over three lines.

# Bibliography


[1] Global Wastewater and Sludge Production, Treatment and Use | SpringerLink https://link.springer.com/chapter/10.1007%2F978-94-017-9545-6_2 (accessed Aug 27, 2019).

[2] Raouf MS, A.; Raheim ARM, A. Removal of Heavy Metals from Industrial Waste Water by Biomass-Based Materials: A Review. *J. Pollut. Eff. Control***2016**, *05* (01). https://doi.org/10.4172/2375-4397.1000180.

[3] (10) (PDF) Methods of Removing Heavy Metals from Industrial Wastewater https://www.researchgate.net/publication/287818349_Methods_of_Removing_Heavy_Metals_from_Industrial_Wastewater (accessed Aug 27, 2019).

[4] Aquaporin Website.

[5] Acar, E. T.; Buchsbaum, S. F.; Combs, C.; Fornasiero, F.; Siwy, Z. S. Biomimetic Potassium-Selective Nanopores. *Sci. Adv.***2019**, *5* (2), eaav2568. https://doi.org/10.1126/sciadv.aav2568.

[6] Shen, Y.; Saboe, P. O.; Sines, I. T.; Erbakan, M.; Kumar, M. Biomimetic Membranes: A Review. *J. Membr. Sci.***2014**, *454*, 359–381. https://doi.org/10.1016/j.memsci.2013.12.019.

[7] Branton, D.; Deamer, D. W.; Marziali, A.; Bayley, H.; Benner, S. A.; Butler, T.; Di Ventra, M.; Garaj, S.; Hibbs, A.; Huang, X.; et al. The Potential and Challenges of Nanopore Sequencing. *Nat. Biotechnol.***2008**, *26* (10), 1146–1153. https://doi.org/10.1038/nbt.1495.

[8] Yusko, E. C.; Johnson, J. M.; Majd, S.; Prangkio, P.; Rollings, R. C.; Li, J.; Yang, J.; Mayer, M. Controlling Protein Translocation through Nanopores with Bio-Inspired Fluid Walls. *Nat. Nanotechnol.***2011**, *6* (4), 253–260. https://doi.org/10.1038/nnano.2011.12.

[9] Han, X.; Studer, A.; Sehr, H.; Geissbühler, I.; Di Berardino, M.; Winkler, F. K.; Tiefenauer, L. X. Nanopore Arrays for Stable and Functional Free-Standing Lipid Bilayers. *Adv. Mater.***2007**, *19* (24), 4466–4470. https://doi.org/10.1002/adma.200700468.

[10] Watson, H. Biological Membranes. *Essays Biochem.***2015**, *59*, 43–69. https://doi.org/10.1042/bse0590043.

[11] Kanduč, M.; Schlaich, A.; de Vries, A. H.; Jouhet, J.; Maréchal, E.; Demé, B.; Netz, R. R.; Schneck, E. Tight Cohesion between Glycolipid Membranes Results from Balanced Water–Headgroup Interactions. *Nat. Commun.***2017**, *8*, 14899. https://doi.org/10.1038/ncomms14899.

[12] Läuger, P.; Lesslauer, W.; Marti, E.; Richter, J. Electrical Properties of Bimolecular Phospholipid Membranes. *Biochim. Biophys. Acta BBA - Biomembr.***1967**, *135* (1), 20–32. https://doi.org/10.1016/0005-2736(67)90004-1.

[13] Mey, I.; Stephan, M.; Schmitt, E. K.; Müller, M. M.; Ben Amar, M.; Steinem, C.; Janshoff, A. Local Membrane Mechanics of Pore-Spanning Bilayers. *J. Am. Chem. Soc.***2009**, *131* (20), 7031–7039. https://doi.org/10.1021/ja809165h.

[14] Mennicke, U.; Salditt, T. Preparation of Solid-Supported Lipid Bilayers by Spin-Coating. *Langmuir***2002**, *18* (21), 8172–8177. https://doi.org/10.1021/la025863f.

[15] Picas, L.; Milhiet, P.-E.; Hernández-Borrell, J. Atomic Force Microscopy: A Versatile Tool to Probe the Physical and Chemical Properties of Supported Membranes at the Nanoscale. *Chem. Phys. Lipids***2012**, *165* (8), 845–860. https://doi.org/10.1016/j.chemphyslip.2012.10.005.

[16] Morandat, S.; Azouzi, S.; Beauvais, E.; Mastouri, A.; El Kirat, K. Atomic Force Microscopy of Model Lipid Membranes. *Anal. Bioanal. Chem.***2013**, *405* (5), 1445–1461. https://doi.org/10.1007/s00216-012-6383-y.

[17] Reimhult, E.; Höök, F.; Kasemo, B. Intact Vesicle Adsorption and Supported Biomembrane Formation from Vesicles in Solution: Influence of Surface Chemistry, Vesicle Size, Temperature, and Osmotic Pressure. *Langmuir***2003**, *19* (5), 1681–1691. https://doi.org/10.1021/la0263920.

[18] Goksu, E. I.; Vanegas, J. M.; Blanchette, C. D.; Lin, W.-C.; Longo, M. L. AFM for Structure and Dynamics of Biomembranes. *Biochim. Biophys. Acta BBA - Biomembr.***2009**, *1788* (1), 254–266. https://doi.org/10.1016/j.bbamem.2008.08.021.

[19] Blanchette, C. D.; Lin, W.-C.; Orme, C. A.; Ratto, T. V.; Longo, M. L. Using Nucleation Rates to Determine the Interfacial Line Tension of Symmetric and Asymmetric Lipid Bilayer Domains. *Langmuir ACS J. Surf. Colloids***2007**, *23* (11), 5875–5877. https://doi.org/10.1021/la7004584.
[20] Gumí-Audenis, B.; Giannotti, M. I. Structural and Mechanical Characterization of Supported Model Membranes by AFM. In *Biomimetic Lipid Membranes: Fundamentals, Applications, and Commercialization*; Kök, F. N., Arslan Yildiz, A., Inci, F., Eds.; Springer International Publishing: Cham, 2019; pp 1–27. https://doi.org/10.1007/978-3-030-11596-8_1.
[21] Garcia-Manyes, S.; Sanz, F. Nanomechanics of Lipid Bilayers by Force Spectroscopy with AFM: A Perspective. *Biochim. Biophys. Acta BBA - Biomembr.***2010**, *1798* (4), 741–749. https://doi.org/10.1016/j.bbamem.2009.12.019.
[22] An, H.; Nussio, M. R.; Huson, M. G.; Voelcker, N. H.; Shapter, J. G. Material Properties of Lipid Microdomains: Force-Volume Imaging Study of the Effect of Cholesterol on Lipid Microdomain Rigidity. *Biophys. J.***2010**, *99* (3), 834–844. https://doi.org/10.1016/j.bpj.2010.04.072.
[23] Attwood, S. J.; Choi, Y.; Leonenko, Z. Preparation of DOPC and DPPC Supported Planar Lipid Bilayers for Atomic Force Microscopy and Atomic Force Spectroscopy. *Int. J. Mol. Sci.***2013**, *14* (2), 3514–3539. https://doi.org/10.3390/ijms14023514.
[24] Canale, C.; Jacono, M.; Diaspro, A.; Dante, S. Force Spectroscopy as a Tool to Investigate the Properties of Supported Lipid Membranes. *Microsc. Res. Tech.***2010**, *73* (10), 965–972. https://doi.org/10.1002/jemt.20834.
[25] El Kirat, K.; Morandat, S.; Dufrêne, Y. F. Nanoscale Analysis of Supported Lipid Bilayers Using Atomic Force Microscopy. *Biochim. Biophys. Acta BBA - Biomembr.***2010**, *1798* (4), 750–765. https://doi.org/10.1016/j.bbamem.2009.07.026.
[26] Picas, L.; Montero, M. T.; Morros, A.; Cabañas, M. E.; Seantier, B.; Milhiet, P.-E.; Hernández-Borrell, J. Calcium-Induced Formation of Subdomains in Phosphatidylethanolamine-Phosphatidylglycerol Bilayers: A Combined DSC, 31P NMR, and AFM Study. *J. Phys. Chem. B***2009**, *113* (14), 4648–4655. https://doi.org/10.1021/jp8102468.
[27] Gumí-Audenis, B.; Costa, L.; Carlá, F.; Comin, F.; Sanz, F.; Giannotti, M. I. Structure and Nanomechanics of Model Membranes by Atomic Force Microscopy and Spectroscopy: Insights into the Role of Cholesterol and Sphingolipids. *Membranes***2016**, *6* (4), 58. https://doi.org/10.3390/membranes6040058.
[28] González-Ramírez, E. J.; Artetxe, I.; García-Arribas, A. B.; Goñi, F. M.; Alonso, A. Homogeneous and Heterogeneous Bilayers of Ternary Lipid Compositions Containing Equimolar Ceramide and Cholesterol. *Langmuir***2019**, *35* (15), 5305–5315. https://doi.org/10.1021/acs.langmuir.9b00324.
[29] Jurak, M.; Mroczka, R.; Łopucki, R.; Wiącek, A. E. Structure and Wettability of Heterogeneous Monomolecular Films of Phospholipids with Cholesterol or Lauryl Gallate. *Appl. Surf. Sci.***2019**, *493*, 1021–1031. https://doi.org/10.1016/j.apsusc.2019.07.065.
[30] Dante, S.; Hauß, T.; Steitz, R.; Canale, C.; Dencher, N. A. Nanoscale Structural and Mechanical Effects of Beta-Amyloid (1–42) on Polymer Cushioned Membranes: A Combined Study by Neutron Reflectometry and AFM Force Spectroscopy. *Biochim. Biophys. Acta BBA - Biomembr.***2011**, *1808* (11), 2646–2655. https://doi.org/10.1016/j.bbamem.2011.07.024.
[31] Gumí-Audenis, B.; Costa, L.; Ferrer-Tasies, L.; Ratera, I.; Ventosa, N.; Sanz, F.; I. Giannotti, M. Pulling Lipid Tubes from Supported Bilayers Unveils the Underlying Substrate Contribution to the Membrane Mechanics. *Nanoscale***2018**, *10* (30), 14763–14770. https://doi.org/10.1039/C8NR03249A.
[32] Andre, G.; Brasseur, R.; Dufrêne, Y. F. Probing the Interaction Forces between Hydrophobic Peptides and Supported Lipid Bilayers Using AFM. *J. Mol. Recognit.***2007**, *20* (6), 538–545. https://doi.org/10.1002/jmr.837.

[33] Sullan, R. M. A.; Li, J. K.; Zou, S. Quantification of the Nanomechanical Stability of Ceramide-Enriched Domains. *Langmuir***2009**, *25* (22), 12874–12877. https://doi.org/10.1021/la903442s.
[34] Picas, L.; Suárez-Germà, C.; Teresa Montero, M.; Hernández-Borrell, J. Force Spectroscopy Study of Langmuir−Blodgett Asymmetric Bilayers of Phosphatidylethanolamine and Phosphatidylglycerol. *J. Phys. Chem. B***2010**, *114* (10), 3543–3549. https://doi.org/10.1021/jp910882e.
[35] Sullan, R. M. A.; Li, J. K.; Zou, S. Direct Correlation of Structures and Nanomechanical Properties of Multicomponent Lipid Bilayers. *Langmuir***2009**, *25* (13), 7471–7477. https://doi.org/10.1021/la900395w.
[36] Steltenkamp, S.; Müller, M. M.; Deserno, M.; Hennesthal, C.; Steinem, C.; Janshoff, A. Mechanical Properties of Pore-Spanning Lipid Bilayers Probed by Atomic Force Microscopy. *Biophys. J.***2006**, *91* (1), 217–226. https://doi.org/10.1529/biophysj.106.081398.
[37] Hennesthal, C.; Steinem, C. Pore-Spanning Lipid Bilayers Visualized by Scanning Force Microscopy. *J. Am. Chem. Soc.***2000**, *122* (33), 8085–8086. https://doi.org/10.1021/ja000940j.
[38] Nussio, M. R.; Oncins, G.; Ridelis, I.; Szili, E.; Shapter, J. G.; Sanz, F.; Voelcker, N. H. Nanomechanical Characterization of Phospholipid Bilayer Islands on Flat and Porous Substrates: A Force Spectroscopy Study. *J. Phys. Chem. B***2009**, *113* (30), 10339–10347. https://doi.org/10.1021/jp811035g.
[39] Jiang, Y.; Pryse, K.; Singamaneni, S.; Genin, G.; Elson, E. Atomic Force Microscopy of Phase Separation on Ruptured, Giant Unilamellar Vesicles, and a Mechanical Pathway for the Co-Existence of Lipid Gel Phases. *J. Biomech. Eng.***2019**. https://doi.org/10.1115/1.4043871.

# Appendix A

## Heavy metals, their permission levels and their removal methods

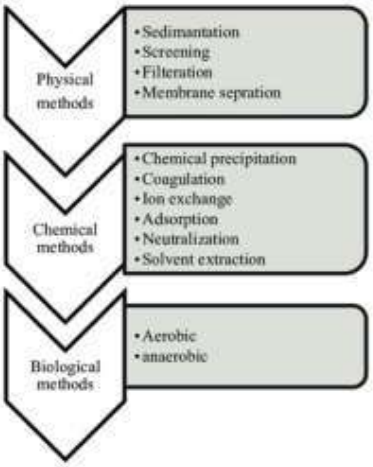


***Figure A.1:*** *Conventional methods for heavy metals removal. Adapted from Abdel-Raouf MS et al.*[2]

| Metal | Source | Route of Entry | Toxicity Effect | Permission level (mg/L) |
|---|---|---|---|---|
| Arsenic | Pesticides, fungicides, metal smelters | Inhalation and ingestion | Irritation of respiratory system, Liver and Kidney damage, Loss of appetite, nausea and vomiting etc. | 0.020 |
| Cadmium | Welding, electroplating, pesticide fertilizer, Cd-Ni batteries | Inhalation and ingestion | Lung, liver and kidney damage; Irritation of respiratory system | 0.06 |
| Chromium | Paints, electro plating and metallurgy | Inhalation, ingestion, and absorption through skin | Lung damage and Irritation or respiratory system | 0.05 |
| Mercury | Pesticides, batteries, paper industry | Inhalation, ingestion and absorption through skin | Irritation of respiratory system; lung, liver kidney damage, and loss of hearing and muscle coordination | 0.01(vapor) |
| Lead | Paint, pesticide, smoking, automobile emission,mining, | Inhalation and ingestion | Lung and liver damage; loss of appetite, nausea | 0.15 |
| Nickel | Electrochemical industries | Inhalation | Lung, liver and kidney damage | 0.1 |

***TableA.1:*** *Source, route of entry, toxicity effects and permission levels of some heavy metals. Adapted from Abdel-Raouf MS. and al. [2]*

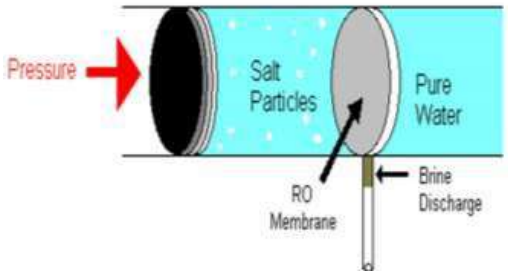


***Figure A.2:*** *Sketch explaining the reverse osmosis (RO) desalination mechanism. The salt particles (in the first compartment) are retained by the semi-permeable RO membrane that only allows pure water to get through to the second compartment. Adapted from https://energy.sandia.gov/wp-content//gallery/uploads/BiomimeticMembranes2.pdf*

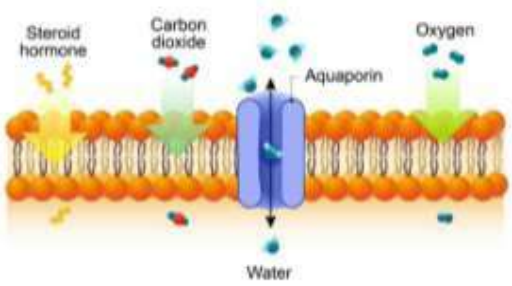


***Figure A.3:*** *Sketch depicting the Aquaporin transmembrane protein embedded in the lipid bilayer of the cell membrane (Only the lipid bilayer is represented here). Thanks to its facilitated diffusion, only water molecules can go through this protein. Adapted from*

# Appendix B

## Structural and nanomechanical characterization of lipid bilayers by AFM

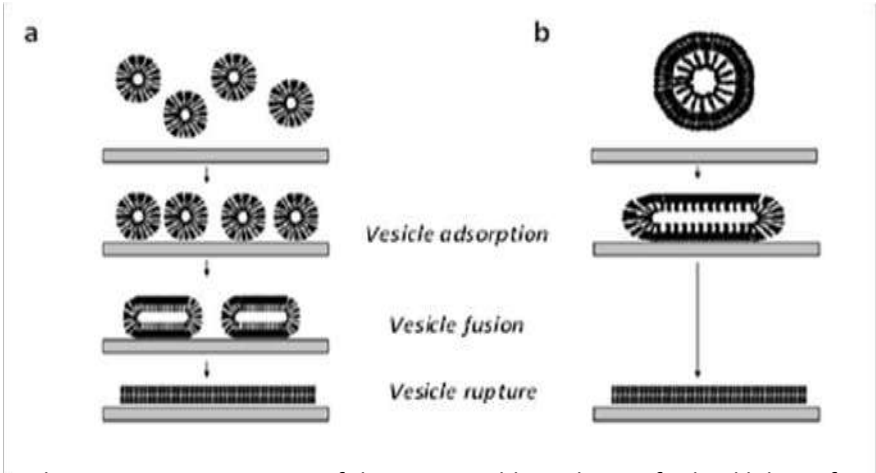


***Figure B.1**: Schematic representations of the two possible pathways for lipid bilayer formation using vesicle fusion technique. a) Three-step process: vesicle adsorption on the substrate, vesicle fusion and vesicle rupture b) Two-step process with vesicle adsorption and direct vesicle rupture to form the lipid layer. Adapted from Goksuet al.*[18] [18]

| | **Lipid deposit method** | | | |
|---|---|---|---|---|
| Features | Drop casting | Spin coating | LB transfer | Liposome fusion |
| Advantages | *Easy<br>*Versatile technique<br>*Good for packing properties study | *Full surface coverage<br>*Defect-free bilayers<br>*Well-controlled film thickness<br>*Well-controlled bilayer number | *Asymmetric bilayer deposition<br>*Controlled bilayer lateral pressure | *Simplicity |
| Drawbacks | *Poor control of lipid bilayer number | *Symmetric bilayers<br>*Difficult single bilayer deposition | *Uncompleted coverage<br>*Defects on bilayers<br>*Reproducibility problem | *Symmetric bilayers<br>*Non-controlled<br>lateral pressure |

***Table B1:** Advantages and disadvantages of the most used lipid deposition methods. Inspired from Picas et al.[15]*

| | FS-based imaging mode | | |
|---|---|---|---|
| Features | FV or force mapping | PFQNM | PFM[++] |
| Advantages | *Suitability to relate FS measurements to topography features<br>*Averaged measurements over the whole image | *Simultaneous imaging and nanomechanical mapping at high resolution<br>*Fast acquisition time | *High-spatial resolution images<br>*Fast scanning speeds<br>*Difficult control of the scanning force<br>*Possible sample damage |
| Disadvantages | *Slow acquisition time<br>*Low resolution images<br>*Huge amount of data to analyze | *Difficult accurate determination of mechanical properties (need of correct fitting model[+]) | *Only stiffness and adhesion values are stored<br>*No possible post-processing of force curves[+++] |

***Table B.2:*** *Advantages and disadvantages of force spectroscopy-based imaging modes. Inspired from An et al.[22] and Picas et al.[15] [+]Correct fitting model taking into account the sample nature and the tip geometry is crucial for extracting reliable parameter values. For example, for soft samples (like lipids), cantilever indentation depths in the sample should be minimal (<20% of sample thickness) to reduce the support effect. [++] In PFM, the cantilever position is sinusoidally modulated at high frequencies (>20 kHz) and force curves are recorded. [+++]Post processing of force curves has been enabled in a more recent version: Digital pulsed force mode (DPFM).*

| | Membrane model | |
|---|---|---|
| | **SLB** | **PSB** |
| Advantages | *Easy to prepare<br>* Improved surface coverage<br>* Improved imaging resolution<br>*Stable | *Freestanding bilayers: no support interaction<br>* Possible mechanical bending and stretching studies |
| Disadvantages | *Interaction with the support needs control<br>* Elastic response linked to that of the substrate<br>*Only compression mechanical studies are possible | *Difficult coverage<br>*Less stability |

***Table B.3:*** *Advantages and disadvantages of the two membrane models: Supported Lipid Bilayers (SLBs) and Pore-Spanning Bilayers (PSBs). Inspired from Picas et al.[15] (2012) and Steltenkamp et al.[36]*

# Appendix C

## Extraction of lipids from Arabidopsis thaliana's leaves:

## From 18/03/2019 to 26 /03/2019

Arabidopsis' leaves were collected in 4 corning tubes of 50 mL, were dropped in liquid nitrogen and stored at – 80°C on 1st of March, 2019

**Monday, 18 of March, 2019: Plant freeze drying**

Lyophilization, freeze drying or cryodesiccation is a low temperature dehydration process consisting in freezing the product, lowering the pressure and removing the ice by sublimation; which is in contrast to most conventional dehydration methods using heat to evaporate water. It will preserve lipid and protein molecules from degradation.

-Make 1 hole in each tube's cap. Put the tubes in the lyophilization bottle and plug the bottle on the freeze dryer

-Open the valve very slowly to avoid air movement. The pressure will increase. Wait until it get down again (to about 0.032mbar at a T= -86°C)

-Leave over night to freeze dry


Arabidopsis leaves on the freeze dryer

**Tuesday, 19 of March, 2019: Lipid extraction**

- Remove the lyophilization bottle by closing the valve very slowly and put back the tubes in liquid nitrogen.
- In a 400-mL Erlenmeyer, boil 120mL of absolute ethanol on a hot plate stirrer to destruct lipase activity.
- With a Potter pestle, grind the frozen plants in powder inside the corning tubes

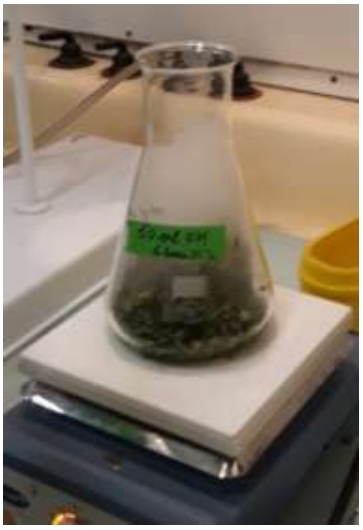

- Put freeze dried leaves in the ethanol Erlenmeyer.

5 minutes later, remove the Erlenmeyer from the hot block and add 40mL of Methanol (MeOH) and 160mL of chloroform ($CHCl_3$).Ligand

- Blow argon in the solvent mixture to remove oxygen.

Put a bar magnet in the Erlenmeyer, close it with foil and leave it for 1h on the stirrer at room temperature.**c**)

- Using a funnel plug with ethanol washed quartz wool, filter the liquid in a separatory funnel. Since the leaves are large, it clogsrapidly. A second is used to finish the solution filtrationss-DNA

- Prepare the CHCl3/MeOH 2/1 solution: 200mL of chloroform and 100mL of methanol.

- To rinse the Erlen, add 60ml of this mixture (with a glass pipette) and pour it on the quartz wool.

- At the end of the filtration (about 45min later), remove the funnel and add 68mL of NaCl 1% directly in the separatory funnel

- Blow argon to remove air and to mix up solvents and close with the funnel cap.

- Leave it overnight for the formation of the two phases the organic phase containing lipids and the inorganic phase containing the small remaining leaves

**Wednesday, 20 of March, 2019**

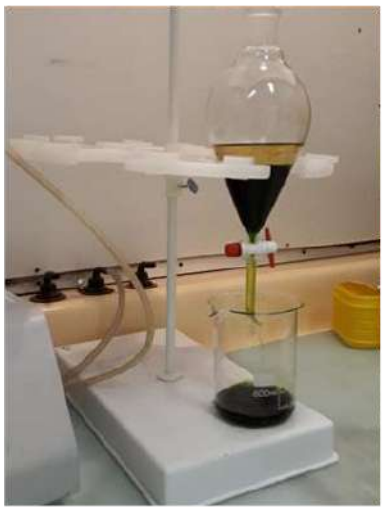

- Take the organic phase (bottom phase) from the separatory funnel and transfer it in a clean 600-ml beaker : remove the funnel cap, open the valve and let the bottom phase flow until the biphase interface is reached (Make sure not to take the top phase).


- Dry all the solvent under argon in a warm water bath (3h30min): change water approximately every 30 minutes to speed up evaporation)

- Extract the lipid with 10x1ml in chloroform and transfer it in a clean Pyrex tube.

- After the methanolysis tubes' preparation, store the lipid solution at -20°C after drying it under argon.

**Quantification of lipid extracts by fatty acids methanolysis (FAME; fatty acid methyl ester; formation) and gas chromatography with flame ionization detector (GC-FID)**

- The C15 (pentadecanoic acid, a linear fatty acid with 15 carbon atoms, is the internal laboratory standard acid) is stored at -20 °C at 0.5 µg/µl in $CHCl_3$: MeOH 2/1 v/v . Defrost it on the bench at least 1h before its use.
- Prepare 3 methanolysis Pyrex tubes (15ml tubes) making sure that every tube has a good screw thread and a Teflon plug seal.
- Turn on the hot block at 100 °C.
- Prepare the methanolysis buffer: 2.5% sulfuric acid $H_2SO_4$ in methanol MeOH (add 5mL of $H_2SO_4$ to 200 mL of pure frozen MeOH in a glass ground-necked bottle).
-


In each methanolysis tube :
- Add 2µl of lipid solution (vortex the lipid-containing tube before pipetting for a better homogeneity).
- With a Hamilton syringe, add 10 µl of C15 (about 5µg of C15).
- Add 3 ml of methanolysis buffer.
- Close tightly the Pyrex tube to avoid solvent evaporation.
- Put 1h at 100°C for the methanolysis reaction to occur.

- Take it out of the hot block and let it cool down few minutes
- Stop the reaction by adding 3 ml of water
- Add 3 ml of hexane and vortex vigorously at least for 10s
- Wait at least 30 min to separate the biphase on the bench
- Take the upper phase with a Pasteur pipette (about the volume of the pipette), transfer it in a 4 ml hemolysis glass tube and dry it under argon. Be careful not to take the bottom phase (which is very acid and can degrade the sample). Try to keep the pipette tip far from the tube walls and from the bottom phase by not taking all the top one; 3 to 4 mm of the latter can be kept in the tube
- Add 3ml of hexane in the Pyrex tube and vortex again for at least 10s. Wait for the biphase

- Take again the upper phase as described previously (this time the volume of the phase is about 1.8 the volume of the Pasteur pipette) and transfer it in the same hemolysis glass tube. Dry it under argon.

For the **GC-FID analysis**, lipid extracts need to be transferred in aninsertput in a crimp vial

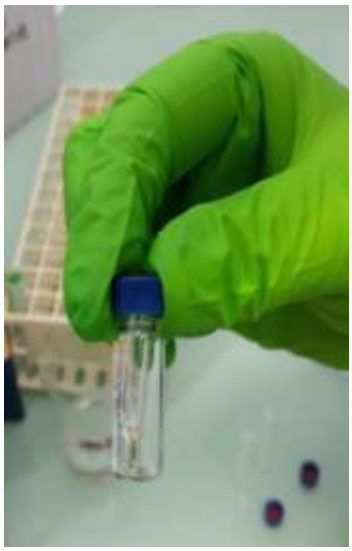

- Resuspend the lipid extracts in 100 µl of hexane by rinsing thoroughly the tube walls. Evaporate carefully in argon in order to let all lipids stick at the tube bottom.
- Resuspend in 40 µl of hexane while rotating the tube for a better lipid solubility. Transfer it in the minitubes.
- Close tightly the crimp vials.
- Inject the vials in the GC-FID (the analysis takes about 34 minutes per sample)

Gas chromatograph

Samples on GC-FID

**GC-FID analysis**

The gas chromatograph is a chemical analysis instrument used to separate and analyze complex compounds able to vaporize without decomposition. As explained in the schematic below, gas chromatograph is composed of a column ; a flow-through narrow silica tube through which chemical constituents of the sample pass in a carrier gas (mobile phase) stream (nitrogen in our case). Depending on their chemical and physical properties, different sample constituents exit the column end at different rates and are detected electronically.

In our case, a flame ionization detector is coupled to the gas chromatograph. Measuring the number of ions, formed upon oxidation of organic compounds in a hydrogen flame, per unit time makes this instrument mass sensitive.

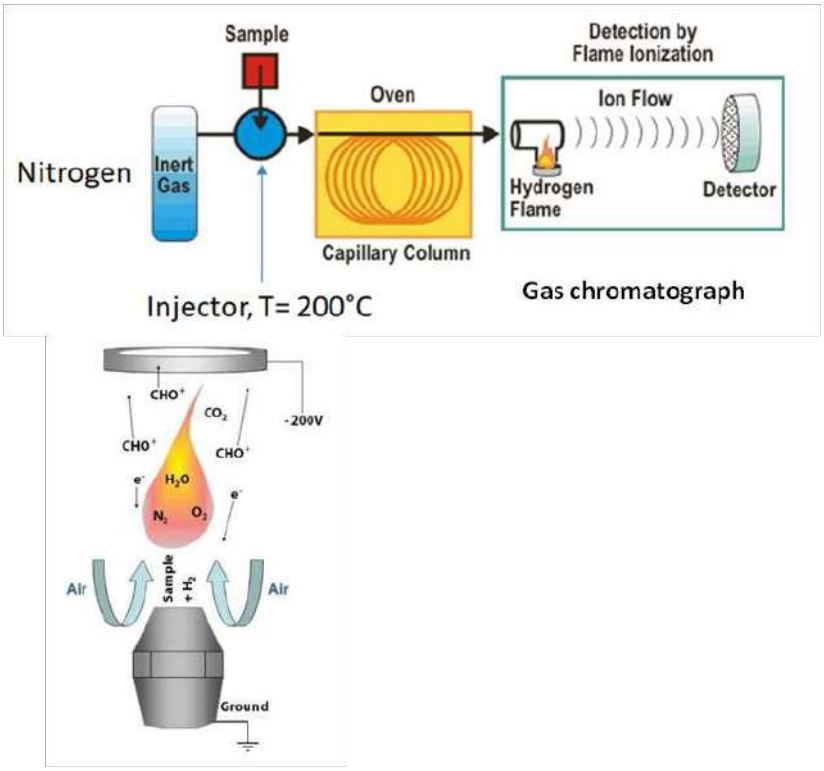


Two electrodes are used to detect ions. The latter (basically, CHO are attracted by the negative electrode inducing a current that is fed in an integrator. This current is proportional to the reduced carbon atoms in the flame and the data is displayed via a software installed on the detector-connected computer. The displayed graph is the real-time change in the electrodes potential difference as function of time.

The potential values are fed to an integrator since the peak area is proportional to the constituent mass. The first peak saturating the detector (the detection limit is 1000mV) corresponds to the hexane, the solvent. It appears about 1min after the analysis begins, which is the minimum time required to reach the column end. 5 min later, the graph displays the peak corresponding to C15, the internal standard. Later, we recognize the C16 and C18 peaks, especially C18:3 which is the abundant acid in our samples. Based on C15 mass (5 µg), the software script determines the other acids 'masses.Retention times were established by running commercially available fatty acid methyl ester (Sigma)

**Thursday, 21 of March 2019**

First, the GC results are extracted: in average, we have 16.56µg for the 2µl analyzed lipids i.e. about 8.3µg/µl

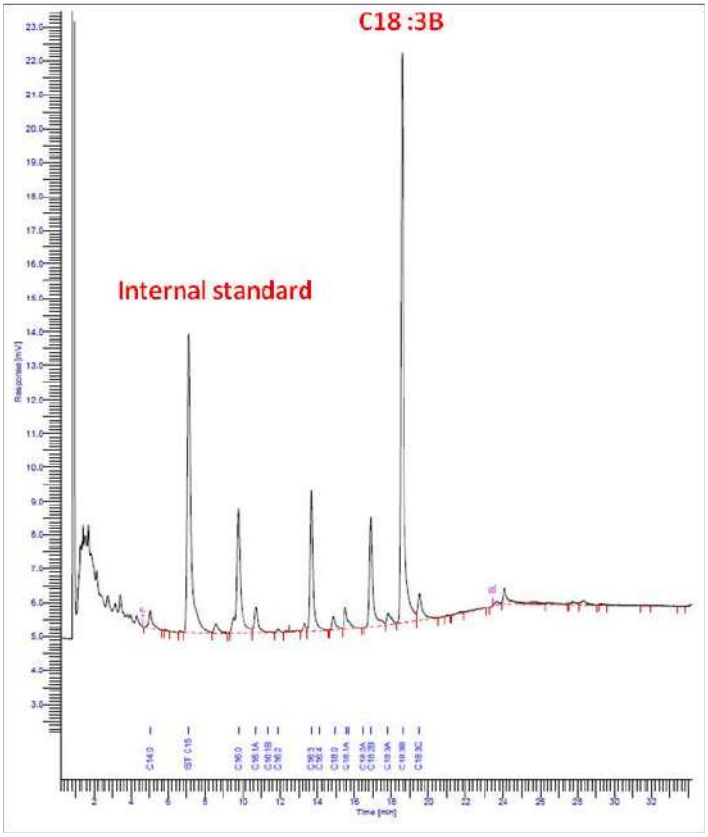


To perform column chromatography, 20 mg of lipids are needed which is the mass contained in 2.4 ml of lipid extract

- Using a 500 µl Hamilton syringe, prepare 4 aliquots of 2.4 ml in hemolysis tubes.
- Dry 3 of them under argon and store them at -20°C. The **fourth aliquot is to be used in the following steps** (dry it under argon in order **to have about 2ml**)

## Column chromatography

This step aims at separating the different lipids through column chromatography; silicic acid holds lipids by different bonding before eluting the column with solvents of increased polarity.

**Silica column preparation**

- For a better stability, put a paper tissue around the column and fix it in the holder

**Column washing**

- Close the column valve.
- Fill the column and allow it to drain completely **three times consecutively** using

- Water
- EtOH
- $CHCl_3$

- In a 150-ml beaker, weigh 900 mg of silicic acid $H_4SiO_4$. Use a mask because it is very volatile.
- Add $CHCl_3$ to cover the silicic acid by about 1 cm
-

**Quartz wool insertion**

- With a tweezer, take a small quartz wool and wash it with ethanol and chloroform $CHCl_3$.
- Close the column valve and half fill it with $CHCl_3$.
- Insert the quartz wool in the column.
- With a thin tip, press the wool and place it in the bottom of the column.
- Add $CHCl_3$ and allow it to sink a little without drying the wool.
- Using a 1 ml pipette tip, add the $CHCl_3$- silicic acid solution while keeping the column valve open, it fills about 7 cm of height. Pay attention not to form air bubbles when filling the column.
- Wash the column with 10ml of $CHCl_3$.
- Define the flow front of the silicic acid (closed valve) with a colored Scotch tape to distinguish silicic acid from lipids (after adding them) giving a green color to the whole column.
- Prepare 3 pyrex tubes with.

    - 40 ml of $CHCl_3$
    - 15 ml of acetone
    - 10ml of MeOH /$CHCl_3$ 1/1 v/v

**First elution**

- On top of the silicic acid, add the lipid solution (2ml) with a Pasteur pipette.
- Elute the lipid solution until the flow front in a beaker. Pay attention not to completely dry the column.
- Elute the 40 ml of $CHCl_3$ in the same beaker. This takes about **2h15min**

3 min

30 min

1 h

2 h

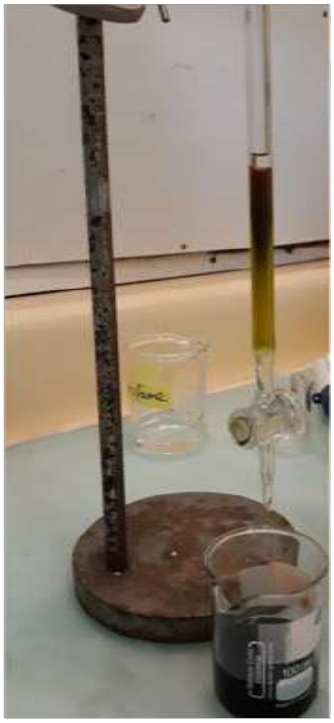

2h15min

**Second elution**

- Elute the 15 ml of acetone. This takes about **40min**

beginning

Eluate 3 min

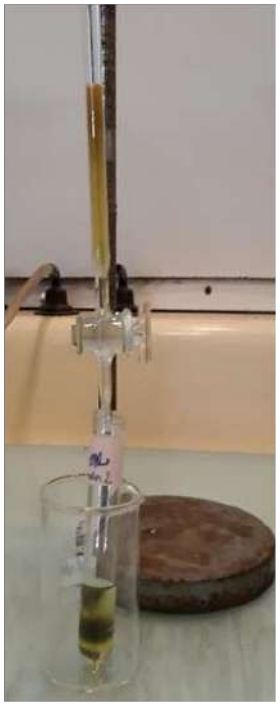

13 min

Eluate 13 min

**Third elution**

- Elute the 10 ml of MeOH /$CHCl_3$ 1/1 v/v. This takes about 11min

- The eluate is «Fraction3» and contains mainly phospholipids.

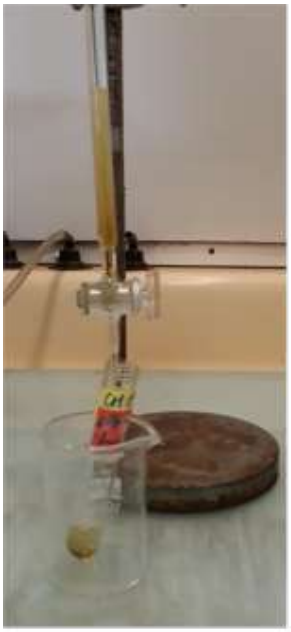

2min

Eluate 3min

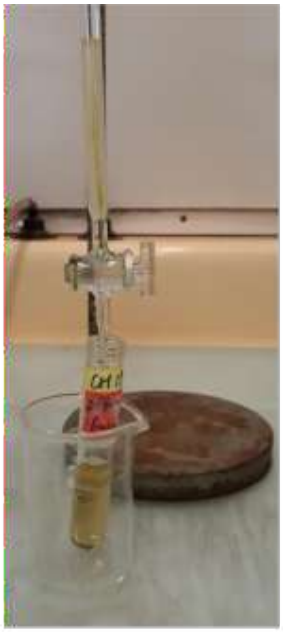

5min

5min (end)

**Fraction2 contains the lipids MGDG and DGDG**

**Fraction3 contains the lipids PI, PC, PG, SQDG and PE**

- Transfer dried lipids from screw-capped tubes into hemolysis tubes (add MeOH/$CHCl_3$ to dried lipids and transfer them), dry under argon and store them at -20°C.

- Prepare the 2 TLC plates (Silica gel 60, Merck, 20cmx20cm) by defining the migration edges with a pencil. Cover them with foil.

## Friday, 22 of March 2019

**Thin Layer Chromatography (TLC)**

- Defrost fraction2 and fraction3 for about 30min

- Prepare the migration cuve (In our case sense 2 is used, cf figure below) at least 30min before starting TLC

| **Migration solvent Sens 2** | |
|---|---|
| $CHCl_3$ | 50 ml |
| Acetone | 20 ml |
| MeOH | 10 ml |
| Acetic acid | 10 ml |
| $H_2O$ | 5 ml |

- Resuspend each fraction in 500µl of $CHCl_3$. Try to add chloroform on the tubes' walls to make sure to suspend the whole lipid sample

- Lay down lipids with a Pasteur pipette on the TLC plate at 2.5 cm of both sides (following the drawn lines). Dry between each drop with argon

- Do it again once with 300µl and once with 200µl (for fraction2) and once with 300µl (for fraction3)

- Put the 2 TLC plates in the migration cuve. Put each plate in front of one cuve's walls. Let lipids migrate for about 1h30min (to about 3cm from the top of the cuve)

- Dry the TLC plates under the fume hood

**ANS revelation**

- Under the fume hood, spray the TLC plates with ANS (anilinonaphtalenesulfonate 0.2% w/v in MeOH: 0.2g in 100ml of MeOH), used as a fluorescent probe, on TLC plates

- Dry few minutes

- Lipid visualization in a TLC visualizer (λ=254 nm)

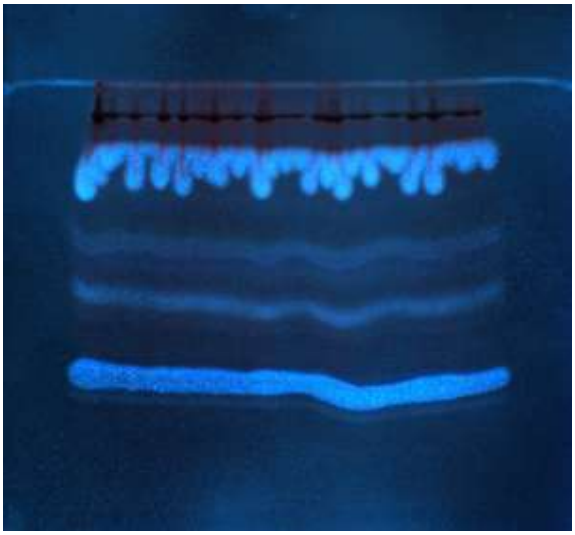

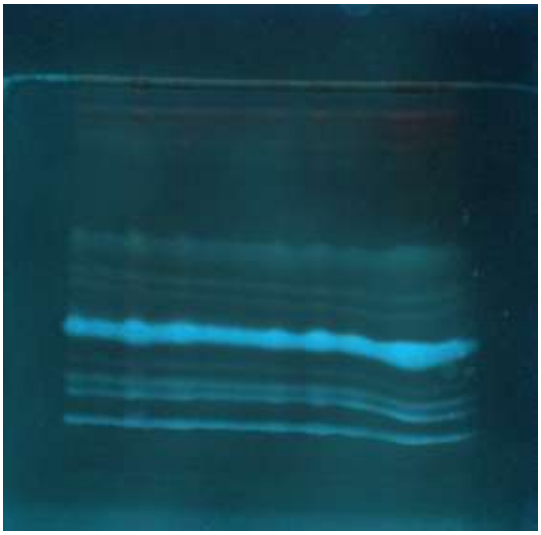

-Lipid visualization under UV light

- Draw around the spots with a pencil. On TLC plate of fraction3, lipids are called 1, 2, 3, 4, and 5 since some lipids are hardly distinguishable after migration (cf TLC lipid map below). These lipids will be well defined later thanks to mass spectrometry

**TLC lipid map**

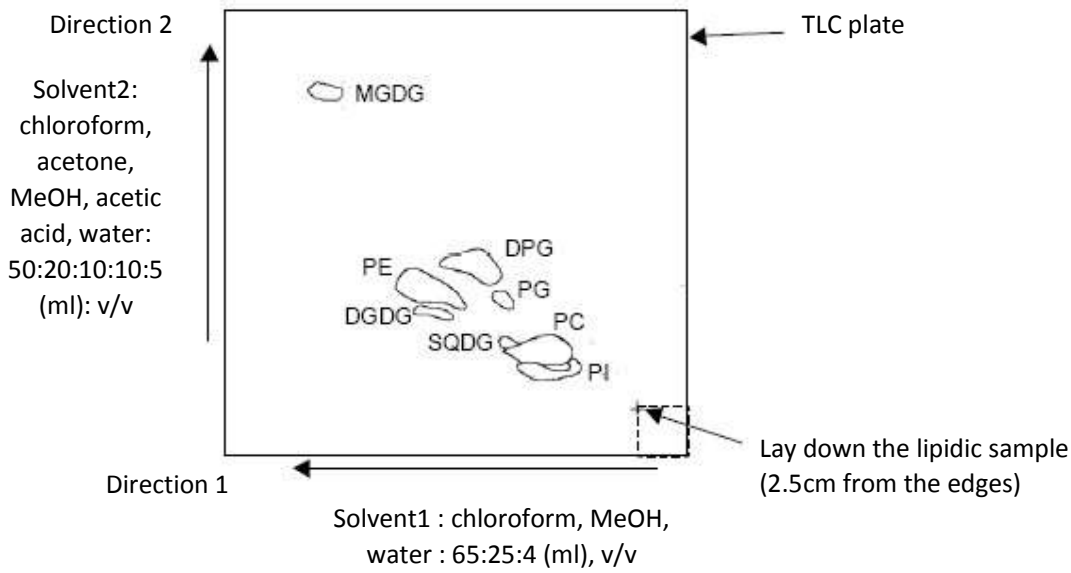

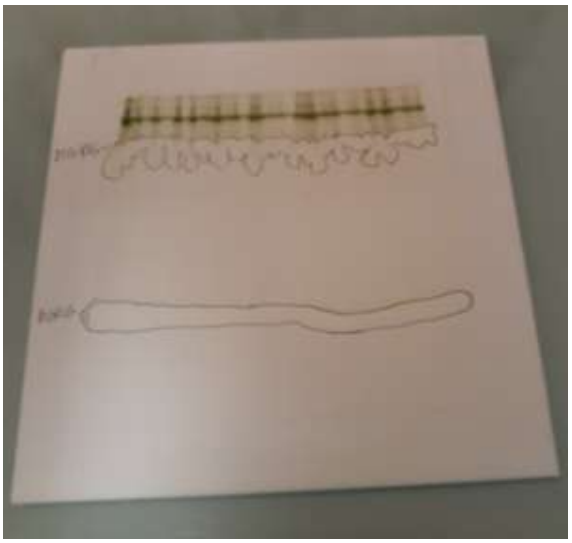

Fraction 2

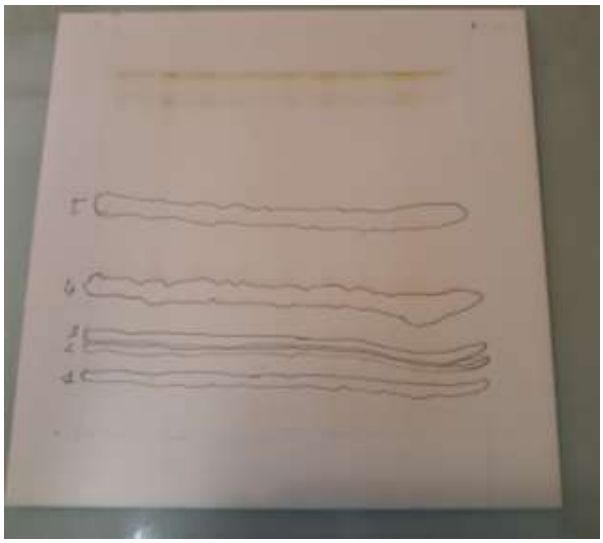

Fraction 3

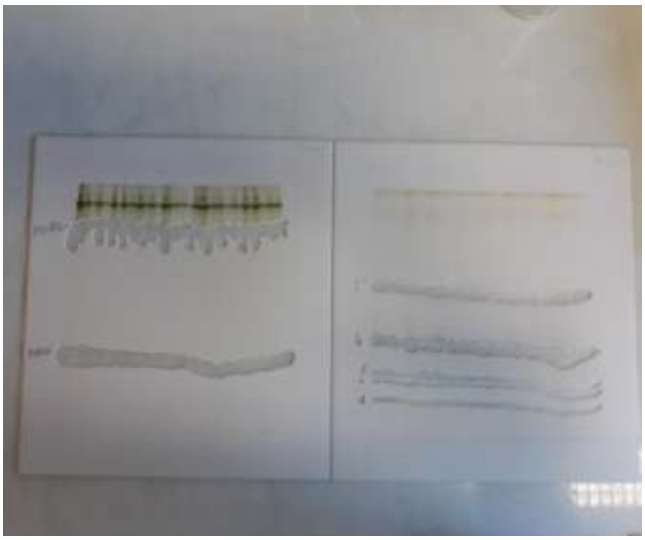

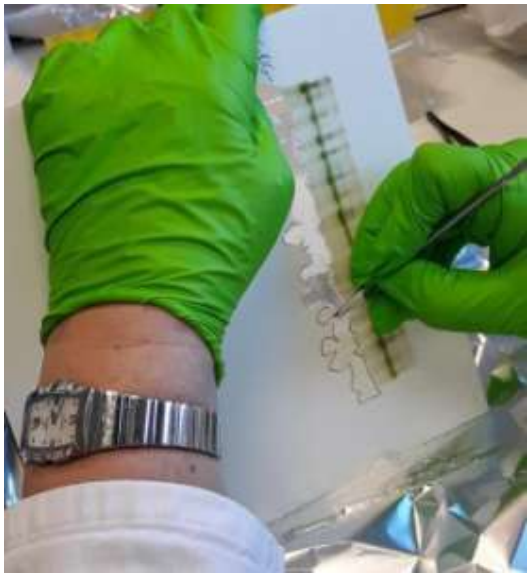

- Scrap each lipid spot with a spatula
- Transfer the silica powder in Pyrex tubes. Dry them with argon to avoid lipid oxidation and store them at -20°C

**Tuesday, 26 of March 2019**

**Lipid extraction from silica (Bligh and Dyer method)**

**For each lipid**

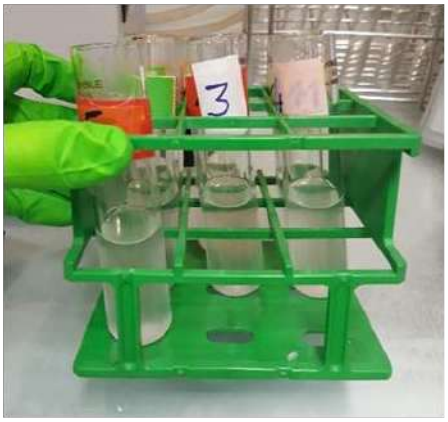


- Transfer silica powder in a 30-ml corex tube
- Add 13.5 ml of $CHCl_3$ /MeOH 1/2 v/v and vortex. Blow argon (about 1min for each lipid).

In order to transfer all the silica, rinse tubes with MeOH

- Add 4.5 ml of $CHCl_3$ and vortex gently
- Add 8 ml of water. Blow argon
- Incubate for 10min at room temperature

- Centrifugate tubes at 3000 rpm (rotations per minute) for 10min

- With a Pasteur pipette, take the lower organic phase in a corex tube. Take care not to take silica. Dry with argon
- In the biphase tube, add 12 ml of $CHCl_3$ to the upper phase and blow argon (about 1min /tube)
- Centrifugate tubes at 2500 rpm for 10min
- Take the lower phase and add it in the tube containing the first lower phase. Dry with argon.


- Resuspend in 1.5ml of $CHCl_3$ in a 5-ml hemolysis tube. Dry with argon

**Methanolysis**

- Resuspend lipids in 500 µl of $CHCl_3$ using a 500-µl Hamilton syringe.
- For each lipid (MGDG, DGDG, lipids 1, 2, 3, 4 and 5), prepare a methanolysis tube:
  - For **MGDG, DGDG and lipid 4, add 2µl of lipid solution+ 10 µl of C15 solution** (equivalent to 5µg since C=0.5mg/mL)
  - For other lipids, **add 5 µl of lipid solution+ 10 µl of C15 solution**
- Perform methanolysis and CPG analysis as described on Wednesday, 20 of March, 2019

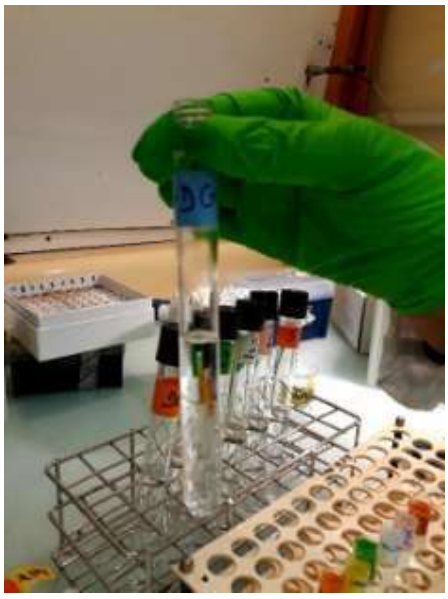

Methanolysis biphase1

Methanolysis biphase2

**GC results (Gas Chromatography):**

**DGDG: 12µg**

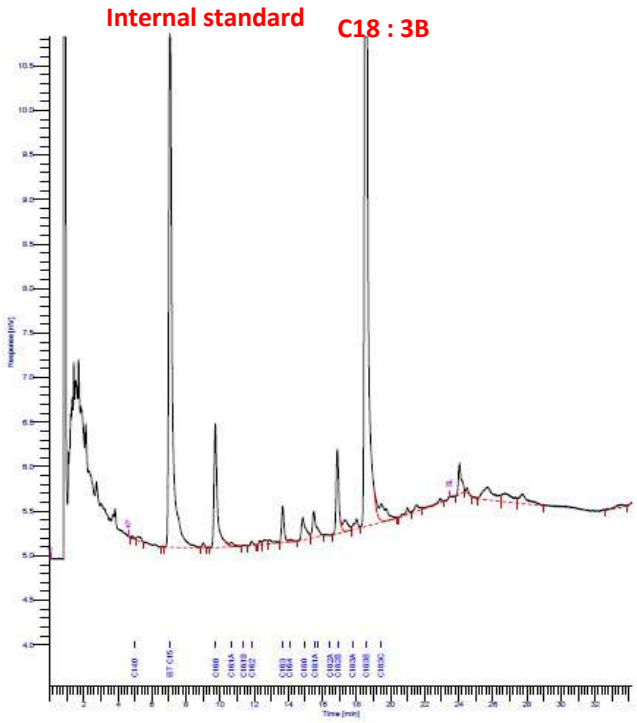


Then mass spectrometry is performed on extracted lipids and lipids are identified from fractions. Identification results are the following

1 : PI

2 : PC

3 : SQDG

4 : PE+PG

5 : PA

# Appendix D

**Objective**
Preparation of PC liposome solution (1mM)

## 1. Materials

### 1.1 Consumables

Lipid stock solution: S3-PC2 (prepared on 18/06)
$CHCl_3$-MeOH solution (1:2)
Standard vesicle buffer: 20mM HEPES pH7.3, 100mM NaCl
MilliQ water solution (ultra-pure filtered water)
Eppendorf tubes
Parafilm

### 1.2 Equipment

Hamilton syringes (500µl, 10µl)
Pipettes + plastic tips
Beakers
Glass tubes
Plastic tubes
Mini-Extruder for LUV Preparation from Avanti Polar Lipids, ref. 610023
Centrifuge
pH-meter with buffer solutions (pH=4 and pH=7)

## 2. Methods

The liposome preparation protocol is the one used in C2: "**Liposome formation and binding protocol". The prepared liposomes are light ones**

**Liposome formation**

The initial lipid solution **S3-PC2** contains **n=234µmol**
Resuspend it in **2340µl=2.34ml**; this makes a solution of **C=0.1M=0.1µmol/µl**

In a glass tube, combine **n=1000nmol=1µmol** of lipids in **organic solvents** ($CHCl_3$-MeOH solution 1:2, v/v) by taking **V=10µl** from the lipid solution
Dry under argon (Ag) for at 1h to be sure all solvents are dried

Resuspend the lipids in 1 mL of buffer solution. The resulting solution is 1mM
Vortex**(about 10sec)** every 15min for about 1h at RT.
After this step, multilamellar liposomes are formed.

Transfer liposomes to a non-sterilized Eppendorf tube to avoid their sticking to the tubes' walls and seal well with parafilm

Subject the liposomes to 8 cycles of freeze/thaw using liquid nitrogen and a water bath at 50°C.Vortex (about 10 sec) between cycles.
This step aims at increasing the efficiency of entrapment of water-soluble compound sand forming unilamellar liposomes

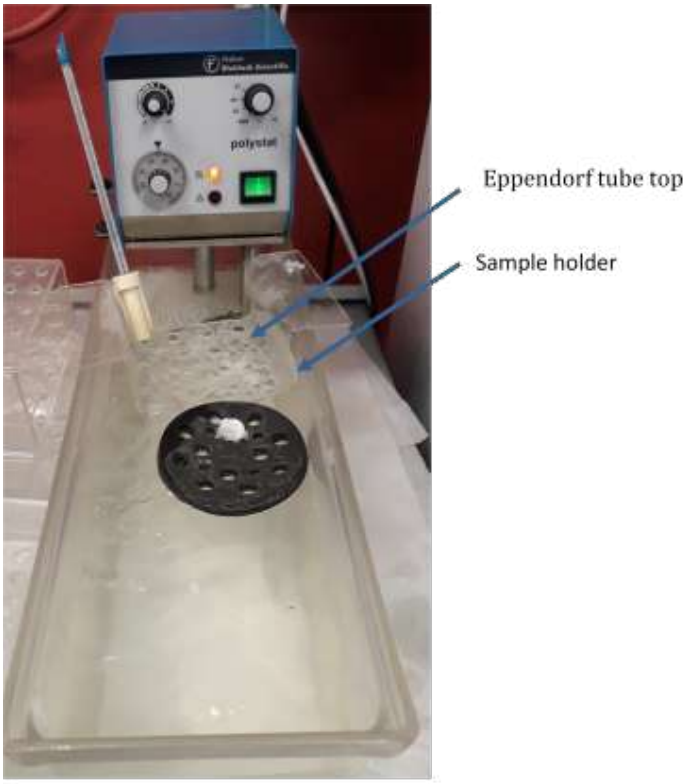


Water bath (50°C)

LiquidNitrogen

Extrude the liposomes through a 0.4µm filter **eight times**. This step controls the liposomes' size

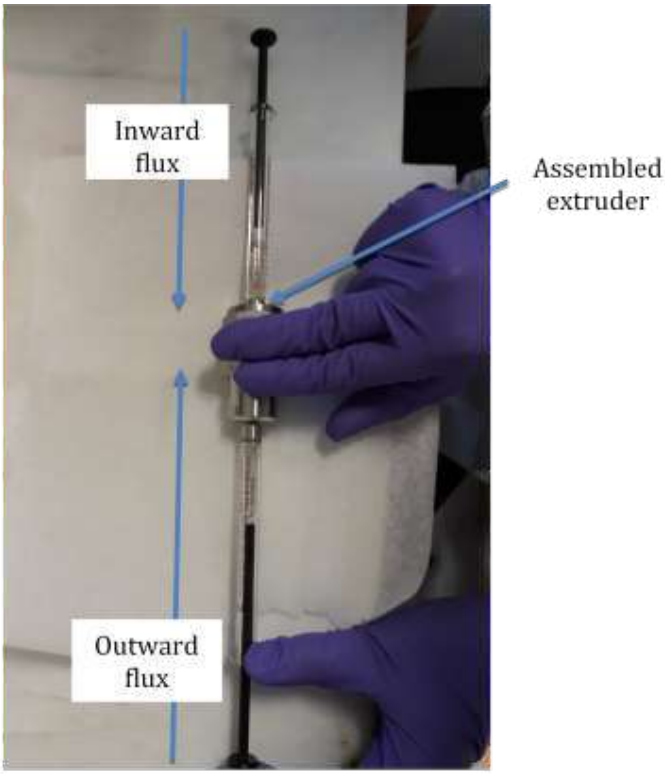


Liposome solution extrusion. Outward and inward flows are with respect to the bottom syringe containing initially the lipid solution

Centrifuge light liposomes at 16,000 g for 10 min at 4°C
Retain the supernatant. This reduces the number of heavy multilamellar vesicles.
The prepared solution is so homogenous that it is difficult to distinguish between its two phases.
Transfer the final solution to a clean Eppendorf tube

**Buffersolution (20mM HEPES pH7.3, 100mM NaCl) preparation:**

**HEPES solution (C=1M) preparation:**
Add m=11.9g of HEPES powder to V=30ml of milliQ water
Stir the solution using magnetic stirrer
While controlling the pH with a pH-meter, add progressively KOH solution (C=10M) using a plastic Pasteur pipette till reaching pH=7.3
In a measuring cylinder, add V=20ml of milliQ water
**This results in a 50ml HEPES solution of 1M at pH=7.3**

Take **V=1ml** from **1M HEPES** solution and **V=2.5ml** from **2M NaCl solution.**
In a plastic graduated tube, add water to have a final volume of 50ml.The resulting solution is the buffer: 20mM HEPES; pH7.3, 100mM NaCl
NaCl is added to regulate the osmotic pressure

Before being stored, buffer solutions (1M HEPES, 20mM HEPES; 100mM NaCl) are filtered with a 0.2µm filter

**Liposome storage and use:**
Liposome solution is stored at 4°C and can be pipetted using standard pipettes with plastic tips
It is preferable to gently pipette liposomes, not to vortex and not to sonicate them

**At the experiment end; the initial solution S3-PC2 is also dried and restored at -20°C**

**General remarks:**
The prepared liposomes are described as light compared to heavy ones usually dissolved in sucrose (instead of NaCl) vesicle buffer. These liposomes are centrifuged at lower accelerations (16,000g) as compared to light liposomes (100,000g)
The adjustment of pH may be not crucial for our application. However, it is very important for binding proteins to liposomes

**Avanti's Mini-Extruder for LUV Preparation kit:**
**From** https://avantilipids.com/divisions/equipment-products

Avanti Mini Extruder allows to prepare large, unilamellar vesicles via extrusion through a polycarbonate membrane. The liposome size ranges from 30nm to 1µm

Extruder kit:
The kit includes:
A mini Extruder made from stainless steel and Teflon
2 O-Rings
2 Gas Tight syringes (1ml)
Polycarbonate Membranes (ref. 800282, pore size : 0.4µm)
Filter supports (ref.610014)
Filter supports and polycarbonate membranes are single-use

**Extruder assembly:** Following assembly instructions of Avanti Polar lipids

**The extruder diagram is shown below:**

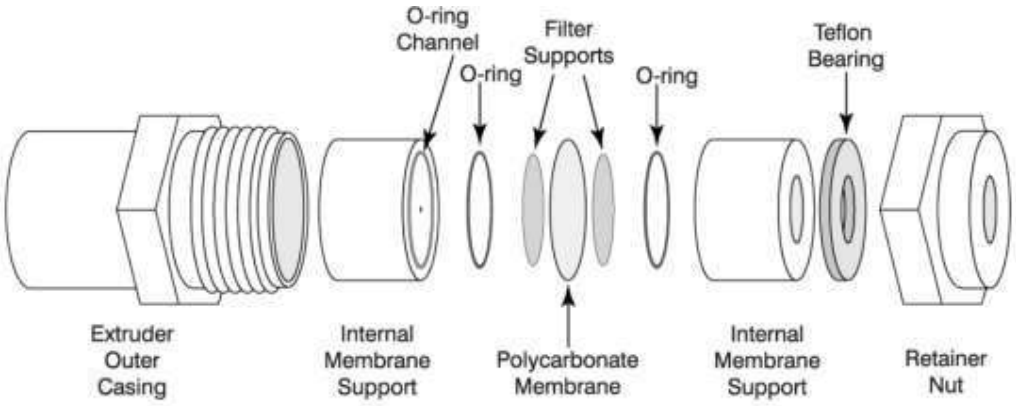


Extruder diagram from *https://avantilipids.com/divisions/equipment-products/mini-extruder-assembly-instructions*

1. Pre-wet the two filter supports and the polycarbonate membrane with deionized water

2. Pre-wet the two internal membrane supports, extruder outer casing and retainer nut with deionized water

3. Pre-wet the two syringes with water

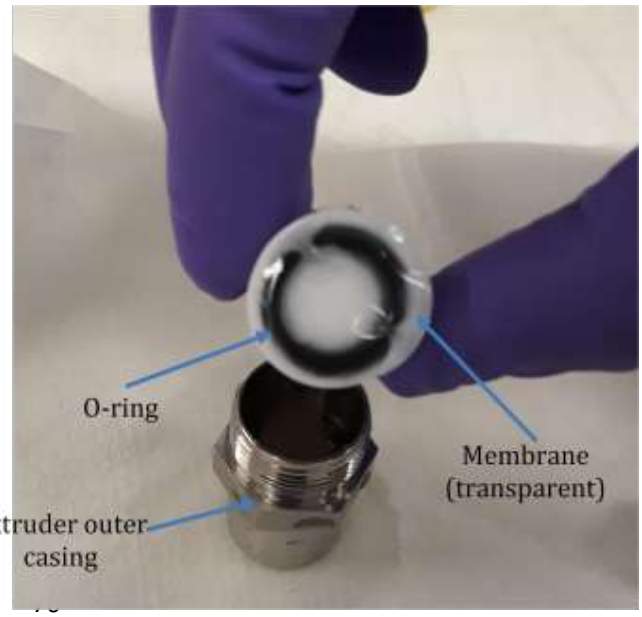


4. Place 1 filter support on the Teflon orifice of a internal membrane (with the O-ring faced up)

5. Insert the internal membrane support, with the filter support, into the extruder outer casing with the O-ring facing up

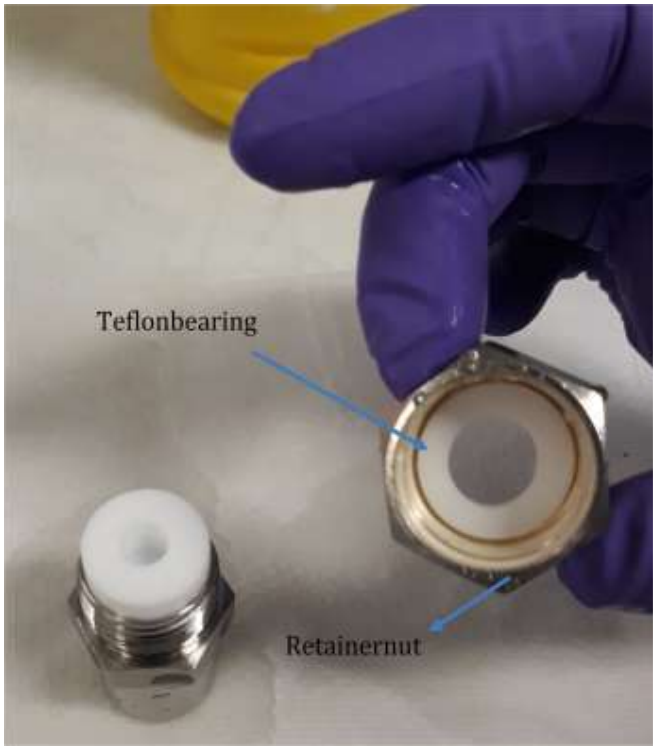


6. Place the polycarbonate membrane in the extruder outer casing over the filter support and O-ring

7. Place the second filter supportover the orifice of the remaining internal membrane support

8. Carefully place the second internal membrane support into the casing (O-ring facing down) being careful not to twist the membrane support when it comes in contact with the membraneP-lace the Teflon bearing into the retainer nut

9. Place the retainer nut on the threaded end of the extruder outer casing and tighten by hand until it is finger tight

10. Place the retainer nut on the threaded end of the extruder outer casing and tighten by hand until it is finger tight

Screwed extruder

**Extrusion steps:**

Using membranes with pore size >0.2µm produce a polydisperse suspension of multilamellar liposomes.

1. Load the sample into one of the syringes and place the latter into one end of the mini-extruder.

2. Gently push the plunger of the filled syringe until the lipid solution is completely transferred to the alternate empty syringe. Repeat this step 8 times.

3. Remove the filled syringe from the extruder and transfer the lipid solution to a clean Eppendorf tube. Liposomes are not stable in aqueous media (at 4°C) and should be used in the next 48h of their preparation.

4. Remove the alternate syringe and detach the mini-extruder.
5. Clean apparatus thoroughly

**Abstract**

Thanks to recent advances in nanotechnology and molecular engineering, biomimicry is emerging at the nanoscale and more particularly in the field of membrane and nanopores. The biological cell is filled with different nanopores and transporters controlling the exchange of ions and molecules between the cell and its environment. However, these biological nanopores are difficult to study in vitro due to their instability and sensitivity to small variations in external parameters (pH, salt concentration…). On the contrary, solid-state nanoporous membranes have advantages over their biological counterparts: enhanced stability, choice of nanopore diameter and potential for integration into devices. In this context, the aim if the internship was to build and characterize **hybrid nanoporous membranes**. These membranes combine the robustness of solid-state nanopores with the specificity of lipids (biomolecules). Biomimetic hybrid membranes are fabricated by depositing plant lipids (PC and DGDG) inside SiN nanopores. Different microscopy techniques (fluorescence, transmission electron microscopy TEM and atomic force microscopy AFM) are used to characterize lateral lipid deposition on nanoporous membranes. Vertical lipid deposition inside nanopores is also quantified using AFM. Surface coverage of lipid deposited with different methods is also evaluated. Further, AFM scan parameters effect on constructed nanopore topography is assessed.

**Résumé**

Grâce aux avancées récentes des nanotechnologies et du génie moléculaire, la biomimétique émerge à l'échelle nanométrique et plus particulièrement dans le domaine des membranes et des nanopores. La cellule biologique est remplie de différents nanopores et transporteurs qui contrôlent l'échange d'ions et de molécules entre la cellule et son environnement. Cependant, ces nanopores biologiques sont difficiles à étudier in vitro en raison de leur instabilité et de leur sensibilité à de faibles variations des paramètres externes (pH, concentration en sel...). Au contraire, les membranes nanoporeuses à l'état solide présentent des avantages par rapport à leurs homologues biologiques : stabilité accrue, choix du diamètre des nanopores et possibilités d'intégration dans les dispositifs. Dans ce contexte, l'objectif du stage est de construire et de caractériser des membranes hybrides nanoporeuses. Ces membranes combinent la robustesse des nanopores à l'état solide avec la spécificité des lipides (biomolécules). Les membranes biomimétiques sont fabriquées en déposant des lipides végétaux (PC et DGDG) dans des nanopores de SiN. Différentes techniques de microscopie (miscroscopie fluorescence, microscopie électronique à transmission TEM et microscopie à force atomique AFM) sont utilisées pour caractériser l'étalement latéral de lipides sur la surface des membranes nanoporeuses. Les dépots de lipides dans les nanopores sont également été quantifiés à l'aide de l'AFM. L'uniformité de dépôt de lipides préparés par différentes manières est aussi évaluée. De plus, l'effet des paramètres de balayage AFM sur la topographie des nanopores construits est évalué.

**Astratto**

Grazie ai recenti progressi delle nanotecnologie e dell'ingegneria molecolare, la biomimesi sta emergendo alla scala nanometrica, in particolare nel campo delle membrane e dei nanopori. La cellula biologica è riempita con diversi nanopori e trasportatori che controllano lo scambio di ioni e molecole tra la cellula e lo suo ambiente. Tuttavia, questi nanopori biologici sono difficili da studiare in vitro a causa della loro instabilità e sensibilità a piccole variazioni dei parametri esterni (pH, concentrazione di sale....). Al contrario, le membrane nanoporose allo stato solido presentano vantaggi rispetto alle loro controparti biologiche: maggiore stabilità, scelta del diametro dei nanopori e possibilità di integrazione in dispositivi. In questo contesto, l'obiettivo dello tirocineo era quello di costruire e caratterizzare membrane nanoporose ibride. Queste membrane combinano la robustezza dei nanopori allo stato solido con la specificità dei lipidi (biomolecole). Queste membrane vengono fabbricate depositando i lipidi vegetali (PC e DGDG) all'interno di nanopori SiN. Diverse tecniche di microscopia (fluorescenza, microscopia elettronica a trasmissione (TEM) e microscopia a forza atomica (AFM)) sono utilizzate per caratterizzare la deposizione laterale dei lipidi sulle membrane nanoporose. Anche la deposizione verticale dei lipidi all'interno dei nanopori è stata quantificata utilizzando l'AFM. Viene valutata anche la copertura superficiale dei lipidi depositati con metodi diversi. *Inoltre, gli effetti dei parametri di scansione AFM sulla topografia dei nanopori sono valutati.*